## Title
A SCHEME FOR CALCULATING FLOW IN FRACTURES USING NUMERICAL GRID GENERATION IN THREE-DIMENSIONAL DOMAINS OF COMPLEX SHAPES



## Authors
Muralidhar, K.
Long, J.C.S.

## Publication Date
1987-09-01

LBL-24453



**Lawrence Berkeley Laboratory**
UNIVERSITY OF CALIFORNIA

## EARTH SCIENCES DIVISION



# A Scheme for Calculating Flow in Fractures Using Numerical Grid Generation in Three-Dimensional Domains of Complex Shapes

K. Muralidhar and J.C.S. Long

September 1987



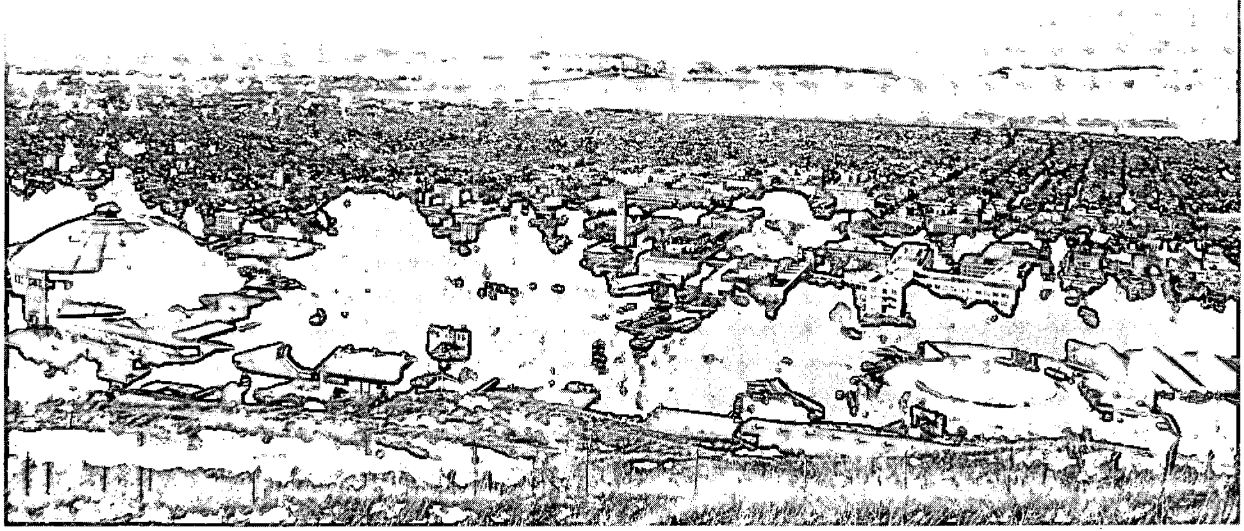

Prepared for the U.S. Department of Energy under Contract DE-AC03-76SF00098

LBL-24453

# A Scheme for Calculating Flow in Fractures Using Numerical Grid Generation in Three-Dimensional Domains of Complex Shapes

*K. Muralidhar and J. C. S. Long*

Earth Sciences Division
Lawrence Berkeley Laboratory
University of California
Berkeley, CA 94720

September 1987

This work was supported by the Repository Technology Division, Office of Civilian Nuclear Waste Management of the U. S. Department of Energy under contract DE-AC03-76SF00098.

# Abstract

A numerical scheme for the solution of fluid flow equations in a complex three-dimensional geometry has been developed in order to study fluid flow in rock fractures. The scheme consists of two parts, the first being a grid generator and the second, a flow solver in a generalized coordinate system. The grid is determined by mapping the irregular flow region of the fracture, onto that bounded by a rectangular parallelepiped. The mapping function is implicitly defined via differential equations, which in turn are derived from a variational principle. This procedure is general enough to incorporate various aspects of grid control such as orthogonality, mesh concentration, treatment of singular points etc. However, only orthogonality has been included in this report. The others are not expected to be significant in the problem of fluid flow in a single fracture. Complete details of the derivation of the governing equations and boundary conditions have been given here. The flow is taken to satisfy the Navier-Stokes equations. These are also solved numerically, by simultaneously solving for the pressure field from a Poisson equation. The complete procedure is validated by computing various test cases, which have been included in this report.

# Table of Contents

## List of Figures

## Nomenclature

| | |
|---|---|
| b | Aperture |
| Du, Duv ... | $(\nabla u)^2$, $(\nabla u \cdot \nabla v)$ etc. expressed in terms of u, v and w as the independent coordinates. |
| EL | Euler-Lagrange operator, $= [\frac{\partial}{\partial \phi} - \sum \frac{\partial}{\partial u} \frac{\partial}{\partial \phi_u}]$ |
| F | Integrand in the variational statement (in the physical space). |
| G | Integrand in the variational statement (in the computational space). |
| $\underset{\sim}{i}, \underset{\sim}{j}, \underset{\sim}{k}$ | Triad of unit vectors in computational space. |
| K | Permeability |
| $K_{eq}$ | Equivalent permeability |
| $K_l$ | Local permeability |
| L | Length of flow region |
| M, N | Number of nodal points in y and z directions. |
| p | Pressure |
| P | Specified value of pressure |
| Re | Reynolds number, $\sqrt{\frac{P}{\rho}}\frac{b}{\nu}$ |
| Ru, Rv, Rw | Residuals of the finite difference equations in the u, v and w component equations. |
| u,v,w | Coordinates in the computational space. Also, components of velocity in Appendices D and E. |
| $u_m$ | Mean velocity in the fracture. |
| $u_1,u_2,u_3$ | Components of velocity in x, y and z directions. |
| x,y,z | Coordinates in the physical space. |
| $\nabla$ | Gradient operator $(\frac{\partial}{\partial x}, \frac{\partial}{\partial y}, \frac{\partial}{\partial z})$. |

| | |
|---|---|
| $\lambda$ | Orthogonality parameter. |
| $\rho$ | Fluid density. |
| $\phi$ | Generic variable on which an operation is performed. |
| $\xi,\eta,\gamma$ | Coordinates defining a transformed computational space, Appendices D and E. |
| $\nu$ | Kinematic viscosity. |

**Subscripts**

| | |
|---|---|
| u,v,w | $\frac{\partial}{\partial u}, \frac{\partial}{\partial v}, \frac{\partial}{\partial w}.$ |
| uu | $\frac{\partial^2}{\partial u^2}$ |
| i,j,k | Location on a finite difference grid in computational space. |

**Superscripts**

| | |
|---|---|
| n | Level of iteration. |

# 1. INTRODUCTION

The science of fracture hydrology is a relatively new field. It is a separate endeavor from classical porous media ground water hydrology because analysis techniques developed for porous media do not work well for fractured rock. Basic research is needed to understand how the features of fractures control flow in the rock. To that end, we are interested in how the features of individual fractures control flow.

Fractures in general have rough sides and these sides are held apart through the contact of asperities on the surfaces. The area of contact, "contact area", is irregular as is the aperture of the fracture where it is open. Thus from the point of view of fluid mechanics, a fracture is an irregular three-dimensional channel with irregularly spaced and sized obstacles.

To characterize the geometry of such a channel is a problem in itself. On going research is focussed on the quantification of void geometry in a fracture. Several laboratory and analytical techniques are under investigation. Casts of the fracture can be made by injecting a low melting point metal into the fracture (Pyrak-Nolte et al., 1987). The fracture can then be taken apart and both sides photographed. In such a photo, the contact area shows up as the color of the rock and the open area show up as the color of the metal. Both photographs and profile data can be used in a conditional geostatistical simulation which provides an estimate of the aperture as a function of location in the fracture plane. Alternatively, it may be possible to quantify the geometry of the fracture directly using parallax photography. These techniques will be described in detail in other reports. Here we discuss how we can proceed to analyze flow through the channel once the geometry is defined.

The problem of fluid flow in an irregular geometry can be solved theoretically only if a numerical approach is adopted. Further, any such scheme must have a definite capability to handle boundary shapes which do not coincide with coordinate lines. In the present work, a three-dimensional grid generation procedure is described, which maps the interior of a complex region onto the interior of a rectangular parallelepiped. This also guarantees that the boundaries of the transformed region represent constant values in terms of the new system of coordinates. The flow computation is performed in the newly defined region, and an inverse transformation rule extracts values of flow velocities and pressure in the geometry of interest. This two-step procedure of grid generation followed by flow calculation is described in detail in this report.

There are several reasons why mesh generation is of central importance in the numerical solution of partial differential equations. First, the profile of the flow boundary is usually different from that of any of the fundamental coordinate systems. This leads to interpolation errors in boundary conditions which in turn could significantly deteriorate the overall accuracy. There are alternative methods, such as the finite element method (FEM), where boundary shape can be included in the formulation of the physical problem, through the use of higher order elements. Whether FEM results in more or less algebraic complexity, than the approach presented here remains as yet unresolved. Second, the cost of computation and the speed of the present day computers limits the number of points that can be used in a flow calculation, and consequently limit the accuracy. Considerable gain in accuracy can be accrued through grid generation by selectively relocating nodal points to represent critical portions of the flow region while keeping the total number of nodes fixed. Lastly, a skewed mesh causes a larger truncation error compared to an orthogonal system. The mesh generation procedure described in this report provides a systematic way to reduce the skewness both in the interior of the physical space, as well as the manner in which the grid line intersects the boundary.

In this report, the emphasis is on grid generation which can, (1) be accomplished via differential equations, (2) handle complex boundary shapes, and (3) impose a predetermined degree of orthogonality on the grid lines. The formulation is presented in three dimensions, suitable for flow analysis in a single rock fracture. It is general enough to be extended to include other mesh properties such as concentration of nodes near a point or line, where severe gradients in the field variable are likely to occur. The governing equations for grid transformation are written with respect to the Cartesian coordinates and the solution for the grid points in the physical space constitutes a transformation law. This procedure falls in the class of techniques which employ boundary transformation to accommodate complex domains. The mapping function is implicit in the differential equations required for the transformation and has only a point wise definition. The rectangular geometry which arises after transformation can be advantageously used for performing computation of the physical problem. This is because the regular boundary shapes permit easy application of boundary conditions. Further, the nodal points in this space are placed at equal intervals, making discretization rules algebraically simple. The whole process of transformation is accommodated in the mathematical model by viewing it as a change of coordinates.

The actual differential equations chosen to define the mapping function depend ultimately on the physical problem prevailing on the flow domain. The interest in this study is restricted to low Reynolds number steady flow in rock fractures, and the respective equations and boundary conditions are known to form an elliptic problem. The grid generated from such a system of equations has built-in smoothing properties, as is observed in related diffusion-dominated problems. Little modification is required to extend this to time-dependent cases. However, in high speed flows, it is necessary to permit the formation of boundary layers, and special treatment is usually required.

The oldest and the simplest method of transforming a given shape to another convenient one is Conformal Mapping (Churchill, 1960), arising from complex variable theory. If an analytical mapping function can be found for the boundary shape at hand, then the grid is generated with little effort, and is naturally orthogonal everywhere in the domain. Further, in many linear problems the governing equations are fully preserved. However, the analytical procedure cannot be generalized and is definitely limited to two-dimensional regions. A related type of mapping based on algebraic formulas and which can be extended to three dimensions has been described by Eisman (1985). It has been found to be useful in the aeronautics industry, where smooth aerofoil shapes are frequently encountered. The approach utilizing differential equations (as opposed to algebraic expressions) is quite recent, and a summary of the procedure involved has been provided by Thompson et al. (1982). The motivation to use differential equations comes from Conformal Mapping Theory, where the real and the imaginary parts of the mapping function must be harmonic, i.e., satisfy Laplace equation. Thompson et al. (1982) also describe the use of Poisson equations for grid generation, where, by a proper choice of source terms, the desired grid control can be accomplished. Winslow (1966) has proposed a variational formulation of the same problem. Brackbill and Saltzmann (1982) have extended this minimization principle to include various measures of grid quality, such as orthogonality and concentration as constraints. The variational method appears to be the most general of all techniques and will be used here. Detailed derivation in three dimensions will form the subject matter of the next chapter.

Grid generation viewed as a numerical procedure for coordinate transformation has been recently used in the solution of two-dimensional continuum problems in both fluid and solid mechanics. Altus and Bar-Yoseph (1983) have studied stress distribution in orthotropic, laminated composites using this method. Projan, Rieger and Beer (1981) have studied free convective movement of a fluid in the gap between eccentric cylinders, by mapping it into a rectangular strip. Goldman and Kao (1981) have described their experience with this technique, applied to heat conduction problems in multiply-connected domains. Napolitano and Orlandi (1985) have published results of a comparison study of laminar flow in a complex geometry, using different numerical schemes. Those employing coordinate transformation are seen to be the most accurate simulations.

This report consists of two parts. First, the equations governing grid generation in three dimensions, including a method to improve orthogonality of the generated coordinates are fully derived. These equations are valid for both simply and multiply connected domains. It is usually simpler to solve for the flow field in a multiply-connected domain where the "holes" overlap the coordinate lines, rather than convert it to one which is simply connected, by use of branch surfaces. This approach could however fail, if the stiffness matrix to be inverted is singular due to these holes in the matrix structure. Secondly, the equations and boundary conditions governing flow are presented in both Cartesian and the transformed coordinates in both two dimensions and three dimensions. The numerical procedure for the solution of these equations is developed in each case and this is followed by results of selected test cases.

# 2.0 FORMULATION OF GOVERNING EQUATIONS OF GRID GENERATION

Figure 2.1 shows an example of a complex planar surface being transformed into a rectangle, where the grid lines have been drawn by joining points for which the generated coordinates take on constants values. In the following discussion, the space covered by the complex boundary (in which the physical process is taking place) will be identified as the *physical space,* and the rectangular (i.e., regularized) region as the *transformed space*. While a mesh in the physical space could be directly used in a numerical solution of the flow problem, there are definite disadvantages in doing so, especially when a finite-difference scheme is used. First, it is difficult to apply boundary conditions directly over a portion of the boundary. Also, unequal spacing of the interior mesh lines requires the use of complicated differencing rules. Both these drawbacks can be overcome by mapping the problem to the simple geometry of the transformed space and transferring the complexity to the transformation of the governing equations. In this case, it is the inverse mapping which is of interest, i.e., the location of the points on the physical space corresponding to those on the transformed space rather than the forward transformation. For this reason, the derivation of the governing equations given below will be for the inverse mapping problem. It is hence appropriate to call the transformed region also as the *computational space* on which the unknown quantities are determined. Differential equations governing the inverse mapping are derived below. The transformation of the governing equations to the computational space are given in Chapter 3.0.

## 2.1 Variational Formulation

The equations governing grid generation are derived through a variational formulation. The minimization principle used by Brackbill (1982) in two dimensions is extended to three dimensions, with the added constraint of partial orthogonality of the mesh lines in the physical space. Let $\underset{\sim}{x}$ = (x,y,z) be the coordinates describing the physical domain and $\underset{\sim}{u}$ = (u,v,w) be that for the computational domain. The transformation of the $\underset{\sim}{x}$

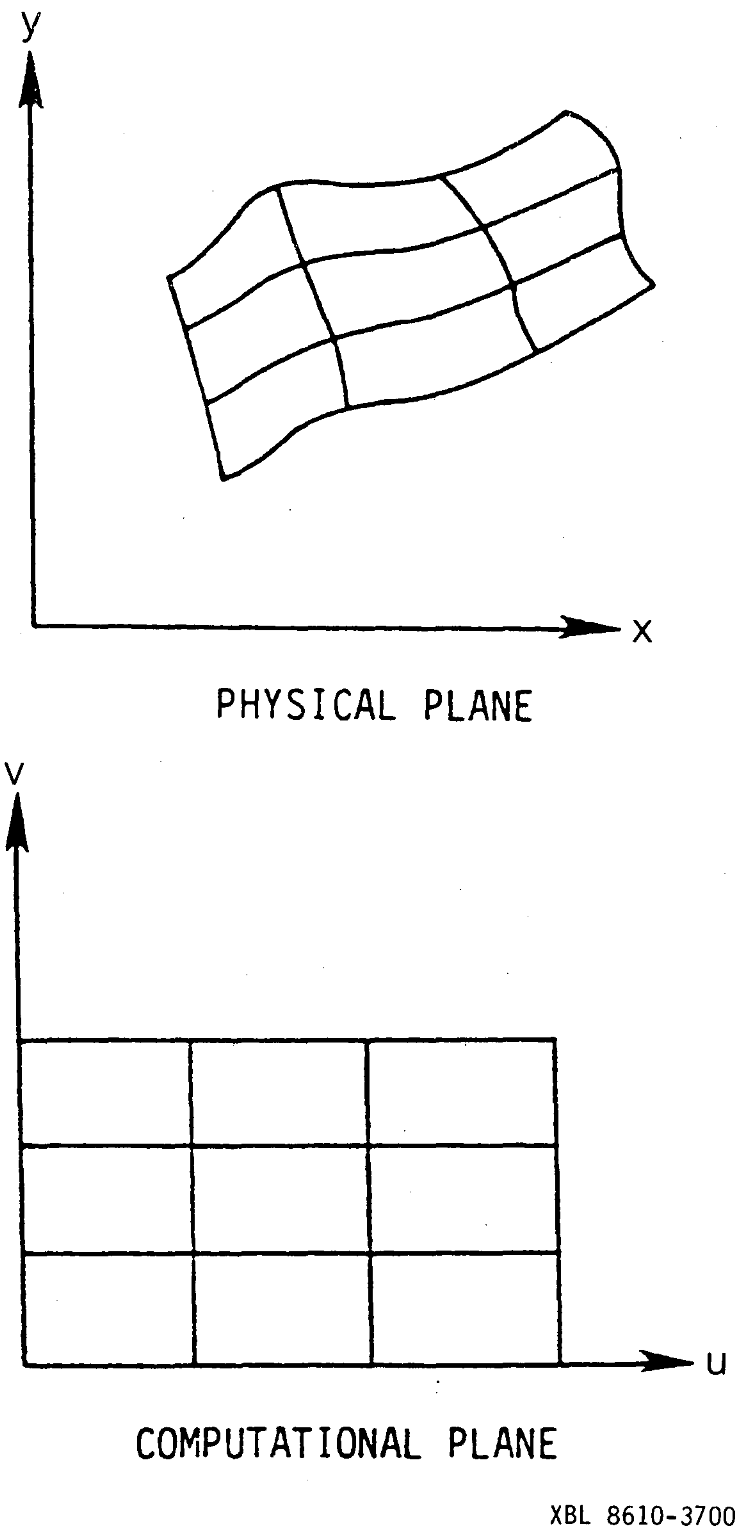


Figure 2.1. Example of Transformation of a Complex Surface to a Rectangle.

space to the $\underset{\sim}{u}$ space is done such that, the boundaries of the region become constant $\underset{\sim}{u}$ lines. The mapping of the interior can be accomplished by minimizing the integral,

$$I = I_s + \lambda\, I_o \tag{2.1}$$

where

$$I_s = \int \left[ (\underset{\sim}{\nabla} u)^2 + (\underset{\sim}{\nabla} v)^2 + (\underset{\sim}{\nabla} w)^2 \right] d\underset{\sim}{x}$$

and

$$I_o = \int \left[ (\underset{\sim}{\nabla} u \cdot \underset{\sim}{\nabla} v)^2 + (\underset{\sim}{\nabla} u \cdot \underset{\sim}{\nabla} w)^2 + (\underset{\sim}{\nabla} v \cdot \underset{\sim}{\nabla} w)^2 \right] J^3\, \underset{\sim}{d}x \quad .$$

Here,

$$\underset{\sim}{\nabla} = \frac{\partial}{\partial x} \underset{\sim}{i} + \frac{\partial}{\partial y} \underset{\sim}{j} + \frac{\partial}{\partial z} \underset{\sim}{k},$$

The Jakobian J, defined as

$$J = \frac{\partial(x,y,z)}{\partial(u,v,w)}$$

is fully given by the determinant

$$J = \begin{vmatrix} x_u & x_v & x_w \\ y_u & y_v & y_w \\ z_u & z_v & z_w \end{vmatrix} \quad , \tag{2.2}$$

where $x_u = \dfrac{\partial x}{\partial u}$ etc. and $\lambda$ is a prescribed weighting parameter.

$I_s$ is called as the *smoothness integral.* The result of minimizing $I_s$ is a grid which is not sensitive to corners or kinks in the boundary data. $I_o$ is called the *orthogonality integral.* $I_o$ is exactly zero when the constant u, v and w lines constructed in the real space are orthogonal to one another. Note that $\lambda$ is similar to but not strictly a Lagrange multiplier because the constraint $I_o = 0$ is not employed. Instead, $I_o$ is made as small as desired by increasing the value of $\lambda$. Hence $I_o$ is a measure of the extent of orthogonality of the coordinate lines. The Jakobian J is a measure of the ratio of corresponding infinitesimal volumes in the $\underset{\sim}{x}$ and $\underset{\sim}{u}$ spaces.

The use of variational principles [such as Equation (2.1)] in describing physical phenomena is quite common in Applied Mechanics, where the quantity to be minimized naturally arises as a measure of potential energy. An advantage of using this variational method is that boundary conditions and incompressibility constraints could be built into the variational statement using the method of Lagrange multipliers. In the present work, only orthogonality has been added to the primary integral $I_s$. When $\lambda = 0$, the solution of Equation (2.1) will generate diffuse grids, and for larger values of $\lambda$, the grid will be fully orthogonal. A mesh with large $\lambda$ invariably conflicts with the requirement of grid refinement, and so only finite values of $\lambda$ are used in practice.

When numerical techniques such as finite differences are used, it is preferable to cast Equation (2.1) in the form of differential equations through variational calculus. The conversion from an integral statement over a finite region to a differential equation applicable pointwise is obtained from the Euler-Lagrange equations of the problem (Greenberg, 1978). As an example in one dimension, the variational problem,

$$\min I = \int F(x,u, \frac{du}{dx})\, dx$$

is equivalent to the Euler-Lagrange equation,

$$\frac{\partial F}{\partial u} - \frac{\partial}{\partial x}\frac{\partial}{\partial u_x} F = 0 \quad ,$$

where F is a functional containing the unknown function u(x). The Euler-Lagrange equations in three dimensions will be the governing equations of grid generation for the present study. In symbolic form, let the inverse problem of Equation (2.1) be stated as,

$$\min I = \int F d\underset{\sim}{u} \tag{2.3}$$

where the complete form of F will be obtained later. The Euler-Lagrange (EL) equations are given as follows, where $x_u = \dfrac{\partial x}{\partial u}$ etc.

$$\left[\frac{\partial}{\partial x} - \frac{\partial}{\partial u}\frac{\partial}{\partial x_u} - \frac{\partial}{\partial v}\frac{\partial}{\partial x_v} - \frac{\partial}{\partial w}\frac{\partial}{\partial x_w}\right] F = 0 \tag{2.4a}$$

$$\left[\frac{\partial}{\partial y} - \frac{\partial}{\partial u}\frac{\partial}{\partial y_u} - \frac{\partial}{\partial v}\frac{\partial}{\partial y_v} - \frac{\partial}{\partial w}\frac{\partial}{\partial y_w}\right] F = 0 \tag{2.4b}$$

$$\left[\frac{\partial}{\partial z} - \frac{\partial}{\partial u}\frac{\partial}{\partial z_u} - \frac{\partial}{\partial v}\frac{\partial}{\partial z_v} - \frac{\partial}{\partial w}\frac{\partial}{\partial z_w}\right] F = 0 \tag{2.4c}$$

and F is treated as $F = F(u,v\ \ldots)$.

$$F = F(u,v,w,x,y,z, \frac{\partial x}{\partial u}, \ldots \frac{\partial z}{\partial w}) \quad .$$

Equations (2.4) constitute an elliptic system of partial differential equations for the unknown variables, x,y,z, and require boundary conditions over the entire flow domain for a solution. These could be of the Dirichlet or Dirichlet-Neumann type. As $\lambda$ is raised more orthogonal grids are generated.

The outline of the rest of the chapter is as follows. The full form of the integrand F (Equation 2.3) is obtained first. The differentiation indicated by Equations (2.4) is evaluated and the terms arranged to form a system of second order, coupled partial differential equations. The discretization rules are described next, to set up the finite-difference equivalent of these equations. The resulting algebraic problem is solved by a Gauss-Seidel scheme. The boundary conditions of the problem are given in detail. Finally, the interpolation rules to extract a coordinate value on the boundary of the real space when a mesh line does not pass through one of the prescribed data points is described.

### 2.2 Derivation of Euler-Lagrange Equations

Complete forms of Equations (2.4) will be obtained here. The solution to these equations provide the inverse transformation from the computational to the physical space. The expression defining F used in Equations (2.4) can be obtained from Equation (2.1) by appropriately interchanging the roles of $\underset{\sim}{x}$ to $\underset{\sim}{u}$ as the independent variables which allows integration to be performed on the computational space. To this end, the following chain rule relationships are useful.

$$\underset{\sim}{\nabla} u = (\underset{\sim}{x}_v \times \underset{\sim}{x}_w)/J$$
$$\underset{\sim}{\nabla} v = (\underset{\sim}{x}_w \times \underset{\sim}{x}_u)/J$$

$$\underset{\sim}{\nabla} w = (\underset{\sim}{x}_u \times \underset{\sim}{x}_v)/J \tag{2.5}$$

Here

$$\underset{\sim}{\nabla} = \underset{\sim}{i}\,\frac{\partial}{\partial x} + \underset{\sim}{j}\,\frac{\partial}{\partial y} + \underset{\sim}{k}\,\frac{\partial}{\partial z} \quad ,$$

the gradient operator and $(\underset{\sim}{i}, \underset{\sim}{j}, \underset{\sim}{k})$ is the unit triad in the $\underset{\sim}{x}$ space. The gradients of u, v and w can be obtained by cyclic permutation in Equation (2.5) and this will be exploited in the derivation of the full equations.

The cross product terms are expanded as below.

$$\underset{\sim}{x}_v \times \underset{\sim}{x}_w = \begin{vmatrix} \underset{\sim}{i} & \underset{\sim}{j} & \underset{\sim}{k} \\ x_v & y_v & z_v \\ x_w & y_w & z_w \end{vmatrix} \quad ,$$

$$\underset{\sim}{x}_w \times \underset{\sim}{x}_u = \begin{vmatrix} \underset{\sim}{i} & \underset{\sim}{j} & \underset{\sim}{k} \\ x_w & y_w & z_w \\ x_u & y_u & z_u \end{vmatrix} \quad , \tag{2.6}$$

and,

$$\underset{\sim}{x}_u \times \underset{\sim}{x}_v = \begin{vmatrix} \underset{\sim}{i} & \underset{\sim}{j} & \underset{\sim}{k} \\ x_u & y_u & z_u \\ x_v & y_v & z_v \end{vmatrix} \quad .$$

Using Equations (2.6), the inverted forms of $(\underset{\sim}{\nabla} u)^2$ and $(\underset{\sim}{\nabla} u \cdot \underset{\sim}{\nabla} v)$ are,

$$(\underset{\sim}{\nabla} u)^2 = \frac{1}{J^2}\left[(y_v\, z_w - z_v\, y_w)^2 + (x_v\, z_w - z_v\, x_w)^2 + (x_v\, y_w - y_v\, x_w)^2\right] \quad ,$$

$$\begin{aligned} \underset{\sim}{\nabla} u \cdot \underset{\sim}{\nabla} v = \frac{1}{J^2}\Big[&(y_w\, z_u - z_w\, y_u)\,(y_v\, z_w - z_v\, y_w) \\ &+ (x_w\, z_u - x_u\, z_w)\,(x_v\, z_w - z_v\, x_w) \\ &+ (x_w\, y_u - y_w\, x_u)\,(x_v\, y_w - y_v\, x_w)\Big] \quad . \end{aligned} \tag{2.7}$$

The indicated differentiation in Equations (2.4) is carried out below by treating F as a function of $u, v, w, x_u, \cdots$ and $z_w$. Note that x, y and z do not appear explicitly in the calculations and so $\frac{\partial F}{\partial x}$, $\frac{\partial F}{\partial y}$ and $\frac{\partial F}{\partial z}$ are identically zero. Using the notation EL for the Euler-Lagrange operator, Equations (2.4) can be restated as, $EL_u(F) = 0$, $EL_v(F) = 0$ and $EL_w(F) = 0$, where the subscripts refer to the component equation. It is enough to derive expressions for $EL_u[(\underset{\sim}{\nabla} u)^2 J]$ and $EL_u[J^4(\underset{\sim}{\nabla} u \cdot \underset{\sim}{\nabla} v)^2]$ and complete the u-equation [i.e., Equation (2.4a)] by rotating indices as u→v→w→u. This will be pursued next.

Equation (2.1) states,

$$\min I = \int G d\underset{\sim}{x} \quad ,$$

where

$$G = \left[ (\nabla u)^2 + (\nabla v)^2 + (\nabla w)^2 \right] + \lambda J^3 \left[ (\nabla u \cdot \nabla v)^2 + (\nabla v \cdot \nabla w)^2 + (\nabla u \cdot \nabla w)^2 \right] \quad .$$

The inverted form of this equation reads,

$$\min I = \int F d\underset{\sim}{u} \quad ,$$

where

$$F = \left[ \sum_u \frac{(\underset{\sim}{x}_v \times \underset{\sim}{x}_w)^2}{J^2} \right] J + \lambda J^4 \left[ \sum_u \frac{(\underset{\sim}{x}_v \times \underset{\sim}{x}_w) \cdot (\underset{\sim}{x}_w \times \underset{\sim}{x}_u)}{J^2} \right] \quad , \qquad (2.8)$$

where the summation sign $\sum$ refers to the addition of terms arising from G, using the rules from Equations (2.6) and (2.7) and the summation index u takes on the symbols u, v and w. In deriving Equation (2.8), the definition of J, i.e.,

$$d\underset{\sim}{u} = \frac{1}{J} d\underset{\sim}{x}$$

has been utilized. As stated above, it is sufficient to evaluate portions of $EL_u(F)$ alone, and obtain the rest by cyclic permutation.

## 2.3 Calculation of $EL_u[J(\nabla u)^2]$

Since

$$\frac{\partial F}{\partial x} = 0 \quad ,$$

$$EL_u = - \frac{\partial}{\partial u} \frac{\partial}{\partial x_u} - \frac{\partial}{\partial v} \frac{\partial}{\partial x_v} - \frac{\partial}{\partial w} \frac{\partial}{\partial x_w} \quad .$$

The complete expression of $(\nabla u)^2$ is given in Equation (2.7).

$$\frac{\partial}{\partial x_u} J(\nabla u)^2 = -\frac{J_{x_u}}{J^2} Du,$$

where

$$Du = (y_v z_w - z_v y_w)^2 + (x_v z_w - z_v x_w)^2 + (x_v y_w - y_v x_w)^2 \quad .$$

$$J_{x_u} = \frac{\partial J}{\partial x_u} = y_v z_w - y_w z_v \quad .$$

Hence,

$$\frac{\partial}{\partial u}\frac{\partial}{\partial x_u} J(\nabla u)^2 = \frac{2}{J^3} J_u (y_v z_w - y_w z_v)\, Du - \frac{Du}{J^2}(y_v z_w - y_w z_v)_u$$
$$- \frac{2(y_v z_w - y_w z_v)}{J^2}[Du]_u$$

Similarly, differentiation of the remaining terms can be carried out.

## 2.4 Calculation of $EL_u[J^4(\nabla u \cdot \nabla v)^2]$

Once again, $\frac{\partial F}{\partial x} = 0$ and it is sufficient to consider the reduced form of $EL_u$, i.e.,

$$EL_u = -\frac{\partial}{\partial u}\frac{\partial}{\partial x_u} - \frac{\partial}{\partial v}\frac{\partial}{\partial x_v} - \frac{\partial}{\partial w}\frac{\partial}{\partial x_w} \quad .$$

$$J^4(\nabla u \cdot \nabla v)^2 = (Duv)^2 = \Big[(y_v z_w - y_w z_v)(y_w z_u - y_u z_w) +$$
$$(x_v z_w - x_w z_v)(x_w z_u - x_u z_w) + (x_v y_w - x_w y_v)\ (x_w y_u - x_u y_w)\Big]$$

$$\frac{\partial}{\partial x_u}(Duv)^2 = 2Duv\left[- z_w(x_v z_w - x_w z_v) - y_w(x_v y_w - x_w y_v)\right]$$

$$\frac{\partial}{\partial u}\frac{\partial}{\partial x_u}(Duv)^2 = 2(Duv)_u\left[- z_w(x_v z_w - x_w z_v) - y_w(x_v y_w - x_w y_v)\right] +$$
$$+ 2Duv\left[- z_w(x_v z_w - x_w z_v) - y_w(x_v y_w - x_w y_v)\right]_u \quad .$$

The next step is to expand each of these terms, and repeat similar calculations for the remaining terms in the Euler-Lagrange operator. Only the final results are given here.

The expanded form of Equation (2.4a) is written as a second order, non-linear partial differential equation as following.

$$\alpha ux \cdot x_{uu} + \alpha vx \cdot x_{vv} + \alpha wx \cdot x_{ww} + \alpha uy \cdot y_{uu} + \alpha vy \cdot y_{vv} + \alpha wy \cdot y_{ww} +$$
$$\alpha uz \cdot z_{uu} + \alpha vz \cdot z_{vv} + \alpha wz \cdot z_{ww} + Ru = 0 \qquad (2.9a)$$

Equation (2.9a) is written in a form convenient for finite difference representation. Ru contains all the mixed derivatives arising from the EL operator. These have been lumped together because their contribution to a selected nodal point is only through its neighbors and not directly on it. This will be seen below. Complete forms of the coefficients in Equation (2.9a) are given in Appendix A. The expanded forms of Equations (2.4b, 2.4c) are symbolically written as the following;

$$\beta ux \cdot x_{uu} + \beta vx \cdot x_{vv} + \beta wx \cdot x_{ww} + \beta uy \cdot y_{uu} + \beta vy \cdot y_{vv} + \beta wy \cdot y_{ww} + \beta uz \cdot z_{uu} + \beta vz \cdot z_{vv} + \beta wz \cdot z_{ww} + Rv = 0 \tag{2.9b}$$

$$\gamma ux \cdot x_{uu} + \gamma vx \cdot x_{vv} + \gamma wx \cdot x_{ww} + \gamma uy \cdot y_{uu} + \gamma vy \cdot y_{vv} + \gamma wy \cdot y_{ww} + \gamma uz \cdot z_{uu} + \gamma vz \cdot z_{vv} + \gamma wz \cdot z_{ww} + Rw = 0 \tag{2.9c}$$

The coefficients in Equations (2.9b) and (2.9c) can be obtained from those in Equation (2.9a) by cyclic permutation of the variables as $x \rightarrow y \rightarrow z \rightarrow x$. This is also explained in Appendix A.

### 2.5 Discretization

A second order, central differencing scheme is employed to approximate both the first and the second derivatives appearing in the governing Equations (2.9a-2.9c). At the boundary, a one-sided difference approximation is used. The following are examples of finite-difference expressions and can be derived from Taylor's series expansion (Anderson et al., 1984). Note that the grid in the transformed space is uniform, and this considerably simplifies the finite-difference formulas.

$$\begin{aligned}
x_{uu} &= \frac{(x_{i+1} + x_{i-1} - 2x_i)_{jk}}{(\Delta u)^2} + O[(\Delta u)^2] \quad , \\
x_{vv} &= \frac{(x_{j+1} + x_{j-1} - 2x_j)_{ik}}{(\Delta v)^2} + O[(\Delta v)^2] \\
x_{ww} &= \frac{(x_{k+1} + x_{k-1} - 2x_k)_{ij}}{(\Delta w)^2} + O[(\Delta u)^2] \\
x_u &= \frac{(x_{i+1} - x_{i-1})_{jk}}{2\Delta u} + O[(\Delta u)^2] \\
x_{uv} &= \frac{(x_{i+1,j+1} - x_{i+1,j-1} - x_{i-1,j+1} + x_{i-1,j-1})_k}{4\Delta u \, \Delta v} + O[(\Delta u)^2, (\Delta v)^2]
\end{aligned} \tag{2.10}$$

The symbol $O(\quad)$ stands for order-of-magnitude, and is also a measure of error when it is dropped in further calculations. The subscripts i, j and k refer to nodal point location in u, v and w directions respectively. It can be seen from Equation (2.10) that all approximations are first order accurate, i.e., have an error of second order. Gradient calculation at the boundaries is performed using a one-sided difference formula, such as,

$$x_u = \frac{(x_2 - x_1)_{jk}}{\Delta u} \quad , \quad \text{when } i = 1 \quad . \tag{2.11a}$$

Equation (2.11) has an error of first order, and can be improved by the formula,

$$x_u = \frac{(4x_2 - x_3 - 3x_1)_{jk}}{2\Delta u} \tag{2.11b}$$

at the expense of increased computation. Assuming L nodal points in the u direction, M in the v direction and N in the w direction, the matrix obtained from the system of equations arising from Equation (2.9) at each nodal point is LMN×LMN for each coordinate x, y and z. Clearly the matrix will be sparse since each node is at most affected by its 26 neighbors, in three dimensions. Since the problem is non-linear, repeated application of a direct method of matrix inversion is not expected to be either efficient or accurate. For this reason, the approach taken circumvents the problem of constructing a matrix, and pursues a fully iterative method for solving the discretized equations.

### 2.6 Gauss-Seidel Iteration

The iteration scheme is constructed as follows. Let $R_x^n$ be the residual of Equation (9a) after the $n^{th}$ iteration. Hence,

$$\begin{aligned} R_x^n = & -2x_{ijk}\left(\frac{\alpha ux}{(\Delta u)^2} + \frac{\alpha vx}{(\Delta v)^2} + \frac{\alpha wx}{(\Delta w)^2}\right) \\ & -2y_{ijk}\left(\frac{\alpha uy}{(\Delta u)^2} + \frac{\alpha vy}{(\Delta v)^2} + \frac{\alpha wy}{(\Delta w)^2}\right) \\ & -2z_{ijk}\left(\frac{\alpha uz}{(\Delta u)^2} + \frac{\alpha vz}{(\Delta v)^2} + \frac{\alpha wz}{(\Delta w)^2}\right) \\ & + \sum_u \sum_x \alpha ux \left(\frac{x_{i+1} + x_{i-1}}{(\Delta u)^2}\right)_{jk} + Ru \end{aligned} \tag{2.12a}$$

In Equation (2.12a), the double summation sign refers to all the terms such as the one shown, arising from Equation (2.9a) and Equations (2.10). For example, $\alpha vx\,(x_{j+1} + x_{j-1})_{ik}/(\Delta v)^2$ would be the second term, and so on. Further, u and x take on the symbols (u,v,w) and (x,y,z) respectively. From Equations (2.9b) and (2.9c) one has the following;

$$\begin{aligned} R_y^n = &- 2x_{ijk}\left(\frac{\beta ux}{(\Delta u)^2} + \frac{\beta vx}{(\Delta v)^2} + \frac{\beta wx}{(\Delta w)^2}\right) \\ &- 2y_{ijk}\left(\frac{\beta uy}{(\Delta u)^2} + \frac{\beta vy}{(\Delta v)^2} + \frac{\beta wy}{(\Delta w)^2}\right) \\ &- 2z_{ijk}\left(\frac{\beta uz}{(\Delta u)^2} + \frac{\beta vz}{(\Delta v)^2} + \frac{\beta wz}{(\Delta w)^2}\right) \\ &+ \sum_u \sum_x \beta ux\frac{(x_{i+1} + x_{i-1})_{jk}}{(\Delta u)^2} + Rv \end{aligned} \tag{2.12b}$$

$$\begin{aligned} R_z^n = &- 2x_{ijk}\left(\frac{\gamma ux}{(\Delta u)^2} + \frac{\gamma vx}{(\Delta v)^2} + \frac{\gamma wx}{(\Delta w)^2}\right) \\ &- 2y_{ijk}\left(\frac{\gamma uy}{(\Delta u)^2} + \frac{\gamma vy}{(\Delta v)^2} + \frac{\gamma wy}{(\Delta w)^2}\right) \\ &- 2z_{ijk}\left(\frac{\gamma uz}{(\Delta u)^2} + \frac{\gamma vz}{(\Delta v)^2} + \frac{\gamma wz}{(\Delta w)^2}\right) \\ &+ \sum_u \sum_x \gamma ux\frac{(x_{i+1} + x_{i-1})_{jk}}{(\Delta u)^2} + Rw \end{aligned} \tag{2.12c}$$

The residuals $R^n$ are treated as functions of x, y and z such that the solution of the Equations (2.9) also form the roots of $R^n$, i.e., reduce $R^n$ to zero. Corrections to previously obtained values of x, y, z are calculated the procedure outlined below. Let

$$R^n = R^n\,(x,y,z)_{ijk} \tag{2.13}$$

Using a Taylor's series expansion up to the first order, one has the following

$$\begin{aligned} R_x^n + A_1\Delta x + B_1\,\Delta y + C_1\,\Delta z &= 0 \\ R_y^n + A_2\Delta x + B_2\Delta y + C_2\Delta z &= 0 \\ R_z^n + A_3\Delta x + B_3\Delta y + C_3\Delta z &= 0 \end{aligned} \tag{2.14}$$

In Equation (2.14), $\Delta x = x_{ijk}^{n+1} - x_{ijk}^{n}$, the correction over a previous value of x, $\Delta y = y_{ijk}^{n+1} - y_{ijk}^{n}$ and $\Delta z = z_{ijk}^{n+1} - z_{ijk}^{n}$. The coefficients are given as,

$$
\begin{aligned}
A_1 &= \frac{\partial R_x^n}{\partial x_{ijk}} = -2\left(\frac{\alpha ux}{(\Delta u)^2} + \frac{\alpha vx}{(\Delta v)^2} + \frac{\alpha wx}{(\Delta w)^2}\right) \\
B_1 &= \frac{\partial R_x^n}{\partial y_{ijk}} = -2\left(\frac{\alpha uy}{(\Delta u)^2} + \frac{\alpha vy}{(\Delta v)^2} + \frac{\alpha wy}{(\Delta w)^2}\right) \\
C_1 &= \frac{\partial R_x^n}{\partial z_{ijk}} = -2\left(\frac{\alpha uz}{(\Delta u)^2} + \frac{\alpha vz}{(\Delta v)^2} + \frac{\alpha wz}{(\Delta w)^2}\right) \\
A_2 &= \frac{\partial R_y^n}{\partial x_{ijR}} = -2\left(\frac{\beta ux}{(\Delta u)^2} + \frac{\beta vx}{(\Delta v)^2} + \frac{\beta wx}{(\Delta w)^2}\right) \\
B_2 &= \frac{\partial R_y^n}{\partial y_{ijk}} = -2\left(\frac{\beta uy}{(\Delta u)^2} + \frac{\beta vy}{(\Delta v)^2} + \frac{\beta wy}{(\Delta w)^2}\right) \\
C_2 &= \frac{\partial R_y^n}{\partial z_{ijk}} = -2\left(\frac{\beta uz}{(\Delta u)^2} + \frac{\beta uz}{(\Delta v)^2} + \frac{\beta wz}{(\Delta w)^2}\right) \\
A_3 &= \frac{\partial R_z^n}{\partial x_{ijk}} = -2\left(\frac{\gamma ux}{(\Delta u)^2} + \frac{\gamma vx}{(\Delta v)^2} + \frac{\gamma wx}{(\Delta w)^2}\right) \\
B_3 &= \frac{\partial R_z^n}{\partial y_{ijk}} = -2\left(\frac{\gamma uy}{(\Delta u)^2} + \frac{\gamma vy}{(\Delta v)^2} + \frac{\gamma wy}{(\Delta w)^2}\right) \\
C_3 &= \frac{\partial R_z^n}{\partial z_{ijk}} = -2\left(\frac{\gamma uz}{(\Delta u)^2} + \frac{\gamma vz}{(\Delta v)^2} + \frac{\gamma wz}{(\Delta w)^2}\right)
\end{aligned}
\tag{2.15}
$$

Equation (2.14) can be solved simultaneously for $\Delta x$, $\Delta y$ and $\Delta z$ and the results are as follows.

$$
\begin{aligned}
\Delta x &= \text{Det } x/\text{Det} \\
\Delta y &= \text{Det } y/\text{Det} \\
\Delta z &= \text{Det } z/\text{Det}
\end{aligned}
\tag{2.16}
$$

where,

$$
\text{Det } x = \begin{vmatrix} -R_x & B_1 & C_1 \\ -R_y & B_2 & C_2 \\ -R_z & B_3 & C_3 \end{vmatrix} \quad ,
$$

$$
\text{Det } y = \begin{vmatrix} A_1 & -R_x & C_1 \\ A_2 & -R_y & C_2 \\ A_3 & -R_z & C_3 \end{vmatrix} \quad ,
$$

$$
\text{Det } z = \begin{vmatrix} A_1 & B_1 & -R_x \\ A_2 & B_2 & -R_y \\ A_3 & B_3 & -R_z \end{vmatrix}
$$

and

$$
\text{Det} = \begin{vmatrix} A_1 & B_1 & C_1 \\ A_2 & B_2 & C_2 \\ A_3 & B_3 & C_3 \end{vmatrix} \quad .
$$

The values of x, y and z are updated by the formula,

$$x_{ijk}^{n+1} \rightarrow x_{ijk}^{n} + \Delta x \ ,$$
$$y_{ijk}^{n+1} \rightarrow y_{ijk}^{n} + \Delta y$$

and

$$z_{ijk}^{n+1} \rightarrow z_{ijk}^{n} + \Delta z \ . \tag{2.17}$$

## 2.7 Boundary Conditions

Equations (2.9a) - (2.9c) constitute a system of second order, elliptic partial differential equations and require the values of x, y and z (Dirichlet) or their derivatives (Neumann) prescribed on all the boundaries. In three dimensions, this has to be done on six surfaces and contact areas, which will be equivalently transformed onto the bounding planes of a rectangular parallelepiped with the contact areas appearing square. Dirichlet boundary conditions are easy to apply, since the solution is already prescribed and no correction is necessary. Neumann conditions are more involved because they require calculation of the normal derivative. Neumann conditions are required whenever the orthogonality of the mesh lines need to be improved. The boundaries of the physical domain are constant u, v or w surfaces, and these conditions permit the mesh lines to be exactly at right angles at least on the boundary of the flow domain. A typical example of a Dirichlet-Neumann condition applied to six sides of a flow region is given below.

**u = constant.**

x is prescribed,

$$\frac{\partial v}{\partial n} = 0 \text{ determines } y \ , \tag{2.18a}$$
$$\frac{\partial w}{\partial n} = 0 \text{ determines } z \ .$$
$$\frac{\partial v}{\partial n} = \underset{\sim}{\nabla} v \cdot \underset{\sim}{n} \quad ,$$

where $\underset{\sim}{n}$ is the unit normal on the u = constant, surface. By definition of the gradient operator, $\underset{\sim}{n} = \underset{\sim}{\nabla} u / | \underset{\sim}{\nabla} u |$ and so, $\frac{\partial v}{\partial n} = 0$ imples that $\underset{\sim}{\nabla} v \cdot \underset{\sim}{\nabla} u = 0$. Using Equations (2.5),

$$(\underset{\sim}{x}_v \times \underset{\sim}{x}_w) \cdot (\underset{\sim}{x}_w \times \underset{\sim}{x}_u) = 0.$$

From Equations (2.6),

$$\begin{gathered}(y_v z_w - z_v y_w)(y_w z_u - z_w y_u) + \\ (x_v z_w - x_w z_v)(x_w z_u - x_u z_w) + \\ (x_v y_w - y_v x_w)(x_w y_u - x_u y_w) = 0.\end{gathered}$$

This can be solved for $y_u$, from which the y boundary condition follows as

$$\begin{gathered}y_1 = y_2 - \Delta u \cdot y_u(i{=}1) \\ y_L = y_{L-1} + \Delta u \cdot y_u(i{=}L).\end{gathered}$$

Similarly, $\dfrac{\partial w}{\partial n} = 0$ leads to $(\underset{\sim}{x}_u \times \underset{\sim}{x}_v) \cdot (\underset{\sim}{x}_v \times \underset{\sim}{x}_w) = 0$, from which an expression for $z_u$ can be obtained.

**v = constant.**

y is prescribed

$$\begin{aligned}&\frac{\partial u}{\partial n} = 0 \text{ determines x.} &&(2.18b)\\ &\frac{\partial w}{\partial n} = 0 \text{ determines z.}\\ &\frac{\partial u}{\partial n} = \underset{\sim}{\nabla} u \cdot \underset{\sim}{n}.\\ &\underset{\sim}{n} = \underset{\sim}{\nabla} v / | \underset{\sim}{\nabla} v | .\end{aligned}$$

Hence,

$$(\underset{\sim}{x}_v \times \underset{\sim}{x}_w) \cdot (\underset{\sim}{x}_w \times \underset{\sim}{x}_u) = 0$$

determines $x_v$ and subsequently x. Similarly

$$\frac{\partial w}{\partial n} = \underset{\sim}{\nabla} w \cdot \frac{\underset{\sim}{\nabla} v}{| \underset{\sim}{\nabla} v |} = 0$$

leads to,

$$(\underset{\sim}{x}_u \times \underset{\sim}{x}_v) \cdot (\underset{\sim}{x}_w \times \underset{\sim}{x}_u) = 0 \quad ,$$

which determines $z_v$ and hence z.

**w = constant.**

z is prescribed.

$$\frac{\partial u}{\partial n} = 0 \text{ determines x.} \tag{2.18c}$$
$$\frac{\partial v}{\partial n} = 0 \text{ determines y.}$$

Since $\underset{\sim}{n}$ for this surface is defined as $\underset{\sim}{\nabla} w / |\underset{\sim}{\nabla} w|$, $\frac{\partial u}{\partial n} = 0$ leads to, $(\underset{\sim}{x}_v \times \underset{\sim}{x}_w) \cdot (\underset{\sim}{x}_u \times \underset{\sim}{x}_v) = 0$, which determines $x_w$ and hence x. Further, $\frac{\partial v}{\partial n} = 0$ requires, $(\underset{\sim}{x}_w \times \underset{\sim}{x}_u) \cdot (\underset{\sim}{x}_u \times \underset{\sim}{x}_v) = 0$ which determines $y_w$ and hence y. Complete forms of Equations (2.18) are given in Appendix B.

The development given above can be reduced to two dimensional regions, either by making the z dimension long, or setting $\frac{\partial}{\partial w} = 0$, except for $z_w$ which is unity. However this is tedious and a separate development of the equations only for two dimensions is given in Appendix C.

### 2.8 Interpolation on a Triangular Grid

Fracture data consists of a typical distribution of nodal points at which the elevation of each of the fracture surfaces is specified. An interpolation scheme for the elevation at points other than the nodes can be developed by constructing triangular elements on the grid. A triangle, as opposed to a rectangular can be expected to eliminate a systematic bias in the interpolation error. This is a unique feature in three dimensions, and does not have a counterpart in two dimensions. Interpolation on a rectangle can however be accomplished unambiguously by using internal nodes.

When two of the three coordinates x, y and z are determined using Equations (2.18), the third one (marked as "specified" in Equations (2.18)) can be obtained using fracture data at the nodes followed by interpolation. The first step towards this end is to identify the smallest triangle bounding the point at which the third coordinate is desired. For definiteness, let (x,y) be given (say from Equations (2.18)) and z is only prescribed pointwise. The value of z at (x,y) can be obtained by linear interpolation using shape functions (Zienkiewicz, 1979).

Let P be a point in triangle 1-2-3 (Figure 2.2), at which the value of z is desired. The values of (x,y,z) are fully known at points 1, 2 and 3 and P is defined as (x,y). The shape functions relative to P are,

$$\begin{aligned} N_1 &= (a_1 + b_1\,x + c_1 y)/2\Delta \\ N_2 &= (a_2 + b_2\,x + c_2 y)/2\Delta \\ N_3 &= (a_3 + b_3\,x + c_3 y)/2\Delta \end{aligned} \tag{2.19}$$

Further,

$$\begin{array}{lll} a_1 = x_2y_3 - x_3y_2 & b_1 = y_2 - y_3 & c_1 = x_3 - y_2 \;, \\ a_2 = x_3y_1 - x_1y_3 & b_2 = y_3 - y_1 & c_2 = x_1 - x_3 \;, \\ a_3 = x_1y_2 - x_2y_1 & b_3 = y_1 - y_2 & c_3 = x_2 - x_1 \;, \end{array}$$

and $\Delta$ is the area of the triangle 1-2-3. Then

$$z(P) = \sum_{i=1}^{3} N_i z_i \quad . \tag{2.20}$$

The area of the triangle can be calculated from the formula,

$$\Delta = \frac{1}{2}\begin{vmatrix} 1 & x_1 & y_1 \\ 1 & x_2 & y_2 \\ 1 & x_3 & y_3 \end{vmatrix} \tag{2.21}$$

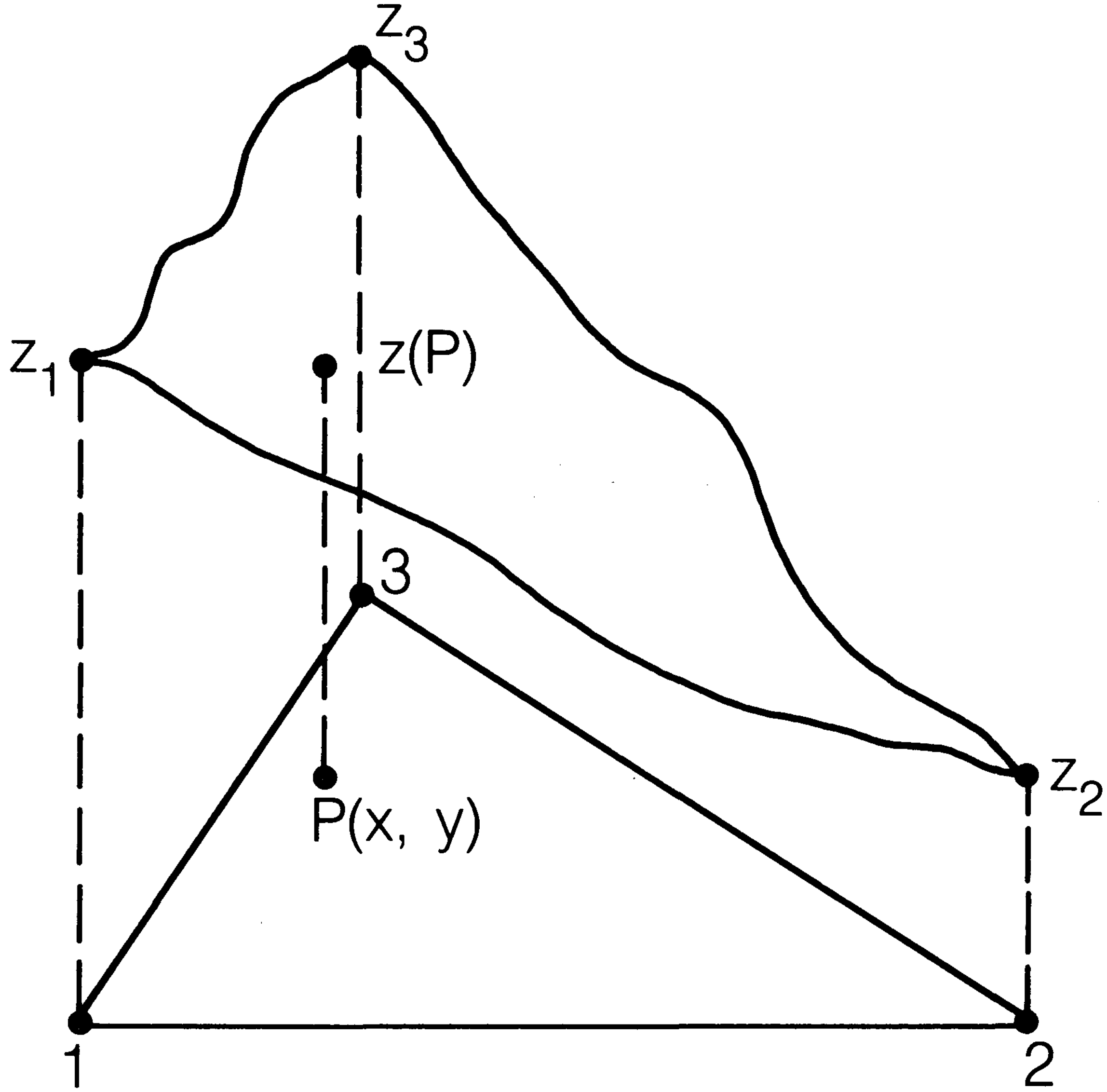


XBL 8610-3703

Figure 2.2. Interpolation on a Triangular Grid.

## 3.0 CALCULATION OF FLUID FLOW

The primary thrust of this work is to replace Darcy's law of fluid motion as a constitutive relationship by the complete momentum equations of flow based on Newton's second law. These are the Navier-Stokes' equations, (Schlichting, 1979), and along with the equation of conservation of mass, determine every state of flow, whether laminar or turbulent, for a wide class of fluids. (Water, air and oil certainly fall in this class.) In this work, the flow is taken as steady and incompressible.

### 3.1 Statement of Equations Governing Fluid Flow

In coordinate-free form, the governing equations are the following.

$$\underset{\sim}{u} \cdot \underset{\sim}{\nabla} \underset{\sim}{u} = - \underset{\sim}{\nabla} p/\rho + \nu \nabla^2 \underset{\sim}{u} \qquad \text{(momentum)} \tag{3.1}$$

$$\underset{\sim}{\nabla} \cdot \underset{\sim}{u} = 0 \qquad \text{(continuity)} \tag{3.2}$$

In three dimensions, there are three components for Equation (3.1) while Equation (3.2) is a scalar equation. $\underset{\sim}{u}$ is the velocity vector ( $u_1$, $u_2$, $u_3$) in the three coordinate directions chosen for study, and p is the total (hydrostatic + dynamic) pressure. $\nu$ and $\rho$ are the kinematic viscosity and density of the fluid, respectively. Equations (3.1) relate the applied forces on a fluid element (namely, pressure and viscous forces) to its acceleration (the left side of the equation), as given by Newton's law of motion. Equation (3.2) states that the flow is divergence free which arises from requiring that the amount of fluid stored in a fixed volume is invariant with time. $\underset{\sim}{\nabla}$ is the usual gradient operator in an orthogonal coordinate system (e.g., $= (\frac{\partial}{\partial x}, \frac{\partial}{\partial y}, \frac{\partial}{\partial z})$)

Let $u_m$ be a velocity scale, h a distance scale and the Reynolds number, $Re = u_m \frac{h}{\nu}$. When the scales are properly chosen, Re is as measure of the ratio of inertial to viscous forces. The pressure scale naturally arises as $\rho\, u_m^2$ from dimensional analyses. The dimensionless forms of Equations (3.1) and (3.2), scaled by these quantities are the following

$$\underset{\sim}{u} \cdot \underset{\sim}{\nabla} \underset{\sim}{u} = -\underset{\sim}{\nabla} p + \frac{1}{Re} \underset{\sim}{\nabla}^2 \underset{\sim}{u} \tag{3.3a}$$

$$\underset{\sim}{\nabla} \cdot \underset{\sim}{u} = 0 \tag{3.3b}$$

The numerical scheme required to solve Equations (3.3) depends on the value of Re. For large values of the Reynolds number (>100), the viscous forces are small, except in regions close to a solid boundary (called boundary layers) and special treatment is usually required. At much higher values, the flow becomes turbulent and the problem either must be treated as unsteady or one with a microstructure. The scope of the present work restricts the Reynolds the number to small values (<50), where the viscous effects are felt uniformly in the flow field. The numerical scheme appropriate for this purpose will be described here.

The two primary difficulties in solving Equations (3.3) are, (a) the non-linear term $\underset{\sim}{u} \cdot \underset{\sim}{\nabla} \underset{\sim}{u}$, Equation (3.3a) and (b) the treatment of incompressibility, Equation (3.3b). The non-linearity causes the matrix equations arising from the numerical approximation to be unsymmetric and to lose diagonal dominance. Since a non-linear problem requires necessarily an iterative solution, the lack of diagonal dominance is likely to provoke divergence of the solution procedure. Special treatment is required to overcome this. The difficulty in using Equation (3.3b) is more fundamental than this. If Equations (3.3a) are solved for the components of $\underset{\sim}{u}$, then Equation (3.3b) must be solved for pressure. However, Equation (3.3b) does not contain the pressure term explicitly. Hence, any iterative scheme or a successive approach, e.g., solution of solving for velocity first followed by pressure can be expected to fail. Specialized methods have been developed to circumvent this problem, each of which depends on the problem to be solved. Two of these are the penalty function method (Carey and Oden, 1983) and the SIMPLE procedure (Patankar, 1980). In the present study, a third approach which uses a Poisson equation of pressure has been used, because it has the following advantages.

1. It identifies pressure as one of the basic variables, instead of eliminating it, as in the penalty function approach.

2. It can be generalized to non-orthogonal coordinate systems, unlike the SIMPLE procedure.

3. It can handle boundary conditions involving specified pressure at the inlet and exit location of the flow domain.

It has the drawback that the source terms in the pressure equation tend to be long and cumbersome, especially in a generalized coordinate system. The accuracy of the overall solution depends on the accuracy of the approximation of these source terms. The Poisson equation of pressure can be derived by taking the divergence of Equation (3.3a). This results in the following.

$$\nabla^2 p = Sp \tag{3.4}$$

where the full form of Sp is given later. Equation (3.4) is used to replace Equation (3.3b) in this work. One final adjustment is made in Equation (3.3a). Because $\underset{\sim}{\nabla} \cdot \underset{\sim}{u} = 0$, $\underset{\sim}{u} \cdot \underset{\sim}{\nabla} \underset{\sim}{u}$ can also be written as $\underset{\sim}{\nabla} \cdot \underset{\sim}{u}\,\underset{\sim}{u}$, which is known as the *conservative* form. The form $\underset{\sim}{\nabla} \cdot \underset{\sim}{u}\,\phi$, for scalar or vector $\phi$, can represent conservation of mass ($\phi = 1$), momentum ($\phi = \underset{\sim}{u}$) or energy ($\phi =$ T, temperature) over a finite flow region (Anderson et al., 1984). The governing equations are hence, the following.

$$\underset{\sim}{\nabla} \cdot \underset{\sim}{u}\,\underset{\sim}{u} = -\,\underset{\sim}{\nabla} p + \frac{1}{Re} \nabla^2 \underset{\sim}{u} \tag{3.5a}$$

$$\nabla^2 p = Sp \tag{3.5b}$$

## 3.2 Boundary Conditions

The appearance of the Laplacian operator ($\nabla^2$) in Equations (3.5) makes each of the equations elliptic, and accordingly requires boundary conditions for both $\underset{\sim}{u}$ and p over the entire flow domain. In contrast, parabolic flow solvers which only require initial conditions along a flow direction to perform the calculation. Boundary-layer flow is an example which can be solved as an initial-boundary value problem. The objective of this study is to look at flows driven by a prescribed pressure drop. Hence the following conditions will apply.

$$\begin{aligned} &\text{Inlet,} \quad p = P, \quad \text{prescribed,} \\ &\text{Exit,} \quad p = 0. \end{aligned} \tag{3.6a}$$

On all solid surfaces of the rock, the no-slip condition is imposed, i.e.,

$$\underset{\sim}{u} = 0 \quad \text{on the walls.} \tag{3.6b}$$

When the fracture is subjected to a given pressure difference, the quantity of flow in the fracture channel becomes a variable, and under suitable conditions (such as a large number of contact areas between the mating faces of the rock), the flow could be zero. However, the distribution of velocity on the inlet plane must be prescribed, up to one undetermined factor, which in turn is evaluated from the mean flow in the fracture. As an example,

$$\underset{\sim}{u} = (\bar{u}, 0, 0) \quad \text{at inlet} \tag{3.6c}$$

where $\bar{u}$ is mean velocity in the fracture. The exit conditions are more ambiguous and in this work, the following gradient condition is recommended, because it is expected to influence the upstream solution by a only a marginal amount (Peyret and Taylor, 1983).

$$\underset{\sim}{\nabla} \underset{\sim}{u} \cdot \underset{\sim}{n} = 0 \quad \text{at exit} \tag{3.6d}$$

The pressure boundary condition on the solid walls is derived by combining Equation (3.5a) with Equation (3.6b), leading to,

$$\underset{\sim}{\nabla} p = \frac{1}{Re} \nabla^2 \underset{\sim}{u} \tag{3.6e}$$

There is no difficulty in applying these constraints. In some examples given in Chapter 4, Equations (3.6c) and (3.6d) have been replaced by the periodicity condition,

$$\underset{\sim}{u} \, (x + L, y, z) = \underset{\sim}{u} \, (x,y,z) \tag{3.7}$$

Hence, when Equation 3.7 is used, the flow past a step is also the solution for flow past a series of identical steps, located a distance L apart.

The specification of pressure as as boundary condition (Equation 3.6a) leaves the mean velocity as a dependent variable of the problem, as noted above. In order to examine flow velocity as a function of pressure drop, a new velocity scale $u_m$ is required in the definition of Reynolds number, related to the driving potential of the problem. One such scale is, $u_m = \sqrt{P/\rho}$ where $\rho$ is the total pressure drop. For fully developed flow in a parallel channel of aperture 2b and length L, $u_m$ is related to $\overline{u}$, the mean velocity in the channel by the formula,

$$\begin{aligned}\overline{u} &= \frac{1}{2b}\int_0^{2b} u\,dz \\ &= \frac{1}{3}\left(\frac{u_m b}{\nu}\right)\left(\frac{b}{L}\right)u_m\end{aligned} \tag{3.8}$$

based on the "cubic law",

$$u = \frac{1}{\mu}\,\frac{\Delta P}{L}\,z(z-2b).$$

The Reynolds number $\overline{Re} = \dfrac{\overline{u}b}{\nu}$ is given by,

$$\overline{Re} = \frac{1}{3}\,Re_m^2\,\frac{b}{L} \tag{3.9}$$

where $Re_m = u_m b/\nu$. In a porous medium, $\overline{Re}$ is usually smaller than unity, and in a fracture, it can take values around unity. Typical values of $Re_m$ are then given by,

$$Re_m \approx \sqrt{3L/b} \tag{3.10}$$

For $L/b \approx 10^2$, $Re_m \approx 17$, based on Equation 3.10.

The rest of the chapter will deal with complete statement of the governing equations and the discretization procedure used in this work.

### 3.3 Expanded Form of Governing Equations

The formulation presented above has been tested for a wide range of flows in Cartesian geometries. The mathematical problem obtained by expanding Equations (3.5) is given as follows:

$$\begin{aligned}\frac{\partial}{\partial x}u_1^2 + \frac{\partial}{\partial y}u_1u_2 + \frac{\partial}{\partial z}u_1u_3 &= -\frac{\partial p}{\partial x} + \frac{1}{Re}\nabla^2 u_1,\\ \frac{\partial}{\partial x}u_1u_2 + \frac{\partial}{\partial y}u_2^2 + \frac{\partial}{\partial z}u_2u_3 &= -\frac{\partial p}{\partial y} + \frac{1}{Re}\nabla^2 u_2,\\ \frac{\partial}{\partial x}u_1u_3 + \frac{\partial}{\partial y}u_2u_3 + \frac{\partial}{\partial z}u_3^2 &= -\frac{\partial p}{\partial z} + \frac{1}{Re}\nabla^2 u_3,\end{aligned} \tag{3.11}$$

$$\nabla^2 p = Sp,$$

where

$$\nabla^2 = \frac{\partial^2}{\partial x^2} + \frac{\partial^2}{\partial y^2} + \frac{\partial^2}{\partial z^2} \ .$$

The source term in the pressure equation is given as,

$$Sp = \frac{1}{Re} \nabla^2 D - \left[ \frac{\partial}{\partial x} (\underset{\sim}{u} \cdot \underset{\sim}{\nabla} u_1) + \frac{\partial}{\partial y} (\underset{\sim}{u} \cdot \underset{\sim}{\nabla} u_2) + \frac{\partial}{\partial z} (\underset{\sim}{u} \cdot \underset{\sim}{\nabla} u_3) \right], \quad (3.12)$$

where

$$D = \underset{\sim}{\nabla} \cdot \underset{\sim}{u} = \frac{\partial u_1}{\partial x} + \frac{\partial u_2}{\partial y} + \frac{\partial u_3}{\partial z} \ .$$

Even though $D = 0$ for incompressible flow, an iterative scheme employing Equations (3.11) may not reach this limit until convergence and it must be retained in the calculation of Sp. Further, the inclusion of D serves to "correct" the pressure field which in turn will annihilate the mass sources (or sinks) in the computed flow field. The boundary conditions for flow and pressure are,

$$\begin{array}{ll} \underset{\sim}{u} = 0 & \text{on solid walls,} \\ p=1 & \text{at inlet, when the velocity scale } u_m \text{ is } \sqrt{P/\rho}\ , \\ p=0 & \text{at exit,} \\ \dfrac{\partial p}{\partial y} = \dfrac{1}{Re}\dfrac{\partial^2 u_2}{\partial y^2} & \text{on solid walls.} \end{array} \quad (3.13a)$$

The gradient boundary condition on the exit plane can be derived from Equation (3.6d) as,

$$\frac{\partial \underset{\sim}{u}}{\partial x} = 0 \quad (3.13b)$$

The system of Equations (3.11-3.13) do not apply when grid transformation is used to map a geometrically complex flow domain into one which can be described easily by Cartesian coordinates. In this case, these equations need to be transformed simultaneously (using chain rule) to a "generalized coordinate system", which is fully describable by its "metric derivatives". (A metric derivative gives the rate of movement of the grid lines in the transformed space relative to its magnitude in the physical space.) Such a coordinate system can be constructed in several ways, and one such method is described in Chapter 2. This transformed grid is central to the flow calculation and steps involved in this process are summarized here.

1. The numerically constructed grid is also the "natural coordinate system" for the flow geometry, because the fracture viewed through the grid appears regular (planar, for the present work).

2. The metric derivatives which quantify the grid layout appear in the flow equations written in terms of the generalized coordinates. The procedure given in Chapter 2 enables one to calculate these coefficients with a high degree of accuracy.

3. The truncation error in the numerical solution of the flow field is proportional to the skewness of the grid lines. The method described in Chapter 2 allows for systematic reduction of skewness by increasing the orthogonality coefficient.

4. The regularization of fracture geometry (via transformation) permits easy application of the flow boundary conditions directly on the boundary, without resorting to interpolation. The choice of a square grid in the transformed space makes finite-differencing rules algebraically simple. Grid refinement can be accomplished within the framework of grid generation, when required.

The Navier-Stokes' equations in a generalized coordinate system $(\xi,\eta,\gamma)$ are given below. Flow calculation proceeds by identifying (u,v,w) (from Chapter 2) as one choice of $(\xi,\eta,\gamma)$. The equations are in the conservative form (Anderson et al., 1984).

$$\frac{\partial}{\partial \xi}\left\{ J[\xi_x\,(\underset{\sim}{E}_i - \underset{\sim}{E}_v) + \xi_y\,(\underset{\sim}{F}_i - \underset{\sim}{F}_v) + \xi_z\,(\underset{\sim}{G}_i - \underset{\sim}{G}_v)] \right\}$$
$$+ \frac{\partial}{\partial \eta}\left\{ J[\eta_x(\underset{\sim}{E}_i - \underset{\sim}{E}_v) + \eta_y(\underset{\sim}{F}_i - \underset{\sim}{F}_v) + \eta_z(\underset{\sim}{G}_i - \underset{\sim}{G}_v)] \right\}$$

$$+ \frac{\partial}{\partial \gamma} \left\{ J \left[ \gamma_x \left( \underset{\sim}{E}_i - \underset{\sim}{E}_v \right) + \gamma_y \left( \underset{\sim}{F}_i - \underset{\sim}{F}_v \right) + \gamma_z \left( \underset{\sim}{G}_i - \underset{\sim}{G}_v \right) \right] \right\} = 0$$

where,

$$\begin{aligned}
\underset{\sim}{E}_i &= (u_1, u_1^2 + p,\ u_1u_2,\ u_1u_3), \\
\underset{\sim}{E}_v &= (0, \tau_{xx}, \tau_{xy}, \tau_{xz}), \\
\underset{\sim}{F}_i &= (u_2,\ u_1u_2,\ u_2^2 + p,\ u_2u_3), \\
\underset{\sim}{F}_v &= (0, \tau_{xy},\ \tau_{yy},\ \tau_{yz}), \\
\underset{\sim}{G}_i &= (u_3,\ u_1u_3,\ u_2u_3,\ u_3^2 + p) \quad \text{and} \\
\underset{\sim}{G}_v &= (0, \tau_{xz},\ \tau_{yz},\ \tau_{zz}).
\end{aligned} \tag{3.15}$$

Further,

$$\begin{aligned}
\tau_{xx} &= \frac{2}{3Re} \Big[ 2(\xi_x\, u_{1\xi} + \eta_x\, u_{1\eta} + \gamma_x\, u_{1\gamma}) - (\xi_y u_{2\xi} + \eta_y\, u_{2\eta} + \gamma_y\, u_{2\gamma}) - \\
&\qquad (\xi_z u_{3\xi} + \eta_z\, u_{3\eta} + \gamma_z\, u_{3\gamma} \Big] \\
\tau_{yy} &= \frac{2}{3Re} \Big[ 2(\xi_y\, u_{2\xi} + \eta_y\, u_{2\eta} + \gamma_y\, u_{2\gamma}) - (\xi_x\, u_{1\xi} + \eta_x\, u_{1\eta} + \gamma_x\, u_{1\gamma}) - \\
&\qquad (\xi_z\, u_{3\xi} + \eta_z\, u_{3\eta} + \gamma_z\, u_3\gamma) \Big] \\
\tau_{zz} &= \frac{2}{3Re} \Big[ 2(\xi_z\, u_{3\xi} + \eta_z\, u_{3\eta} + \gamma_z\, u_{3\gamma}) - \gamma_x\, u_{1\gamma}) - \\
&\qquad (\xi_y\, u_{2\xi} + \eta_y\, u_{2\eta} + \gamma_y\, u_{2\gamma}) \Big] \\
\tau_{xy} &= \frac{1}{Re} \Big[ \xi_y\, u_{1\xi} + \eta_y\, u_{1\eta} + \gamma_y\, u_{1\gamma} + \xi_x\, u_{2\xi} + \eta_x\, u_{2\eta} + \gamma_x\, u_{2\gamma} \Big] \\
\tau_{xz} &= \frac{1}{Re} \Big[ \xi_z\, u_{1\xi} + \eta_z\, u_{1\eta} + \gamma_z\, u_{1\gamma} + \xi_x\, u_{3\xi} + \eta_x\, u_{3\eta} + \gamma_x\, u_{3\gamma} \Big] \\
\tau_{yz} &= \frac{1}{Re} \Big[ \xi_z\, u_{2\xi} + \eta_z\, u_{2\eta} + \gamma_z\, u_{2\gamma} + \xi_y\, u_{3\xi} + \eta_y\, u_{3\eta} + \gamma_y\, u_{3\gamma} \Big]
\end{aligned} \tag{3.16}$$

The first of the equations in (3.14) is the continuity equation, and for reasons mentioned earlier, will be replaced by the Poisson equation of pressure, as given below.

$$\begin{aligned}
&\frac{\partial}{\partial \xi} \Big[ J\, (\xi_x p_1 + \xi_y p_2 + \xi_z p_3) \Big] + \frac{\partial}{\partial \eta} \Big[ J(\eta_x p_1 + \eta_y p_2 + \eta_z p_3) \Big] + \\
&\qquad \frac{\partial}{\partial \gamma} \Big[ J(\gamma_x p_1 + \gamma_y p_2 + \gamma_z p_3) \Big] = - JS_p^T \quad ,
\end{aligned} \tag{3.17}$$

where,

$$\begin{aligned}
p_1 &= \xi_x p_\xi + \eta_x p_\eta + \gamma_x p_\gamma \quad , \\
p_2 &= \xi_y p_\xi + \eta_y p_\eta + \gamma_y p_\gamma \quad ,
\end{aligned}$$

$$p_3 = \xi_z p_\xi + \eta_z p_\eta + \gamma_z p_\gamma \tag{3.18}$$

and

$$S_p^T = (\underset{\sim}{u} \cdot \nabla u_1 - \nabla^2 u_1)_1 + (\underset{\sim}{u} \cdot \nabla u_2 - \nabla^2 u_2)_2$$
$$+ (\underset{\sim}{u} \cdot \nabla u_3 - \nabla^2 u_3)_3 \quad . \tag{3.19}$$

In Equation (3.19), the notation $(\ )_i$, $i = 1,2,3$ is the same as in Equation (3.18). The gradient operator in the transformed space is given as,

$$\nabla \phi = (\phi_1,\ \phi_2,\ \phi_3) \qquad \text{with}$$
$$\phi_1 = \xi_x \phi_\xi + \eta_x \phi_\eta + \gamma_x \phi_\gamma \quad \text{etc.,}$$

as in Equation (3.18), and $\nabla^2 = \nabla \cdot \nabla$. The boundary conditions remain symbolically the same, except that the new definition of $\nabla$ is required to be used and the unit normal on a surface $(\underset{\sim}{n})$ is calculated by the methods of Chapter 2.

The test cases in Chapter 4 cover the following problems.

- Two dimensional flow in a Cartesian geometry.
- Three dimensional flow in a Cartesian geometry.
- Two dimensional flow in a complex geometry, solved in a generalized coordinate system.
- Three dimensional flow in a complex geometry.

### 3.4 Discretization of Governing Equations

The purpose of discretization is to replace the differential equations by algebraic equations applicable at every point of the finite-difference grid in the computational space. This system of equations has been solved in this study by a Gauss-Seidel iterative approach, similar to what has been outlined in Chapter 2. Only the important steps have been presented here.

The use of hybrid differencing for the inertial terms reduces the accuracy of the computation, formally to first order in $\Delta x$, $\Delta y$ and $\Delta z$, which is the grid spacing in x, y and z coordinates. The finite difference approximations are as follows:

$$\frac{\partial \phi}{\partial x} \approx \frac{(\phi_{i+1} - \phi_{i-1})_{jk}}{2\Delta x} \tag{3.20}$$
$$\frac{\partial^2 \phi}{\partial x^2} \approx \frac{(\phi_{i+1} + \phi_{i-1} - 2\phi_i)_{jk}}{\Delta x^2}$$

On the bounding planes, one-sided differencing of second order has been used. This is particularly important in the calculation of the dilatation term $D = \underset{\sim}{\nabla} \cdot \underset{\sim}{u}$, which appears in the source term in the pressure equation. As an example,

$$\left.\frac{\partial \phi}{\partial x}\right|_{i=1} \approx \frac{(4\phi_2 - \phi_3 - 3\phi_1)_{jk}}{2\Delta x} \quad , \tag{3.21}$$

$$\left.\frac{\partial^2 \phi}{\partial x^2}\right|_{i=1} \approx \frac{(-\phi_4 + 4\phi_3 - 5\phi_2 + 2\phi_1)_{jk}}{\Delta x^2}$$

The hybrid differencing scheme for the inertial terms is developed below. We seek an approximation to $\frac{\partial}{\partial x}(u\phi)$, or terms similar to it, where u is velocity in the x direction. Consider the nodal arrangement shown below, where P is the point of interest.

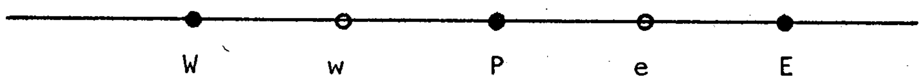


A valid second order approximation is given as,

$$\frac{\partial}{\partial x}(u\phi) \approx \frac{u_e\phi_e - u_w\phi_w}{\Delta x} \quad ,$$

where

$$u_e = (u_E + u_p)/2$$
$$\phi_e = (\phi_E + \phi_p)/2$$

$$u_w = (u_w + u_p)/2$$
$$\phi_w = (\phi_w + \phi_p)/2 \tag{3.22}$$

Experience and preliminary analysis (Hughes, 1979) has shown that Equation (3.22) has only limited validity, and when embedded in an overall iterative solution scheme, causes the velocity field to diverge. This is related to the loss of diagonal dominance of the matrix equations, especially when the grid Peclet number Pe ($= u\Delta x/\nu$) equals two (Patankar, 1980) based on one-dimensional analysis.

The hybrid scheme used in this work calculates the grid Peclet number at every point, and uses Equation (3.22) only if $|\mathrm{Pe}| < 2$. Otherwise, it is replaced by a full (first order) upwind approximation given below.

$$\frac{\partial}{\partial x}(u\phi) \approx \frac{u_e\phi_e - u_w\phi_w}{\Delta x} \quad , \tag{3.23}$$

where

$$\phi_e = \phi_p \text{ if } u_e > 0$$
$$\phi_e = \phi_E \text{ if } u_e < 0$$
$$\phi_w = \phi_W \text{ if } u_w > 0$$
$$\phi_w = \phi_p \text{ if } u_w < 0$$

The need to use Equation (3.23) can be eliminated by grid refinement, which keeps $|\mathrm{Pe}| \leq 2$ and maintains a second order approximation. The use of upwind differencing is justified in this work because:

(a) Only low Reynolds number flows are of interest here. Hence, the numerical diffusion due to Equation (3.23) is only expected to be a small fraction of the total diffusion.

(b) Only steady flows are considered in this work.

(c) There are no expected fronts or discontinuities in flow and pressure, whose resolution is likely to be damaged by upwinding.

The discretization of boundary conditions is given below. When Equation (3.6c) is used as an inflow boundary condition along with Equation (3.6b) as the no-slip requirement on the impermeable side walls, a singularity arises at the corner points (0,0) and (0,b), where b is the aperture. This is circumvented by replacing the equation

$$u = u_m, \quad x = 0, \quad 0 \leq y \leq b,$$

by $u = u_m + \delta, \quad x = 0, \quad 0 < y < b,$ where in two dimensions,

$$\delta = \frac{2u_m}{3N{-}5} \quad \text{and in three dimensions,}$$

$$\delta = \frac{u_m(1{-}\beta)}{\beta}, \quad \beta = \frac{(3N{-}5)(3M{-}5)}{(3N{-}3)(3M{-}3)} .$$

These equations can be derived by requiring that the average value of u is still $u_m$, u is zero on the solid walls and constant everywhere else. This permits application of the no-slip condition on the entire length of the side walls, including the inlet.

The pressure boundary condition at the walls is discretized in the following manner. For a Cartesian system,

$$\frac{\partial p}{\partial y} = \frac{1}{Re}\frac{\partial^2 v}{\partial y^2}$$

on a wall. The left side is approximated by,

$$\frac{\partial p}{\partial y} \approx \frac{(p_2{-}p_1)_{ik}}{\Delta y} \quad \text{, or}$$

$$\approx \frac{(4p_2{-}p_3{-}3p_1)_{ik}}{2\Delta y} .$$

The second higher order formula for the pressure gradient lacks diagonal dominance, and is to be used only after a reasonably converged solution has been obtained. The right side is,

$$\frac{\partial^2 v}{\partial y^2} \approx (v_2{+}v_0{-}2v_1)_{ik} \quad ,$$

where 1 is the wall node and 0 is a ghost node below the wall. From continuity equation, at a wall.

$$\frac{\partial v}{\partial y} \approx \frac{v_2{-}v_0}{2\Delta y} = 0 .$$

Hence,

$$\left.\frac{\partial^2 v}{\partial y^2}\right|_{\text{wall}} \approx \frac{2(v_2)_{ik}}{\Delta y^2}. \tag{3.24}$$

Lastly, when the periodicity boundary conditions are used as in the test cases of Chapter 4, they have been implemented by substituting the following in the nodewise calculations.

$$\phi_{i+1}\Big|_{exit} = \phi_2 \quad ,$$

$$\phi_{i-1}\Big|_{inlet} = \phi_{L-1} \quad , \quad 1 \leq i \leq L. \tag{3.25}$$

A convergence criterion of 0.1 percent has been used in all the iterative calculations presented in Chapter 4.

Principles of discretization outlined above for a Cartesian coordinate system remain unchanged as one moves to any other coordinate system. Appendix D gives the finite-difference formulas arising from discretization of the two dimensional Navier-Stokes' equations in generalized coordinates. Appendix E gives the same in three dimensions.

The finite difference procedure described in Chapters 2 and 3 has been used to solve a test problem of flow past a circular contact area in a square region with uniform flow at inlet. This solution has been compared to that of a finite element calculation given by Muralidhar and Bodvarsson (1987) and the comparison of the two results is presented in Chapter 4.

### 3.5 Calculation of Permeability

For a given pressure drop, the quantity of flow through the fracture is a measure of its permeability. Since the pressure drop is measured by the Reynolds number, the permeability of a rock fracture can be determined from the slope of the mean velocity curve plotted as a function of Reynolds number. A constant slope (i.e., a linear response of $u_m$ to changes in Re) indicates the unimportance of non-linear effects arising from acceleration terms of the Navier-Stokes equations. The equivalent permeability of the fracture is calculated by normalizing this slope by the slope of the $u_m$ – Re curve of a plane parallel channel which has a height equal to the maximum fracture aperture and no contact areas.

### 3.6 Solution of Darcy Equations

Permeability calculated by using Navier-Stokes equations has been compared to that obtained from Darcy's law. The relationship between these two sets of equations is described in Appendix F. In the Darcy calculation, the local permeability distribution is chosen to reflect the variable geometry of the fracture. For example, contact areas are assigned zero permeability, whereas open areas are given unit value. When the aperture is a spatial variable, the local permeability is taken as proportional to the square of aperture, h. Darcy's law as described here, is equivalent to the conventional cubic law, which is based on parabolic flow behavior everywhere in the fracture. The governing equations of Darcy flow are as follows:

$$\nabla \cdot K_l \, h \, \nabla p = 0 \tag{3.26}$$

$$\begin{aligned} &p(0,y) = 1 \\ &p(L,y) = 0 \\ &p_y(x,0) = p_y(x,L) = 0 \end{aligned} \tag{3.27}$$

In Equation (3.26), $K_l$ is the local permeability, p is pressure, $\nabla$ is a two dimensional gradient operator, and L is the region size. The boundary conditions given by Equation (3.27) correspond to a specified pressure drop across the fracture and no flow out of the side boundaries. The average flow through the fracture is then a measure of the Darcy permeability.

Equations (3.26) and (3.27) have also been solved by a finite difference method for prescribed distributions of $K_l$. In a two dimensional channel with varying aperture but no contact points, the equivalent permeability can be obtained from the one-dimensional version of Equation (3.26). It has a closed-form expression given by,

$$K_{eq} = \frac{L}{h(0)\, K_l(0)} \frac{1}{\displaystyle\int_0^L \frac{dx}{K_l(x) h(x)}} \tag{3.28}$$

where L is the channel length, and

$$K_{l(x)} = b(x)^2$$

where b is the local aperture. Clearly from Equation (3.28), $K_{eq} = 0$ when $b = 0$ anywhere in the channel.

# 4. Test Cases

## 4.1 General Remarks

In principle, flow in fractured rocks can be completely determined by solving Navier-Stokes equations in the fluid region, bounded by a geometrically complex surface. However, when one considers the fact that fractures are interconnected and form a network, the Navier-Stokes approach becomes unattractive for the following reasons.

(1) Prescribing the geometry of the flow path is tedious, and in most cases, inaccurate.

(2) The inherent complexity at both small and large scales, i.e., the presence of contact areas and variable aperture on the scale of a single fracture and a network on the scale of a rock, requires a grid which is too large for present day computers to handle.

This necessitates looking for an alternative formulation for calculating flow. One such alternative is Darcy's law, which states that the local flow rate is proportional to the local pressure gradient. This approach has found considerable success in determining flow in a porous media, because the proportionality constant is strictly a function of geometry and the fluid viscosity. This has not been conclusively established for flow in fractures, and even when proportionality of flow and pressure drop is observed, no systematic way is available to predict the proportionality constant (to be called permeability below).

A popular method of determining permeability is to equate it to the square of local fracture aperture. This can be derived from parabolic flow behavior between parallel plates and is called the "cubic law". The equation governing the pressure field based on Darcy's law with permeability determined from the cubic law can be derived from Navier-Stokes equations using a series of simplifying assumptions. This is outlined in Appendix F.

The solution of the complete Navier-Stokes equations can be used to estimate the error involved in calculation of flow rate using cubic law. Secondly, the assumption of linearity in Darcy's law can also be examined by solving the full flow equations. The Navier-Stokes' solver described in the earlier chapters has been developed to fulfill this role of providing a reference answer to flow in single fractures, rather than a tool to deal with practical problems.

Techniques described in Chapters 2 and 3 have been tested for a variety of problems and some examples are given here. Programming and testing of two and three dimensional grid generation, two and three dimensional flow in Cartesian and generalized coordinates has been completed, and several examples are given below.

None of the results is truly grid independent, and no systematic study has been carried out in this regard. However, a limited series of calculation were performed by doubling the total number of grid points and the results were seen to alter by about 5 percent. Hence, the present level of discretization ($\approx$ 10 percent) has been considered to be adequate to reveal the qualitative features of the flow system. A convergence criterion of 0.1 percent has been used for all flow calculations. The grid meets this limit easily, and it is possible to refine the value further, with little increase in computational effort.

In case of the flow field, the region which converges last is that containing the recirculation pattern, where zero velocity is encountered. When this region converges, all other portions of the flow field show convergence to a much lower value ($\approx$ 0.01 percent). Convergence is rapid in flow problems which do not contain a flow structure, as the one mentioned above. These convergence trends are typically independent of Reynolds convergence number, though for a given grid distribution, there is a lower value of Re below which convergence is significantly delayed, and upper value of Re, beyond which the iteration procedure fails to converge. The difficulty at low Reynolds numbers is to be expected, since the rate of movement of information among various parts of the flow domain (which is a function of Re) has already become small. The difficulty at the other extreme of high Reynolds number can be overcome by under-relaxation, to some extent. Ultimately, it must be resolved by grid refinement.

Many of flow fields computed in this study would not converge on a coarser mesh than the one employed (especially in three dimensions). However, error analysis of the finite difference procedure has not been carried out in this work, and no quantitative results are available in this regard. The nonlinear nature of the problem, and its dependence on geometry-related derivatives makes such analysis theoretically intractable.

## 4.2 Examples of Grid Generation

Figure 4.1 shows grid generation in a wavy channel. Figure 4.1a is the physical domain in which the flow process is expected to take place. Figure 4.1b is the transformed domain in which the flow equations are solved. The wavy edges of the channel are now represented by straight edges in the computational plane and there is a one-to-one correspondence between nodal points in Figure 4.1a and 4.1b. Each horizontal line in Figure 4.1b is mapped into a unique wavy line in Figure 4.1a, which constitutes the grid system in the physical domain. The boundary conditions for this problem are prescribed end points for each coordinate line (i.e., Dirichlet BC) and along with the symmetry of the channel, the vertical lines remain undistorted during the transformation. Each of the lines in the physical plane is the contour on which the newly generated coordinates has constant values. The grid generation procedure in Chapter 2 starts with the regular domain (as in Figure 4.1b) and calculates the location of each nodal point in the physical geometry, subject to the boundary shapes as constraint. Since flow is computed in the regularized geometry, it is only this inverse transformation law which is of interest. Figure 4.2 shows grid generation in the same wavy channel considered above. However, orthogonality has been introduced in the calculation, both in the interior ($\lambda = 2$) and at the boundary (Neumann conditions). This requires the gradient of the grid line in the physical domain be prescribed, and hence makes the location itself

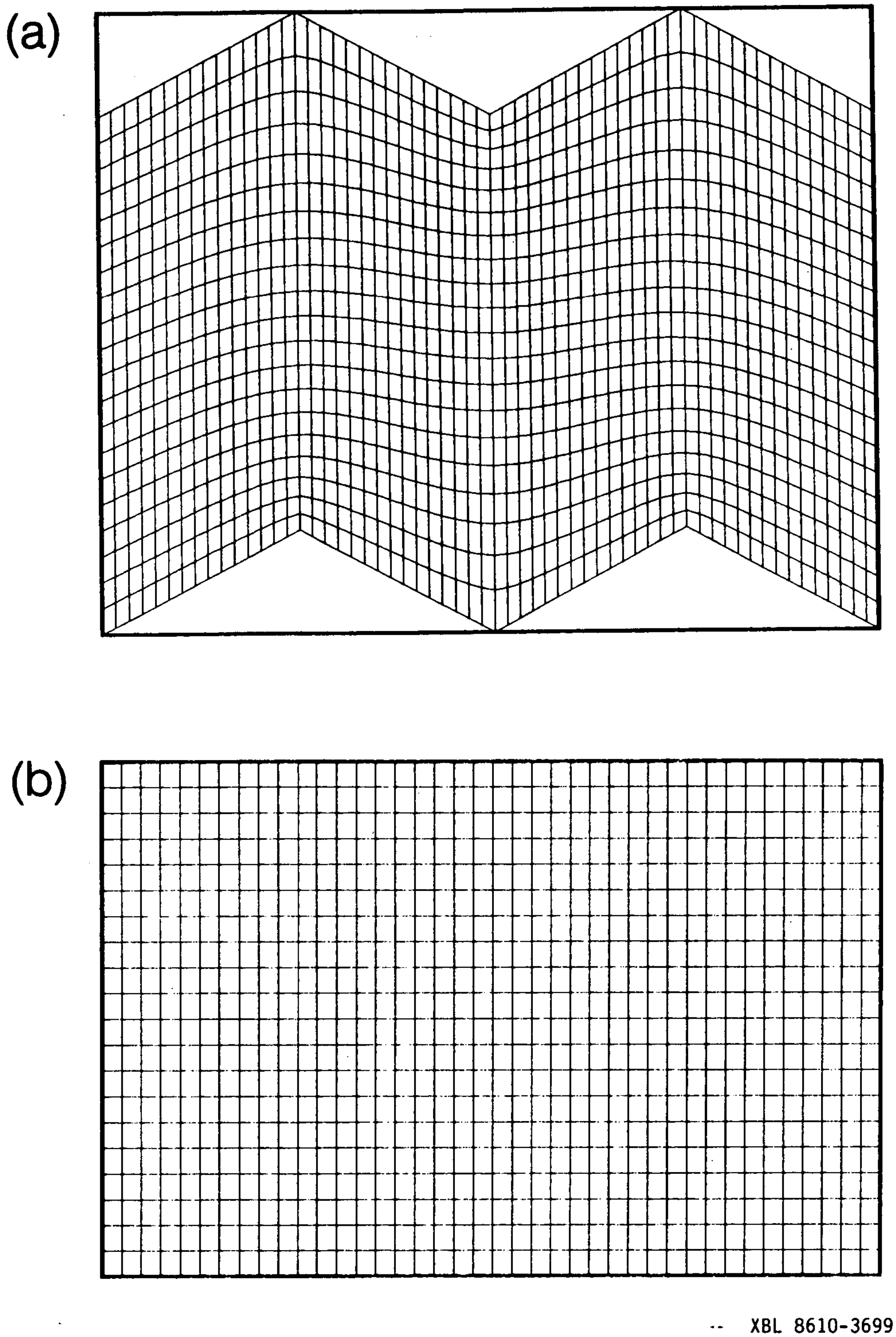


Figure 4.1. Grid Generation in a Wavy Channel of Aperture = 2, length = 6, $\lambda = 0$. (a) Physical Region; (b) Transformed Region.

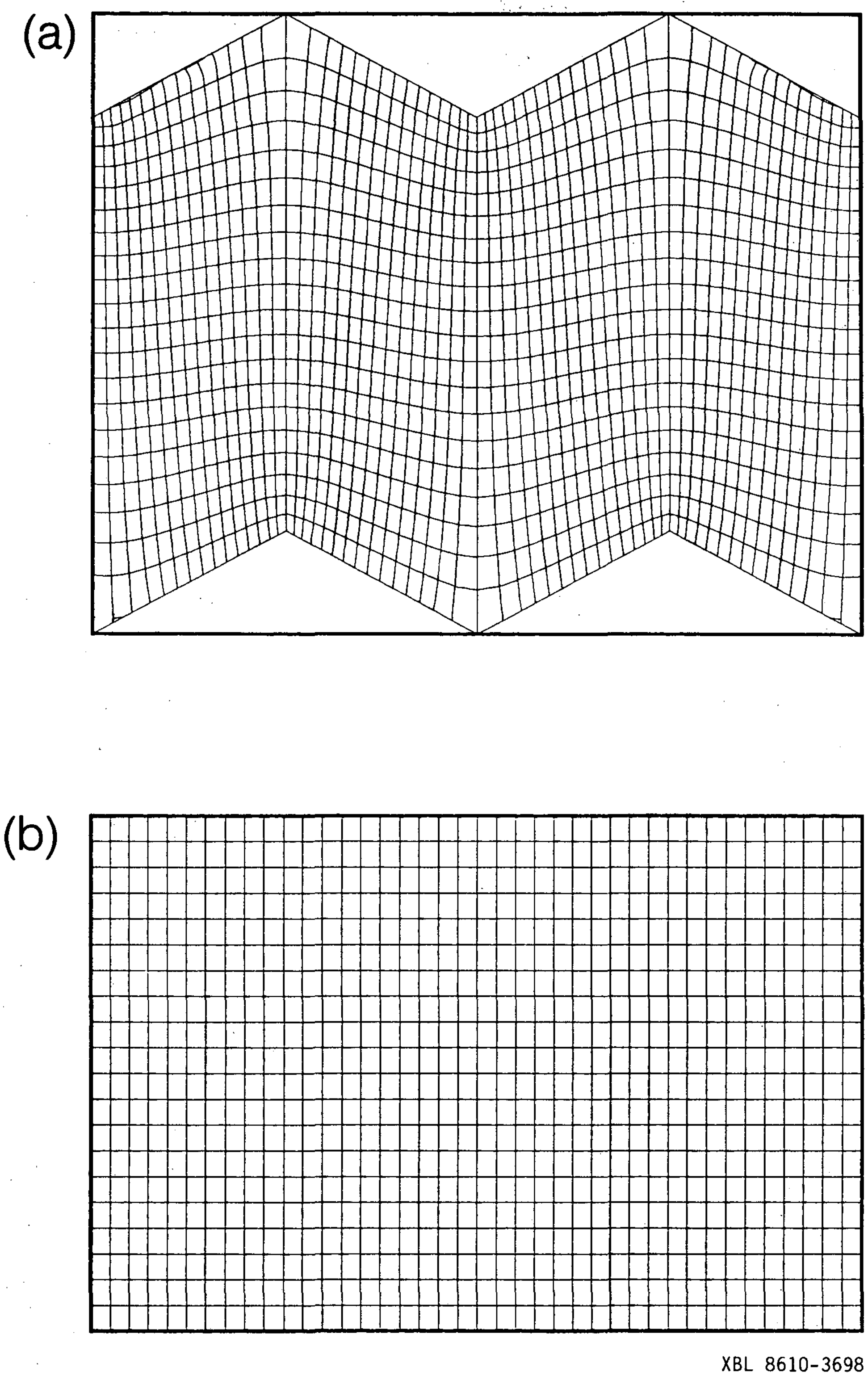


Figure 4.2. Grid Generation in a Wavy Channel of Aperture = 2, length = 6, $\lambda$ = 2. (a) Physical Region. (b) Transformed Region.

indeterminate. During the iteration process, this location is computed by interpolation, and convergence in this case refers to both points in the interior and on the boundary. Singular points (where the gradient is multi-valued) require special treatment, and in this work, have been provided with Dirichlet boundary conditions to circumvent the gradient calculation. The use of nearly orthogonal grids is desirable from the viewpoint of flow calculation, since the truncation error can be shown to follow the law (Thompson, 1982),

$$\mathrm{TE} \approx \frac{\mathrm{A}}{\sin\theta} \qquad 4.1$$

where A depends on the mesh size and $\theta$ is the local angle between the grid lines. Clearly, TE is minimum when $\theta = 90$ degrees.

Figure 4.3 shows a second example of grid generation in a wavy channel which has a constriction. The grid has been computed using Dirichlet boundary conditions, i.e., with prescribed end points for the grid lines, which are equally spaced. The symmetry of the channel about the horizontal mid-plane keeps the corresponding grid line also horizontal. One check on the calculation is that the overall symmetry of the problem should be reproduced in the computed grid. Figure 4.4 shows the grid in the same channel with partial orthogonality imposed on the interior ($\lambda = 2$) and Neuman boundary conditions.

As described in Chapter 1, a single rock fracture is expected to be a channel with rough side walls and a number of contact areas serving as obstacles to fluid flow. In this work, these contact areas will be mapped to rectangles, of about the same total area, and on which flow boundary conditions are easily applied. An example of this procedure is shown in Figure 4.5. In the physical space, the contact area is taken as circular (Figure 4.5a) and in the transformed plane, it is a square (Figure 4.5b). The grid in the physical domain is gradually distorted to accommodate the boundary shape which is not coincident with a rectangular mesh pattern. The procedure described in Chapter 2 permits accurate calculation of the nodal coordinates (Figure 4.5a) which in turn allows

(a)

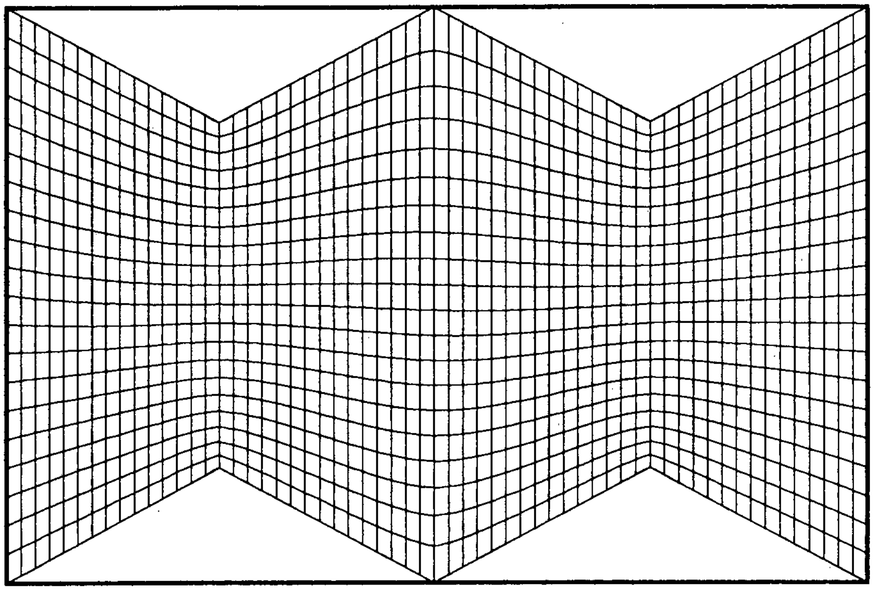

(b)

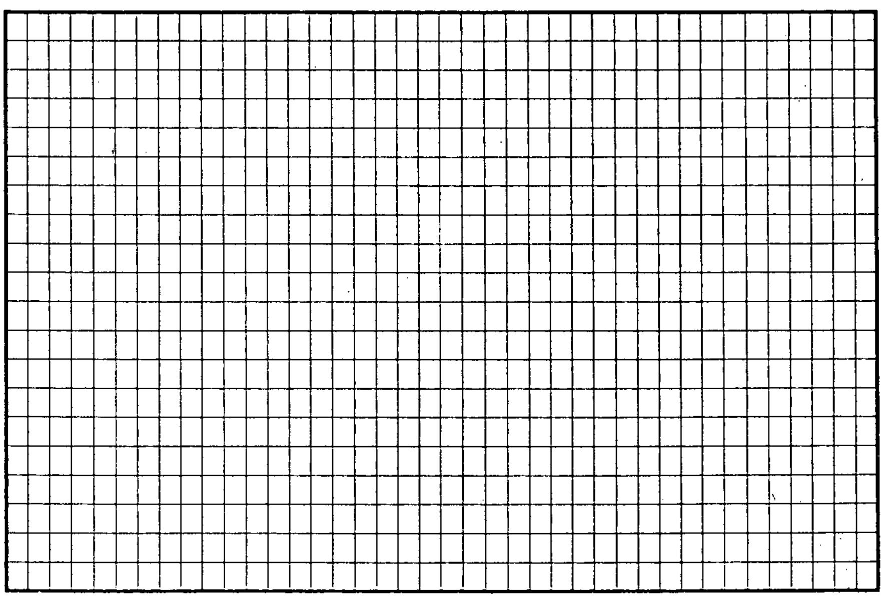

XBL 8610-3691

Figure 4.3. Grid Generation in a Channel with Constriction, Aperture = 2, Length = 6, $\lambda = 0$. (a) Physical Region. (b) Transformed Region.

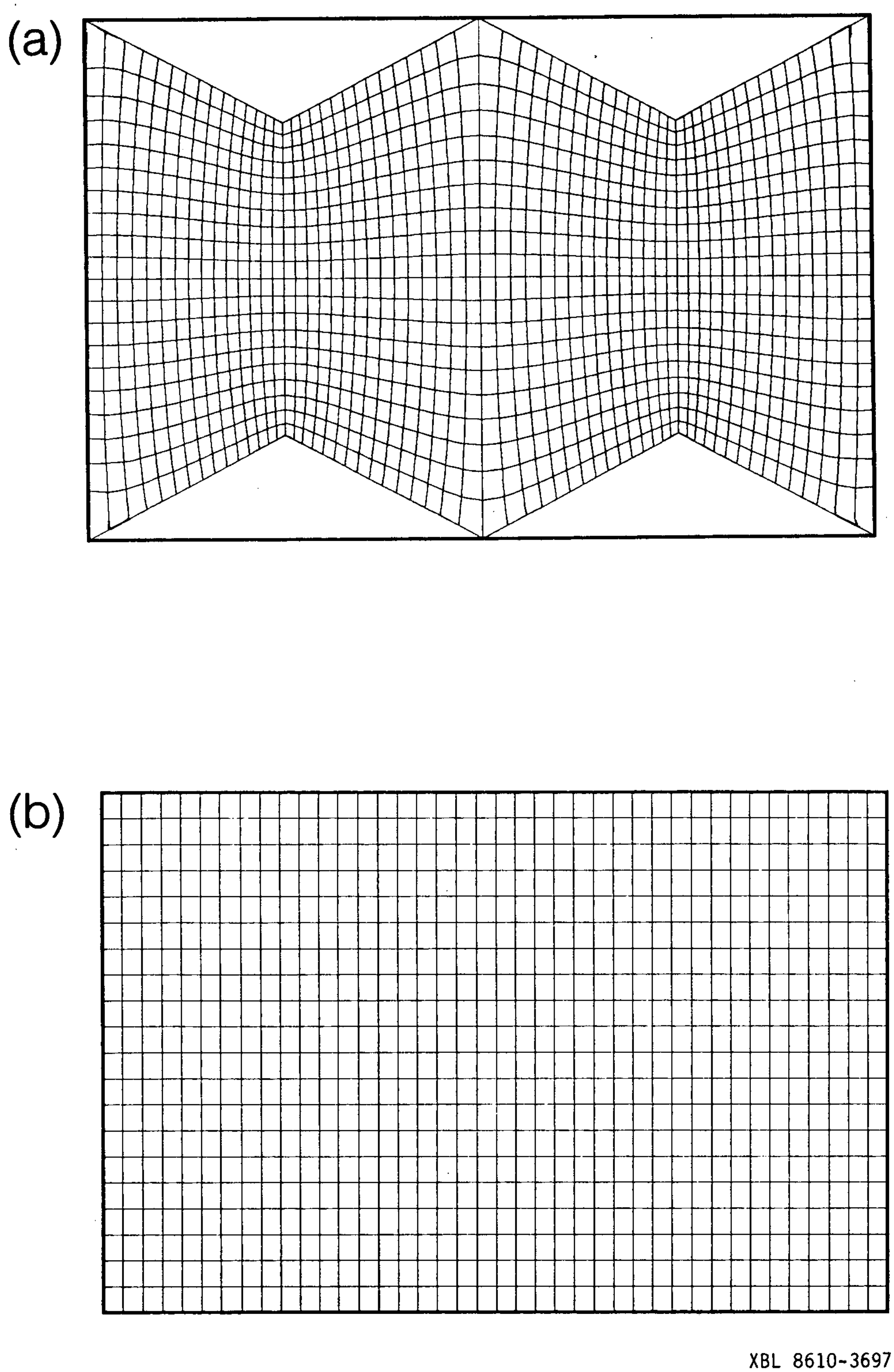


Figure 4.4. Grid Generation in a Channel with Constriction, Aperture = 2, Length = 6, $\lambda = 2$. (a) Physical Region. (b) Transformed Region.

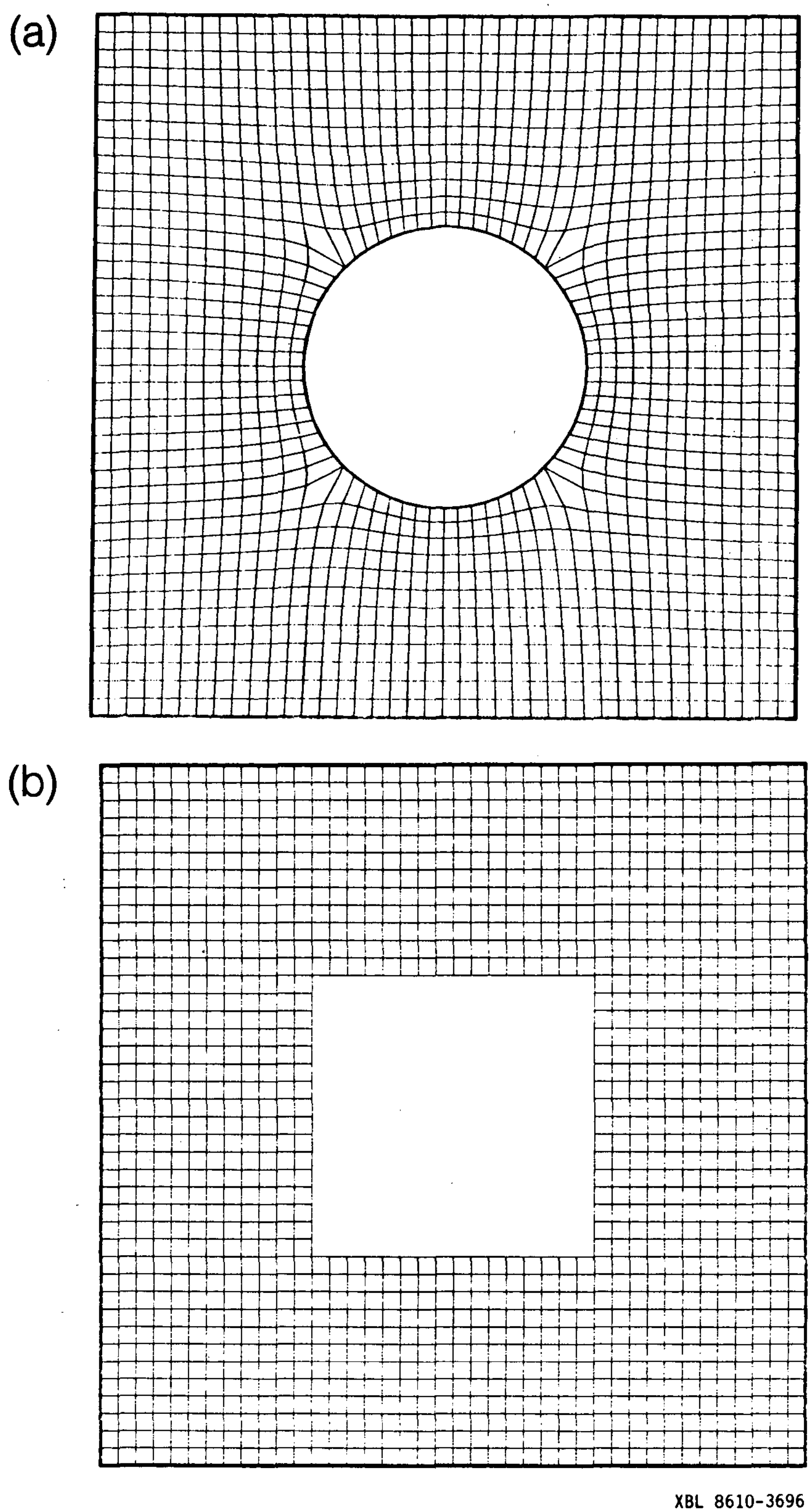


Figure 4.5. Grid Generation in a Square Region with a Circular Obstacle(Contact Area). $\lambda = 0$. (a) Physical Region; (b) Transformed Region.

accurate calculation of the metric derivatives.

### 4.3 Examples of Flow Calculation

The procedure to solve for a flow field has been described in Chapter 3. Results given below have been obtained with specified pressure values at inlet and exit, and a periodicity condition for the flow field over the length of the channel considered for calculation. The Reynolds number is based on pressure drop in the channel.

Figure 4.6 shows flow in a channel with a step. The flow boundary conditions transform this problem to one of a channel with successively located steps, a distance L, the channel length, apart. This accounts for the skewed shape of the inlet velocity profile, which has a maximum at a level above the step. It is possible to prescribe velocity profiles at the inlet (as parabolic, or constant), up to one undetermined multiplying factor (the mean flow) which must be calculated during the iterative process. Results for this case of prescribed velocity profile have also been presented in this report.

The velocity vector plot in Figure 4.6b shows considerable deceleration of flow ahead of the step, and a small recirculation pattern beyond. The extent of a recirculation pattern is a function of Reynolds number. This Reynolds number dependence is seen in the solution only when the inertial terms are retained in the flow model. Otherwise, the flow shows a simple scaling relationship with Re. The use of a model which resolves these local details of the flow field, and using which the behavior of the entire flow system is predicted is expected to be the primary contribution of this work.

Figure 4.7 shows the mean velocity in a channel, with and without a step, as a function of Reynolds number. The straight line relationship for a parallel channel is well-known, and the slope of the line is proportional to the square of the aperture. The curve for the channel with a step predictably lies below that of the parallel channel, since the flow encounters greater resistance in this case. This curve is also close to linear, over the range of values of Re plotted in Figure 4.7. This suggests that an

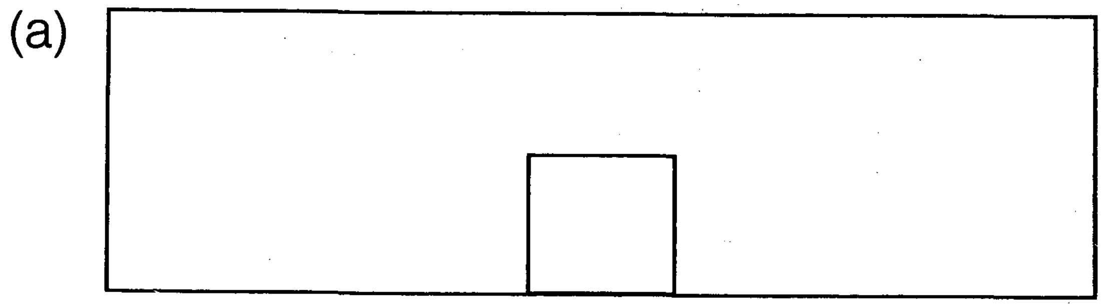

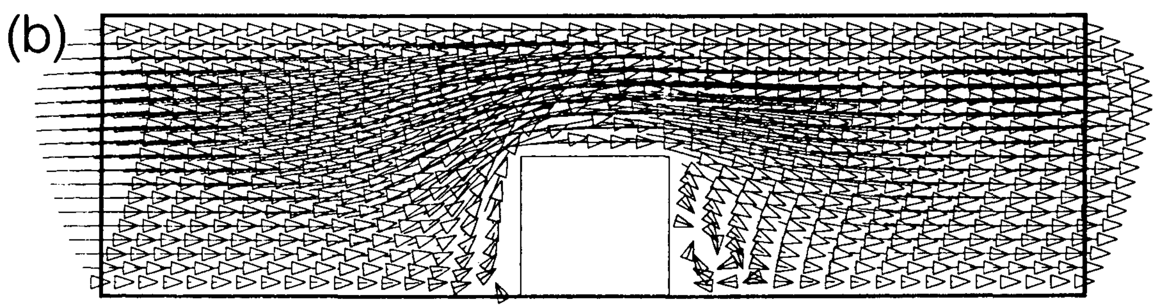

XBL 8610-3694

Figure 4.6. Flow in a Channel with a Step. (a) Flow Geometry: Aperture = 2, Length = 7, Step Size = 1 × 1. (b) Velocity Vector Plot at Re = 25.

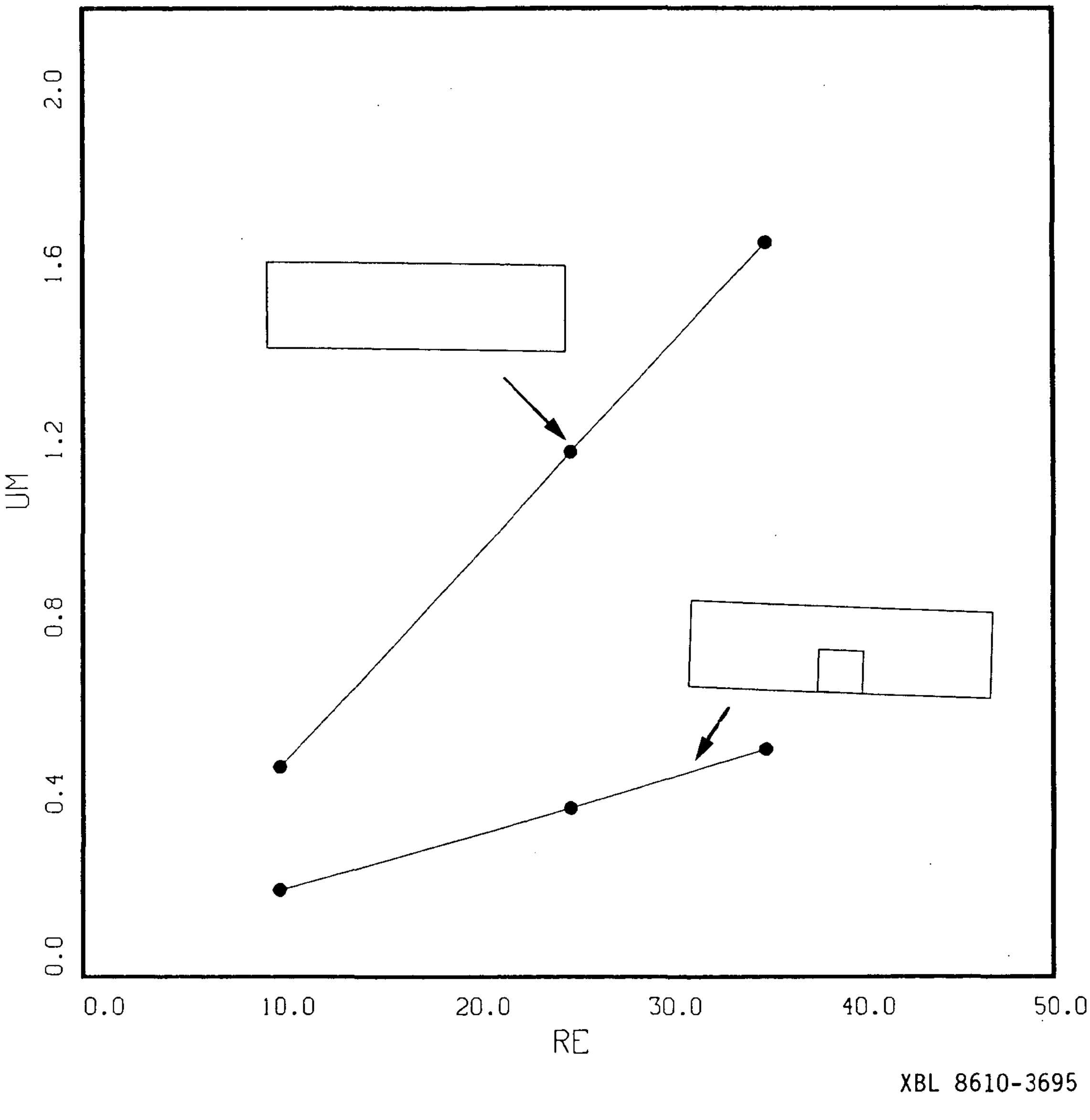


Figure 4.7. Plot of Mean Velocity in a Channel with a Step, Compared to a Parallel Channel, as a Function of Reynolds Number.

equivalent aperture can still be calculated, even though the velocity profiles are far from parabolic.

Figure 4.8 shows flow in a channel with two steps at two values of Reynolds number (10 and 25). The overall flow pattern remains unchanged, and flow features including rolls and the non-zero y-component of velocity at the inlet and exit are reproduced at both Reynolds numbers. Figure 4.9 shows velocity profiles at three x-locations along the channel at Re = 25. The negative velocities seen in the plot are representative of the recirculation pattern and can be loosely identified with vorticity production in the flow. The flow is taken as incompressible and so the area under each curve is a measure of the flow rate (flux) and is a preserved quantity at every x-location. The continuity equation, which represents mass conservation, has been replaced in this work by a pressure equation and so the mass is not conserved strictly in the calculation. The extent of mass production, measured by the difference in areas under the velocity curves (Figure 4.9), is also an indicator of the accuracy of the overall numerical scheme. These mass sources (or sinks) can be reduced further by,

(a) Increasing the number of grid points,

(b) Grid refinement,

(c) Higher order representation of the wall pressure gradient,

(d) Accurate calculation of the source terms in the pressure equation.

For a second-order formulation of factors (c) and (d) above (see Section 3.4), the mass balance has been observed to be within 5 percent for the examples studied here. Figure 4.10 shows a plot of mean velocity as a function of Re, for both a parallel channel and one with two steps located inside. The plot of $u_m$ versus Re for the stepped channel clearly is not linear, and this behavior is proof that constitutive relationships such as Darcy's law do not apply to this class of problems and range of flow rates. The nonlinearity arises from the recirculation pattern in the region beyond the steps, as the flow separates from a bluff surface. The fluid does not adhere to the geometry of the

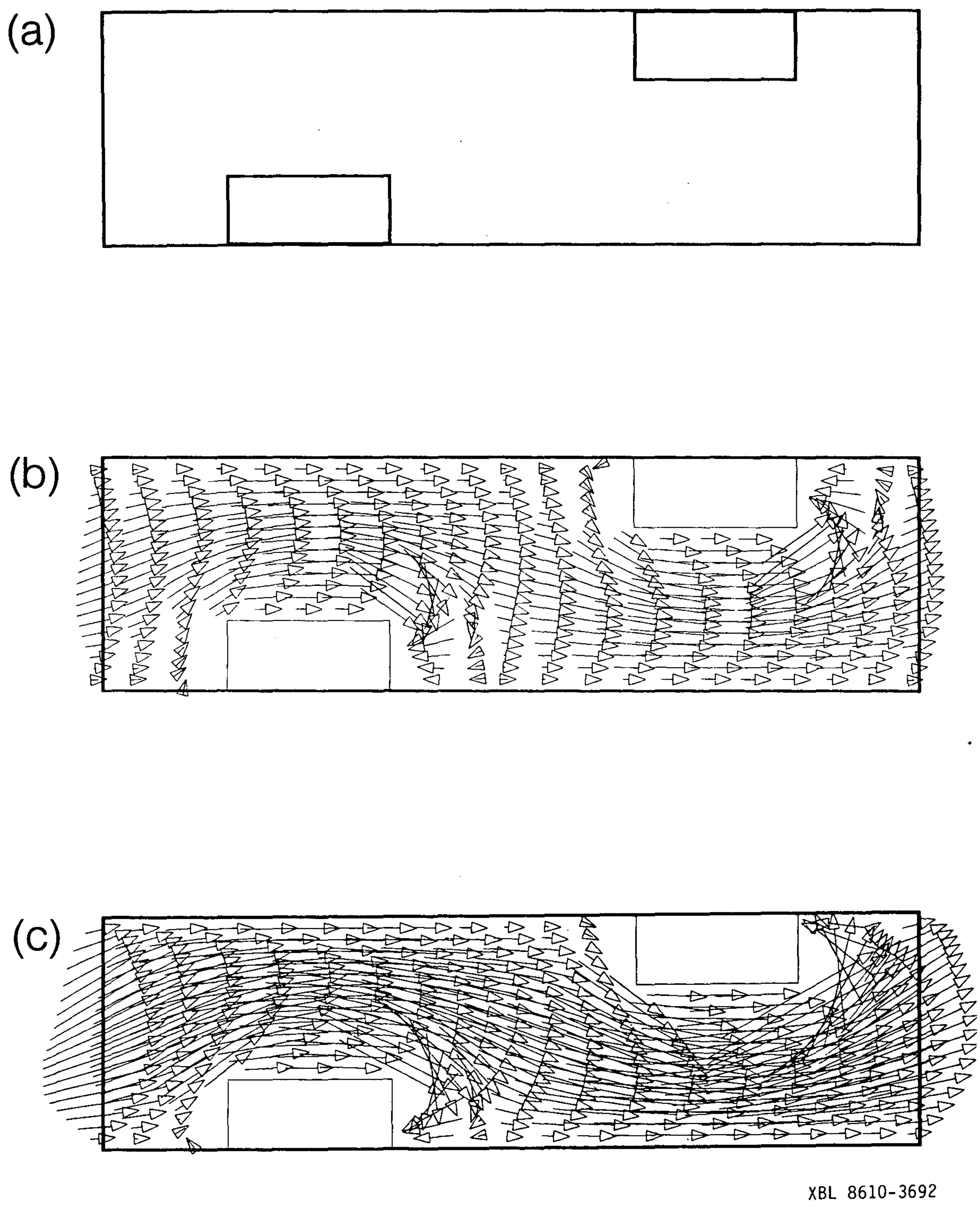


Figure 4.8. Flow in a Channel with Two Steps. (a) Flow Geometry; Aperture = 2, Length = 7, Step Size = 1.4 × 0.6; (b) Velocity Vector Plot at Re = 10; (c) Velocity Vector Plot at Re = 25.

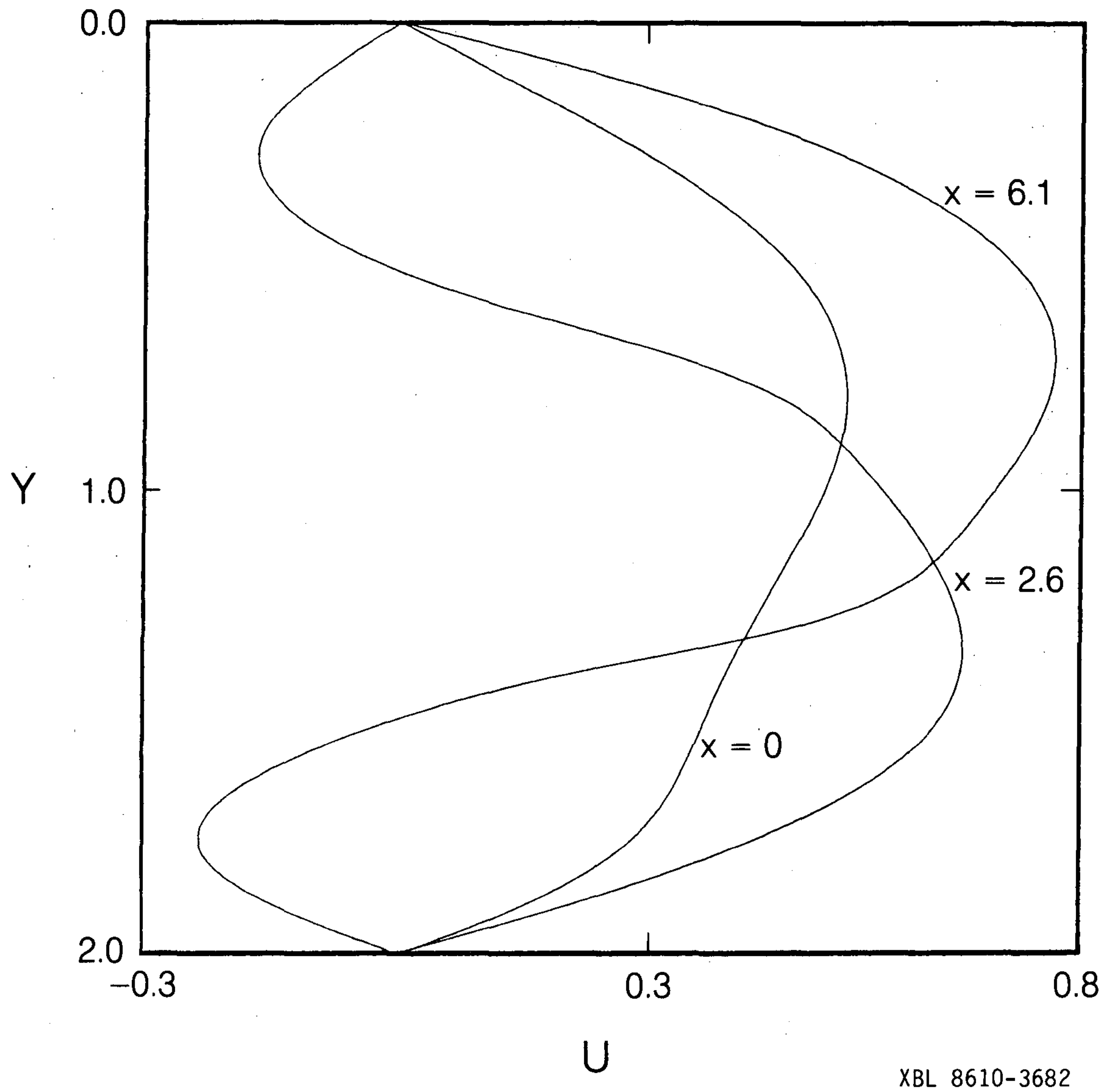


Figure 4.9. Velocity Profiles at Three x-Locations in a Channel with Two Steps. Re = 25.

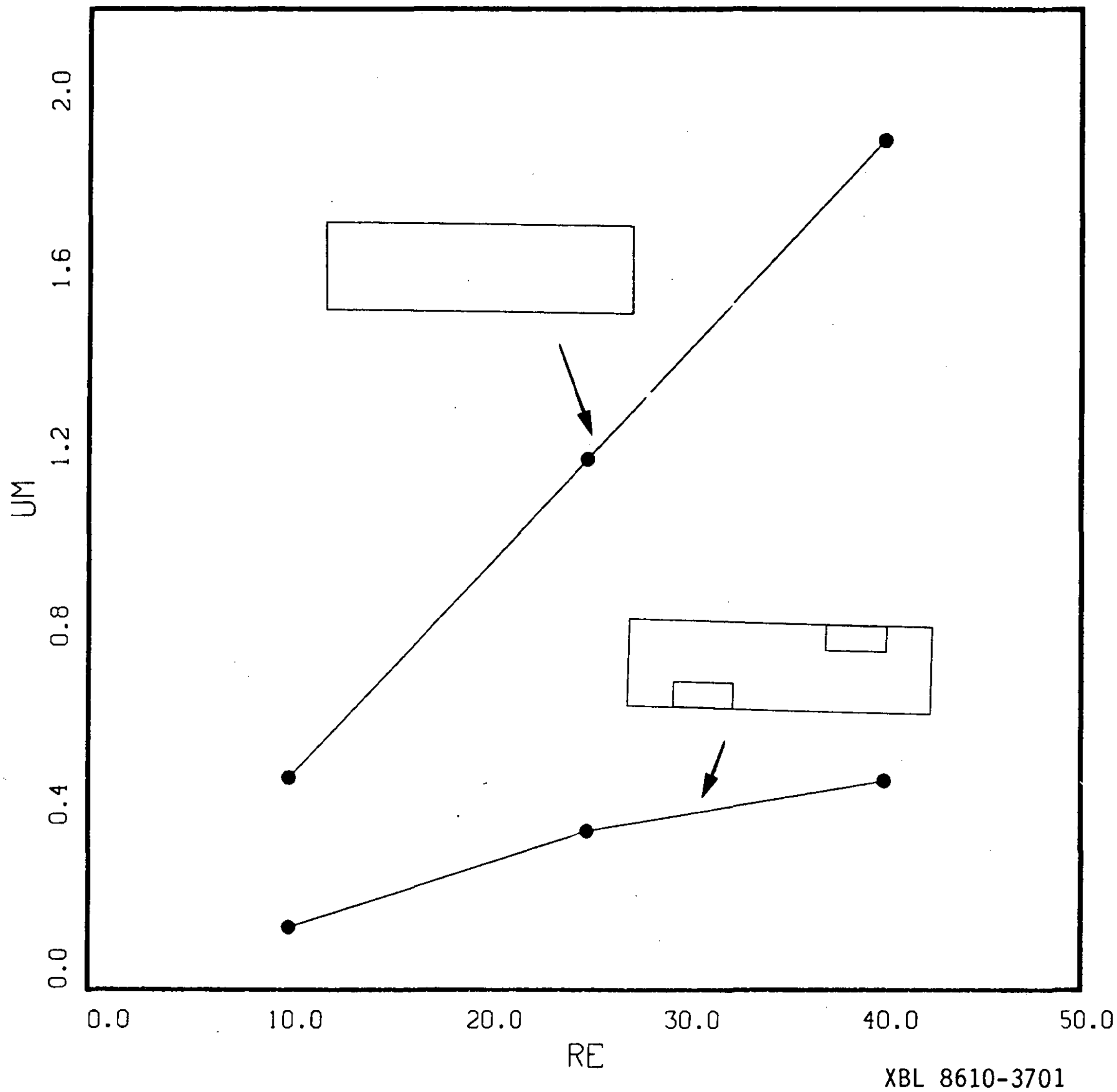


Figure 4.10. Plot of Mean Velocity in a Channel with Two Step, Compared to a Parallel Channel, as a Function of Reynolds Number.

bounding surface because large negative acceleration values are generated which would require large pressure drops to hold the fluid on the surface. As the governing equations show, the acceleration terms are nonlinear, thus making the flow system nonlinear. Only a detailed analysis of flow patterns (such as the one presented in this report) will reveal these effects.

Figure 4.11 shows velocity profiles in a parallel wavy channel at three x-locations, for Re $=$ 25. Figure 4.12 shows a velocity vector plot in the channel at Re $=$ 10. Though not shown, the plot of mean velocity versus Reynolds number for this channel is close to that for a parallel channel, for Re $<$ 50. This is surprising, but the reason can be traced back to the plot in Figure 4.11. The acceleration of flow at x $=$ 3.0, near the upper half of the channel and the consequent retardation in the bottom half, (and the reverse at x $=$ 6) is simply not large enough to create a large y-component of velocity. Hence, the vorticity production is just too weak to cause additional pressure drop and significantly reduce the flow rate. This trend can be expected to change at higher values of Re, where the irregular boundary will promote turbulence.

Figure 4.13 shows flow in a wavy channel with constriction, at Re $=$ 5. Figure 4.14 shows a plot of mean velocity as a function of Reynolds number, for both the wavy and the parallel channels. The parallel channel is constructed with an aperture equal to the maximum aperture of the wavy channel. The trend is close to linear for the former and can be used to determine an equivalent aperture. In the wavy channel pressure drop is larger than the parallel channel due to the acceleration of flow at the throat locations. Non-linearity can be expected at Reynolds numbers which cause the flow to separate in the expanding portion of channel.

Figure 4.15 shows two views of a three-dimensional duct with an obstacle located in its center. The duct is $6 \times 6 \times 2$, dimensionless units and the obstacle is $1.2 \times 1.2 \times 2$. The duct is closed at the top and the sides and flow enters on the left side and leaves the right side, in response to a prescribed pressure drop. Figure 4.16

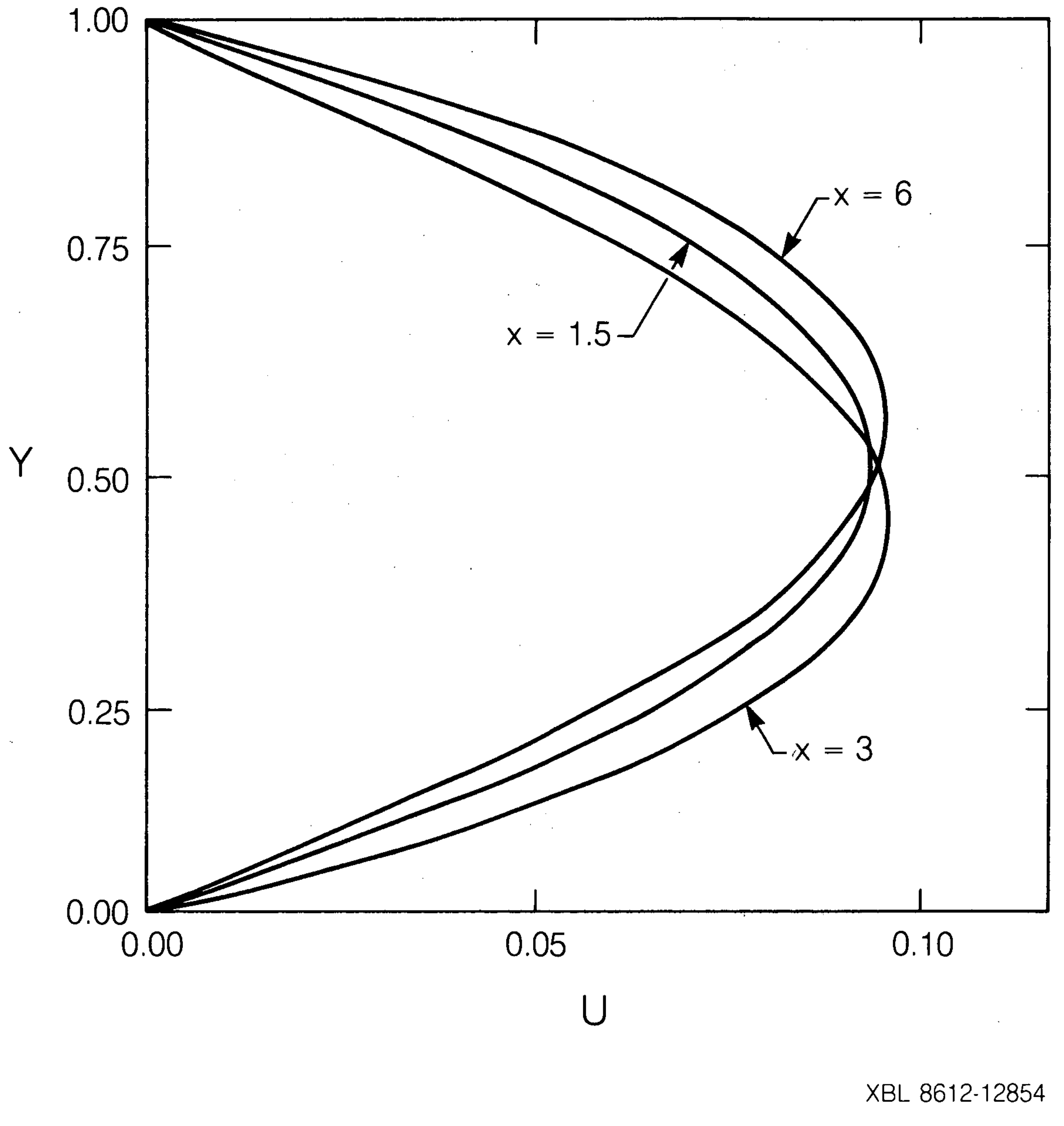


Figure 4.11. Velocity Profiles at Three x-Locations in a Wavy Parallel Channel. Re = 5.

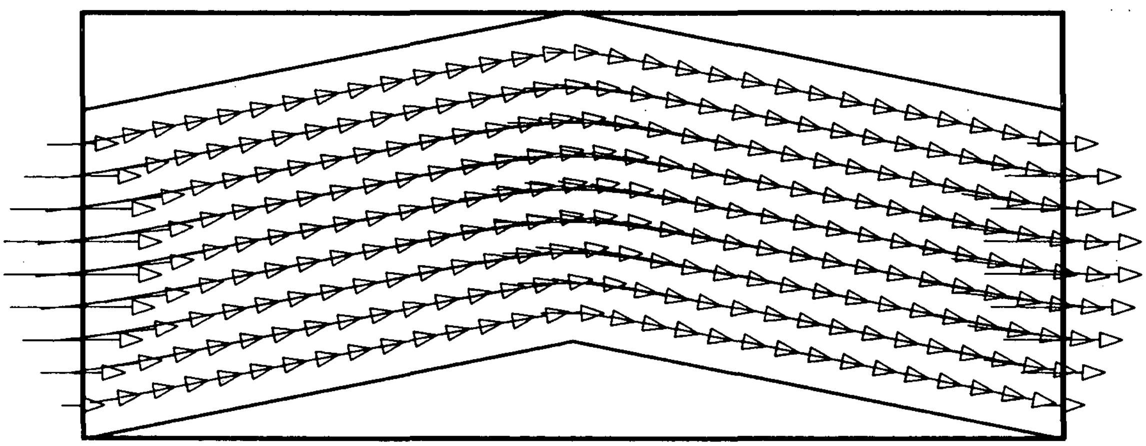

XBL 8612-4969

Figure 4.12. Velocity Vector Plot in a Parallel Wavy Channel Re = 5.

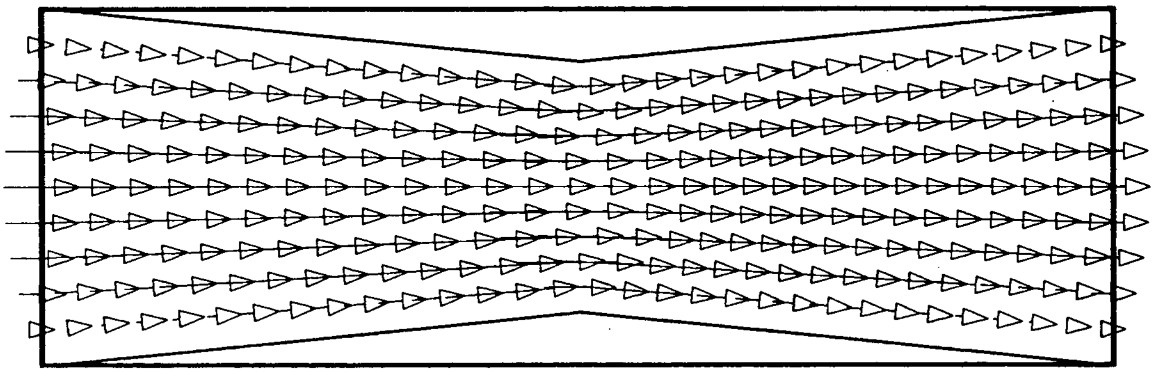

XBL 8612-4966

Figure 4.13. Velocity Vector Plot in a Wavy Channel with Constriction. Re = 5.

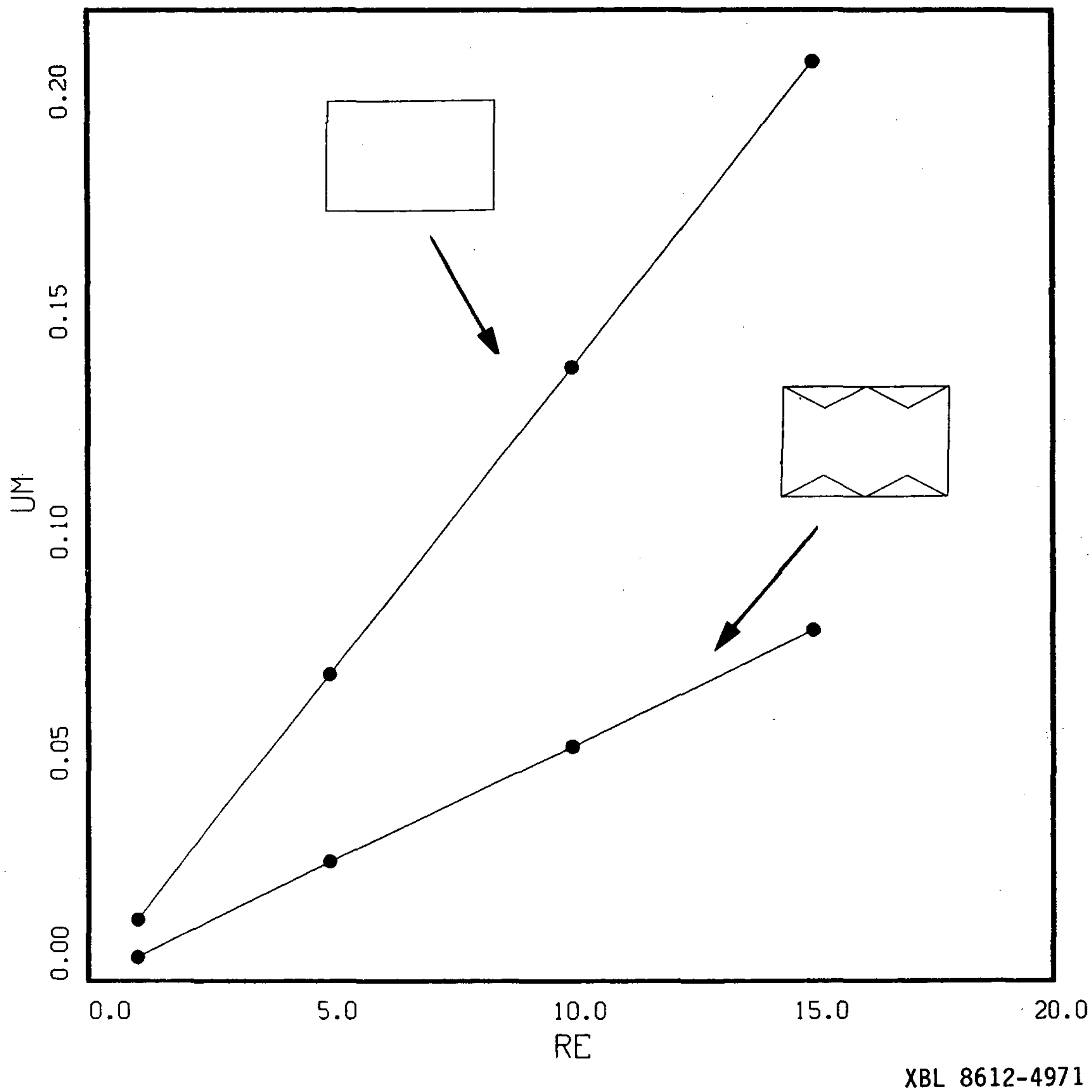


Figure 4.14. Plot of Mean Velocity in a Wavy Channel with Constriction, Compared to a Parallel Channel, as a Function of Reynolds Number.

(a)

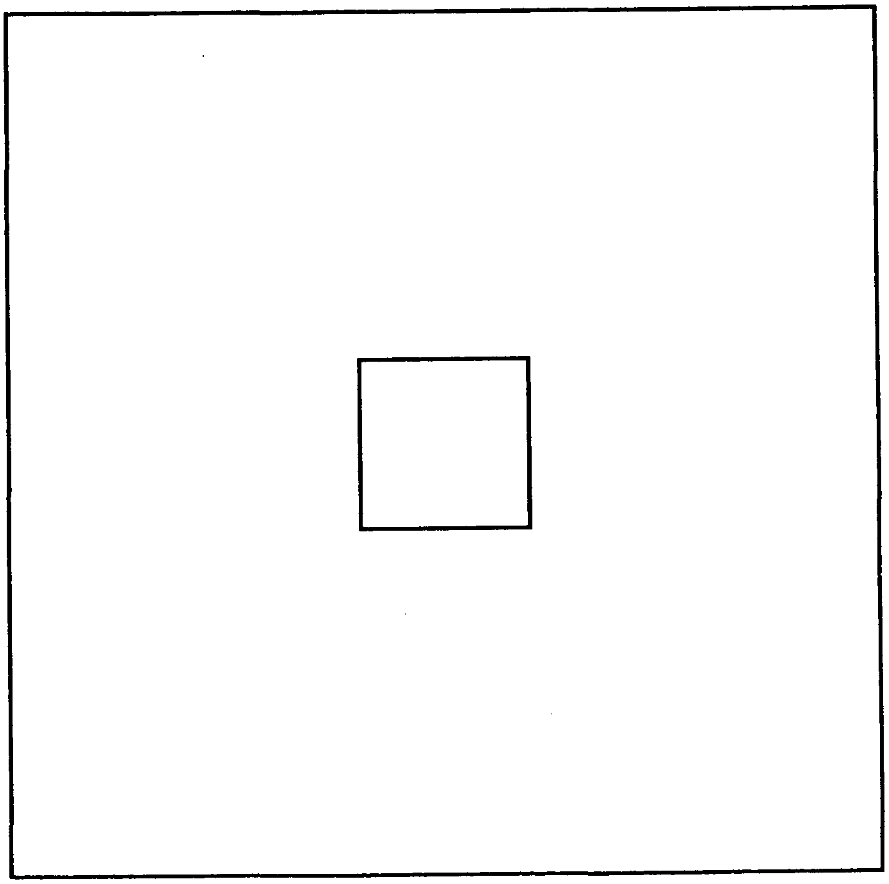

(b)

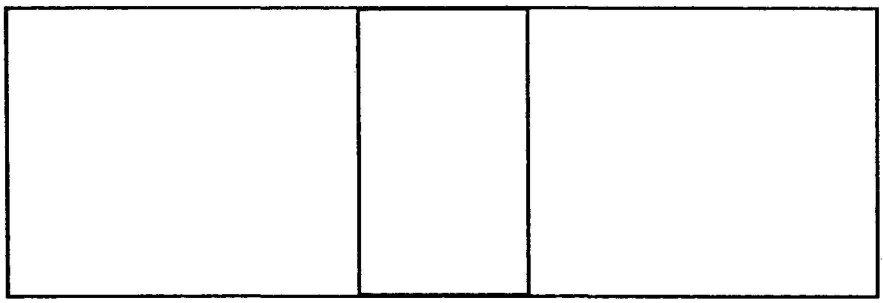

XBL 8610-3693

Figure 4.15. Sections of a Three-dimensional Duct with an Obstacle. Length = Width = 6, Height = 2, Obstacle cross-section = 1.2 × 1.2, (a) Plan (b) Elevation.

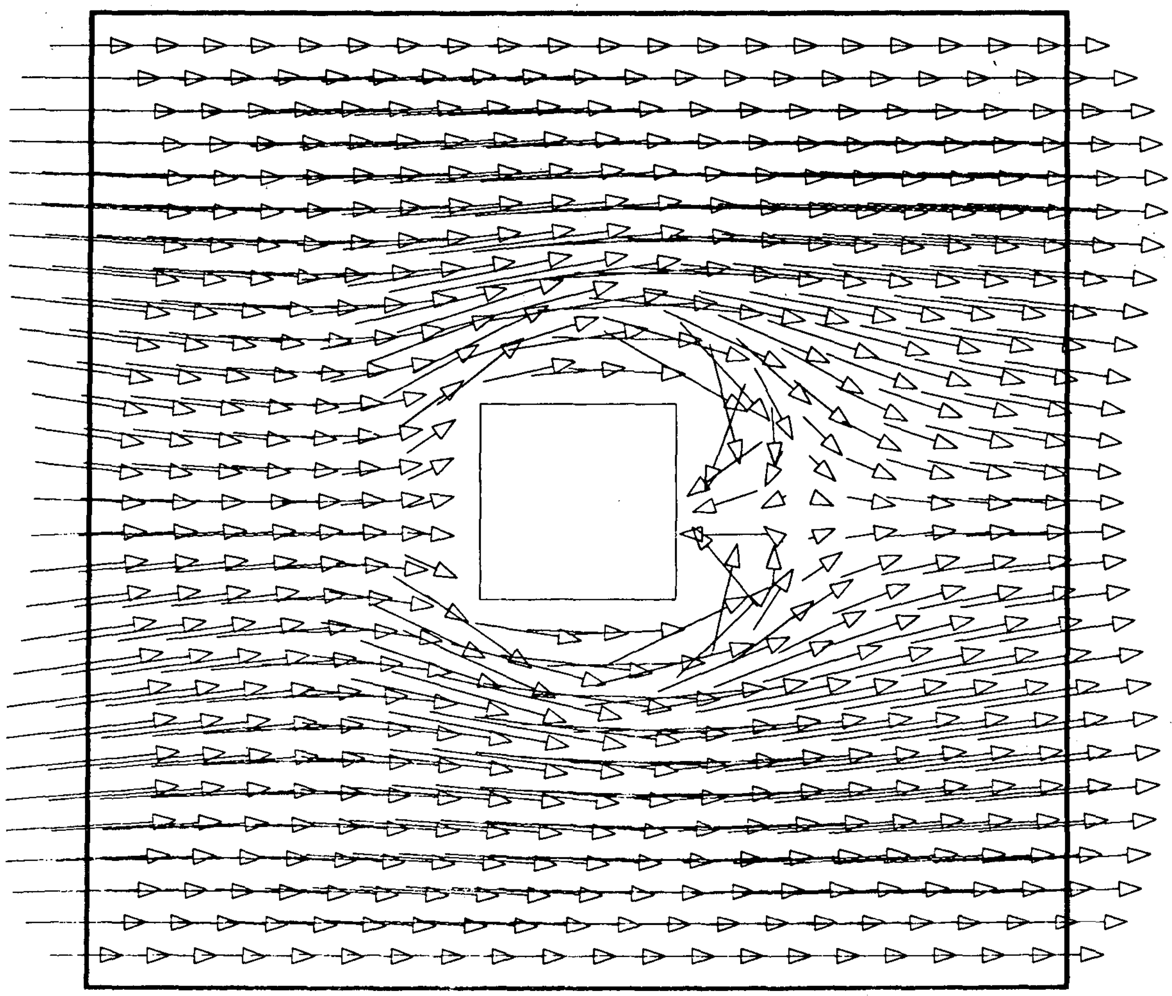

XBL 8610-3686

Figure 4.16. Velocity Vector Plot in a Three-Dimensional Duct with Obstacles, z = 1. Re = 25.

shows a velocity vector plot at the mid-plane of the duct (z = 1), at Re = 25. A symmetric roll pattern is clearly visible on the rear side of the obstruction. The roll pattern is symmetric because the steady flow is, subject to symmetric boundary conditions and geometry must also exhibit symmetricity. As the Reynolds number is raised, the steady state computation retains the symmetric form of the recirculation region, except that it grows in size. It is known from experiments in flow past cylinders and spheres that the symmetric bubble is stable only for low Re.

At higher flow rates, the flow becomes unsteady, and a trailing vortex street is produced behind the cylinder, which destroys symmetry. The onset of unsteadiness in Figure 4.16 would have to be determined from a full transient calculation. It is to be expected that this onset is delayed when more than one obstacle is included in the flow field and when side walls are present. Each of these provides a stabilizing influence to the flow. In the example considered, a pressure-based Re = 25 corresponds to a velocity-based Re = 34 (see Equation 3.9), and at this value, steady state approximation is certainly a reasonable one (Schlichting, 1979, p. 18). Figure 4.17 shows a velocity vector plot closer to the bottom wall (z = 0.1) at Re = 25. The lower wall reduces the magnitude of the velocity, but the flow pattern is otherwise similar to that at z = 1.

Figure 4.18 shows a velocity vector plot at a cross-section of the duct (y = 3) including the obstacle. Small velocities are generated at right angles to the mean flow, but much of the flow goes around the obstacle. The extent of the reverse flow region is a plane of small total velocity, almost parallel to the obstacle side. Figure 4.19 shows flow at a cross-section of the duct excluding the obstacle (y = 2). The flow is mostly parallel, with the darkened regions revealing higher velocities caused by the presence of an obstruction. Figure 4.20 shows plot of mean velocity as a function of Reynolds number for the three-dimensional duct considered above (curve 2) compared to a two dimensional parallel channel (curve 1). As must be expected, the flow in the duct encounters greater resistance and the non-linearities in flow bring out an overall non-

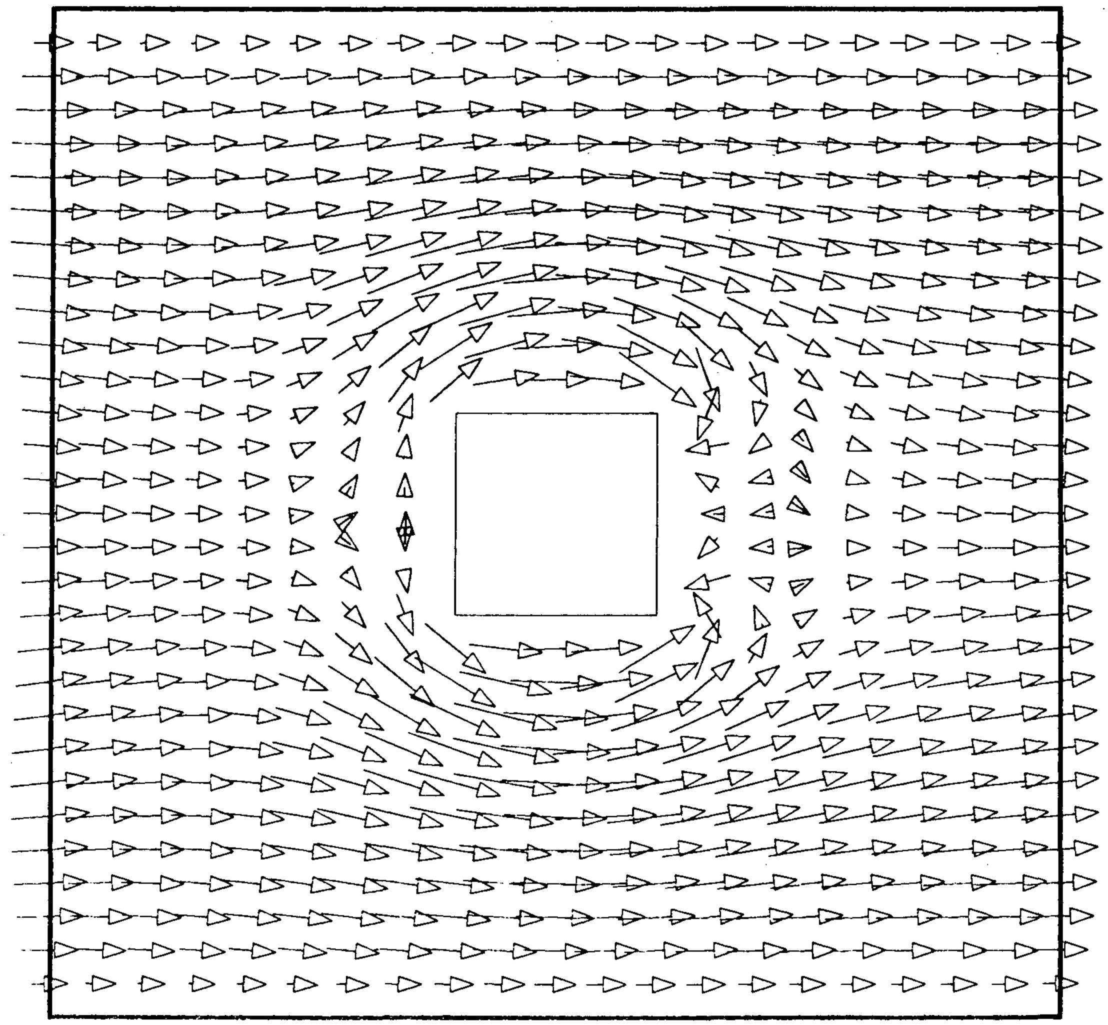


Figure 4.17. Velocity Vector Plot in a Three-Dimensional Duct with an Obstacle, z = 0.1. Re = 25.

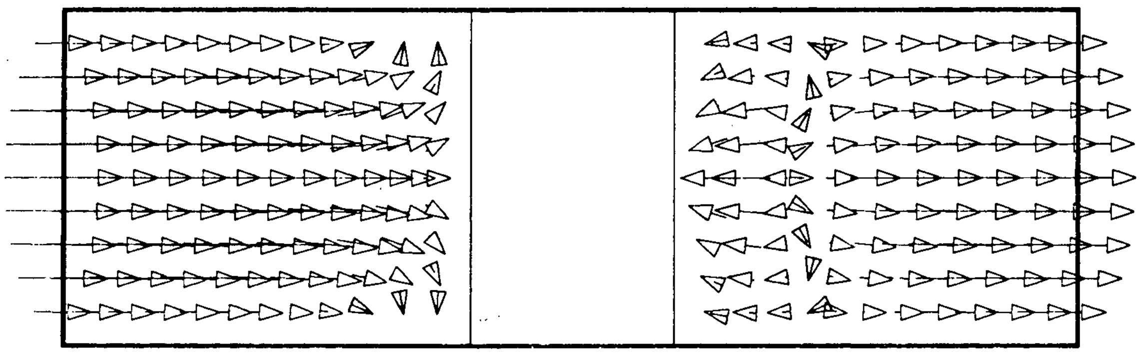

XBL 8610-3688

Figure 4.18. Velocity Vector Plot in a Three-Dimensional Duct with an Obstacle, y = 3. Re = 25.

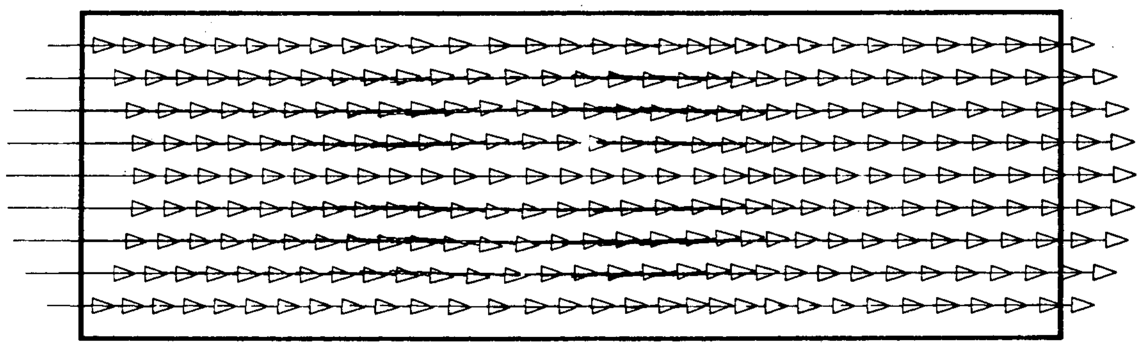

XBL 8610-3689

Figure 4.19. Velocity Vector Plot in a Three Dimensional Duct with an Obstacle, y = 2. Re = 25.

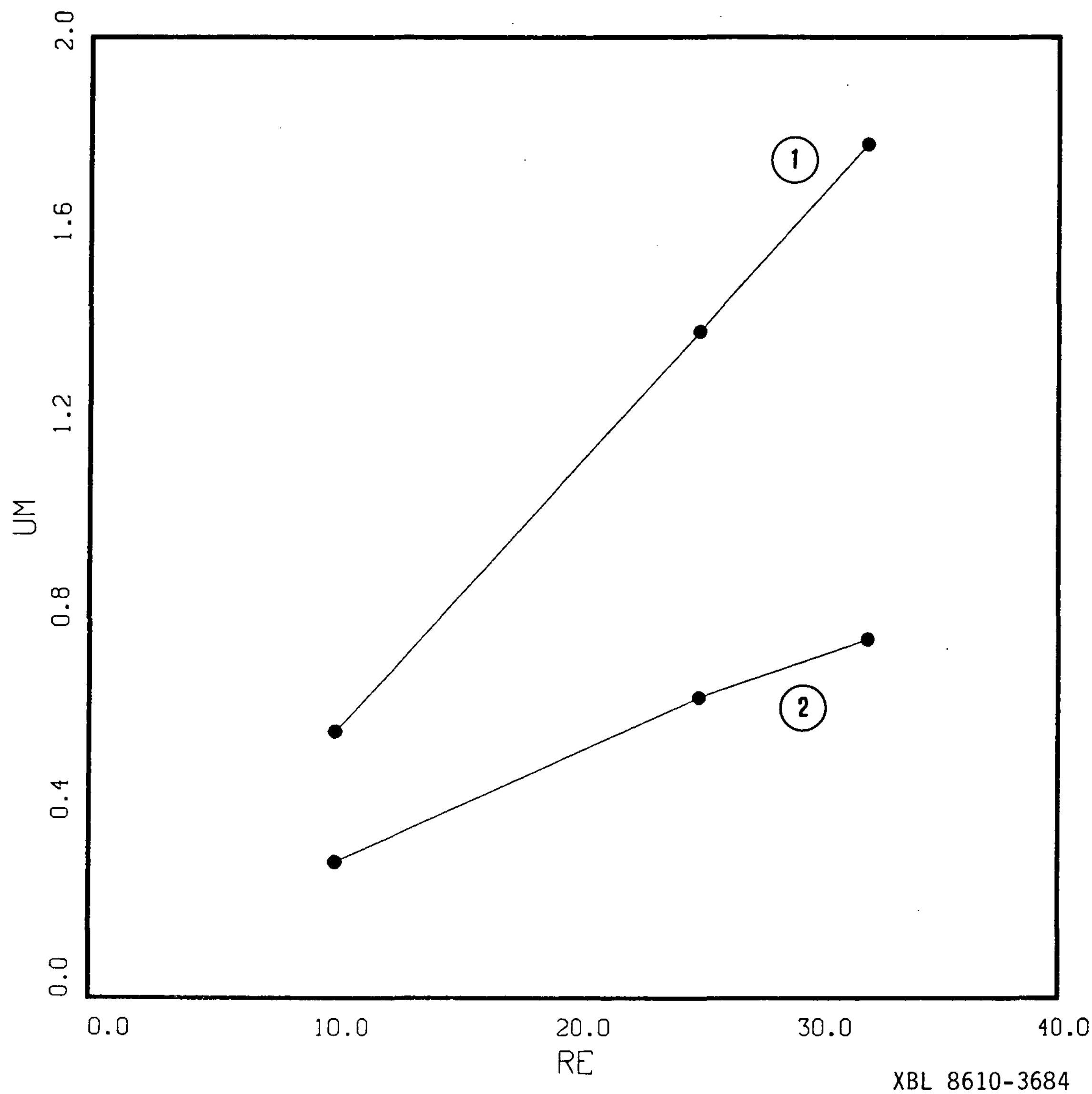


Figure 4.20. Plot of Mean Velocity in a Three Dimensional Channel as a Function of Reynolds Number. (1) Flow in a Parallel Duct. (2) Flow in a Duct with an Obstacle.

linear behavior of the system.

Figure 4.21 shows a velocity vector plot of flow past a circular contact area in a square flow region. The periodicity condition implies that this solution is valid for a geometry repeating indefinitely on both sides of the fracture. The solution has been obtained by using the transformation shown in Figure 4.5, which converts the circular obstacle to a square. Figure 4.22 shows the plot of mean velocity through this region as a function of Reynolds number. The curve is almost linear, over the range $0 < \mathrm{Re} < 15$. However, the equivalent permeability of this system, measured as a slope of the curve is only 12 percent of the permeability without the obstruction.

A comparison of equivalent permeability of all two dimensional periodic geometries considered above, using Navier-Stokes equations and Darcy's law is given in Table 4.1. It can be seen that Darcy's law consistently predicts a permeability larger than the Navier-Stokes value. The reason for this discrepancy is related to the physics ignored by Darcy's law. For example, in Figure 4.1, the channel has a constant aperture even though the flow path is tortuous. This results in a Darcy permeability which is identical to that of a parallel straight channel with the same aperture. On the other hand, the Navier-Stokes equations correctly include tortuosity and determine a permeability smaller than unity.

Solutions based on Darcy's law require a significantly smaller computational effort compared to the solution of Navier-Stokes equations, especially when three dimensional flow fields are considered. For this reason, it is definitely worthwhile to look for correction factors which would improve either the Darcy calculation or its results, without altering the structure of the governing equations (Equations 3.27). It can be seen from Table 4.1 that the difference between the two flow models is quite large under certain conditions, (as in Figure 4.5). This justifies the development of a Navier-Stokes solver, which can serve to determine flow patterns and pressure drops in geometries where Darcy's law has serious shortcomings. Results in Table 4.1, are only for two dimensional

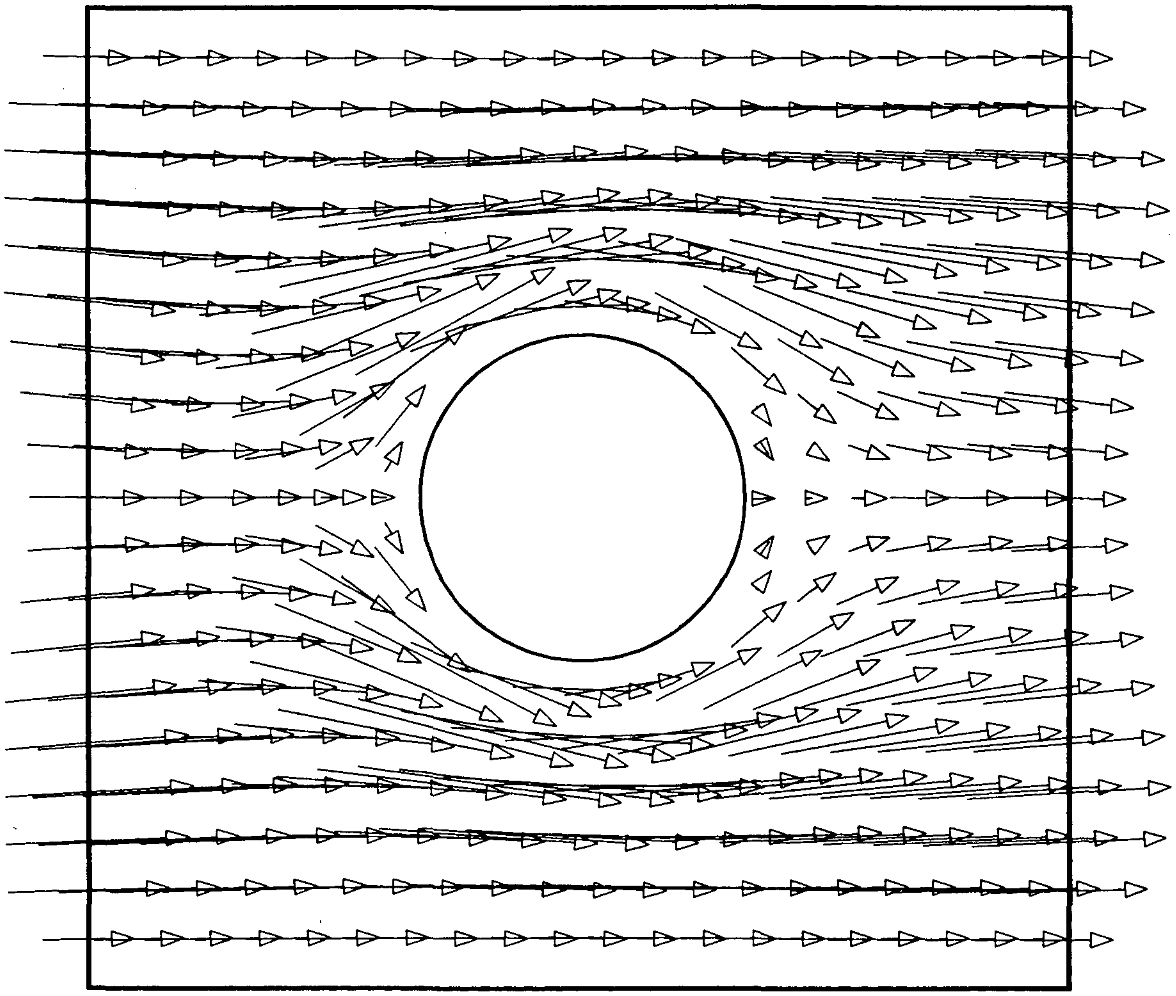


Figure 4.21. Velocity Vector Plot in a Region with a Circular Contact Area. Re = 5. Region size = 6 × 6; Obstacle radius = 1.

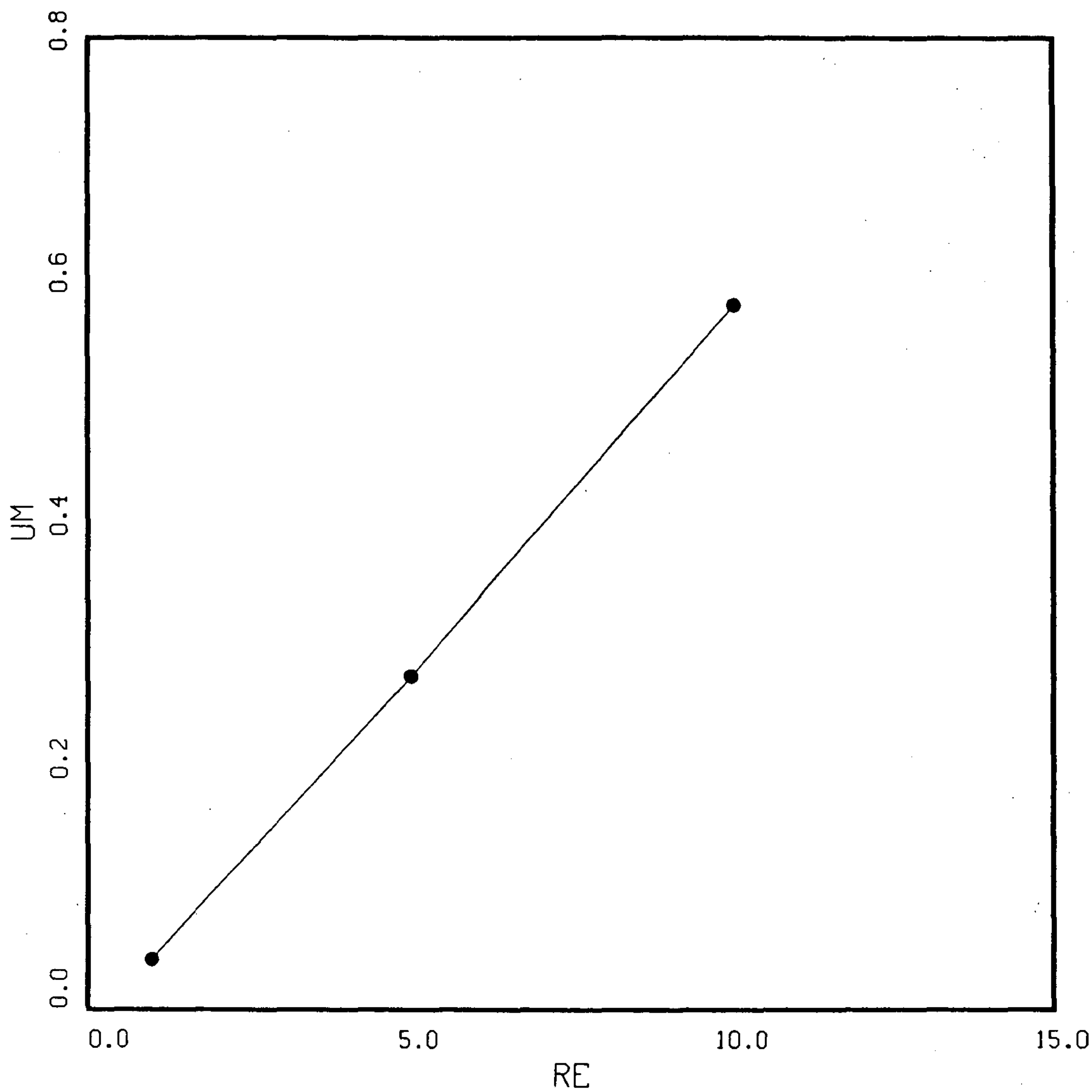


XBL 8612-4967

Figure 4.22. Plot of Mean Velocity as a Function of Reynolds Number, for Flow in a Region with a Circular Contact Area.

geometries. It is clear that Darcy and Navier-Stokes models are in better agreement when the fracture is modeled as a channel with varying aperture, compared to the model of a channel with contact areas. These statements however, require complete validation from the solution of three dimensional Navier-Stokes equations.

Some examples of flow in complex three dimensional channels are given below. In these cases, the geometry is non-periodic and a nearly parallel inlet velocity (Equations 3.6c) is prescribed and a gradient condition is prescribed at the exit (Equation 3.6d). The flow is driven by a given pressure drop, determined by the Reynolds number.

Figure 4.23 shows grid generated by the method of Chapter 2, in a three dimensional channel with a constriction at its center. It is useful to think of the channel as formed by two inverted pyramids whose peaks define the constriction. Figure 4.24 shows flow in this channel, obtained by solving Navier-Stokes equations, as in Chapter 3. It can be seen from this figure that flow is close to parabolic everywhere along the channel length. This suggests that the permeability of the channel should be closely approximated by using the cubic law, which is equivalent to Darcy's law given by Equation 3.27. However, Navier-Stokes equations calculate additional pressure drop due to tortuosity of the flow path.

In two dimensional simulations pressure drop due to tortuosity was observed to be a major difference between the two flow models. This also holds true in three dimensions. Two additional factors arise. These are, (a) the fluid particles have an additional degree of freedom to move in the direction of the third coordinate, and (b) the pressure drop due to tortuosity is a smaller fraction of the overall pressure drop (compared to the two dimensional case), because of the large surface areas encountered in a three dimensional channel. Figure 4.25 shows a plot of equivalent permeability as a function of minimum aperture ("throat") of the channel. When this aperture is unity, a parallel channel is obtained. Both Darcy and Navier-Stokes results are shown. The Darcy permeability is taken from cubic law as the square of the local aperture. The discrepancy

## Table 4.1.

## Comparison of Navier-Stokes and Darcy Solution for Permeability of Two Dimensional Periodic Geometries.

| Geometry | Equivalent Permeability | |
|---|---|---|
| | Navier-Stokes | Darcy |
| Figure 4.1 | 0.92 | 1.0 |
| Figure 4.3 | 0.38 | 0.57 |
| Figure 4.5 | 0.12 | 0.905 |
| Figure 4.6 | 0.305 | 0.48 |
| Figure 4.8 | 0.27 | 0.55 |

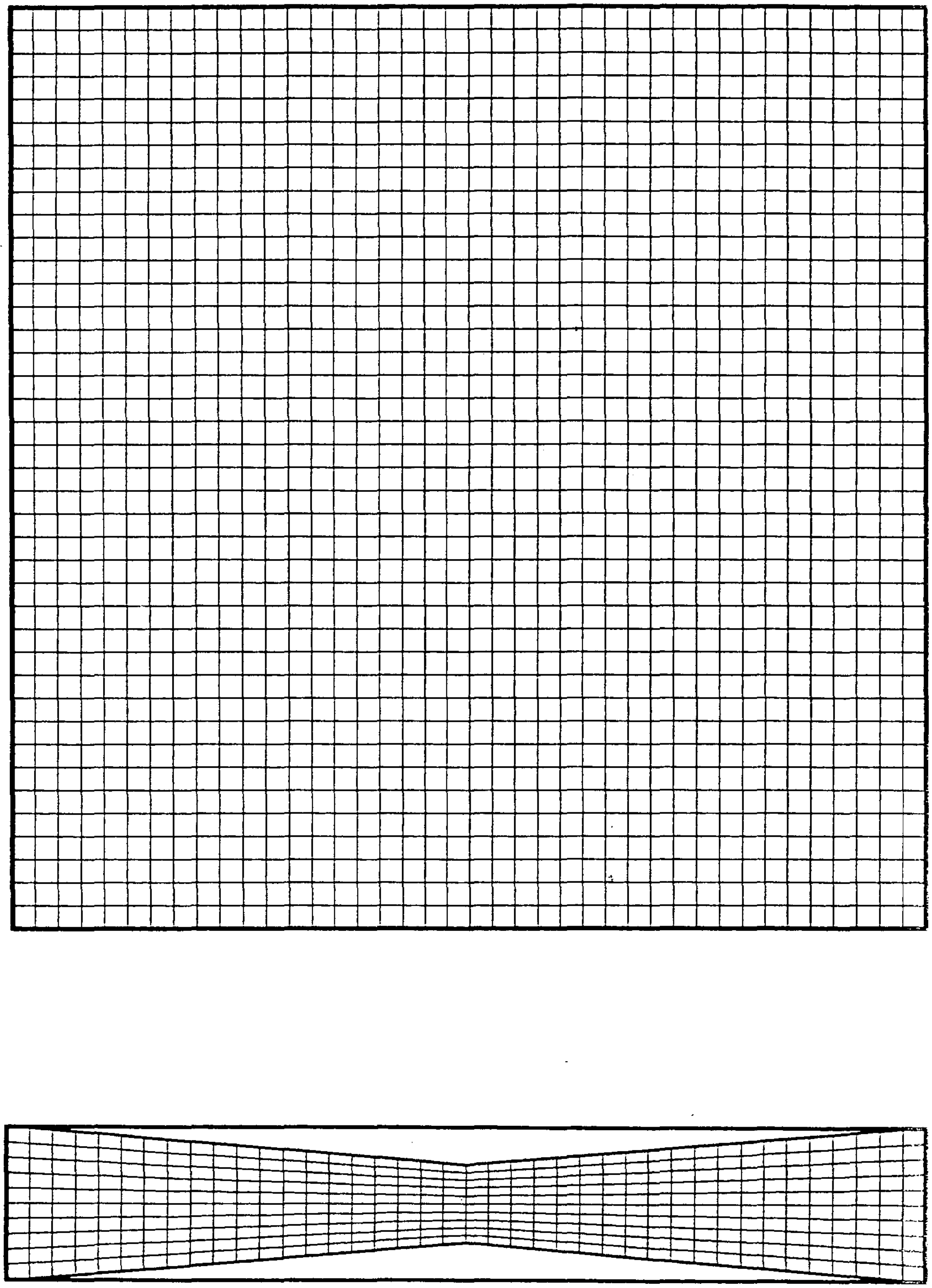

XBL 873-1430

Figure 4.23. Grid in a Three-Dimensional Channel with a Constriction at the Center.

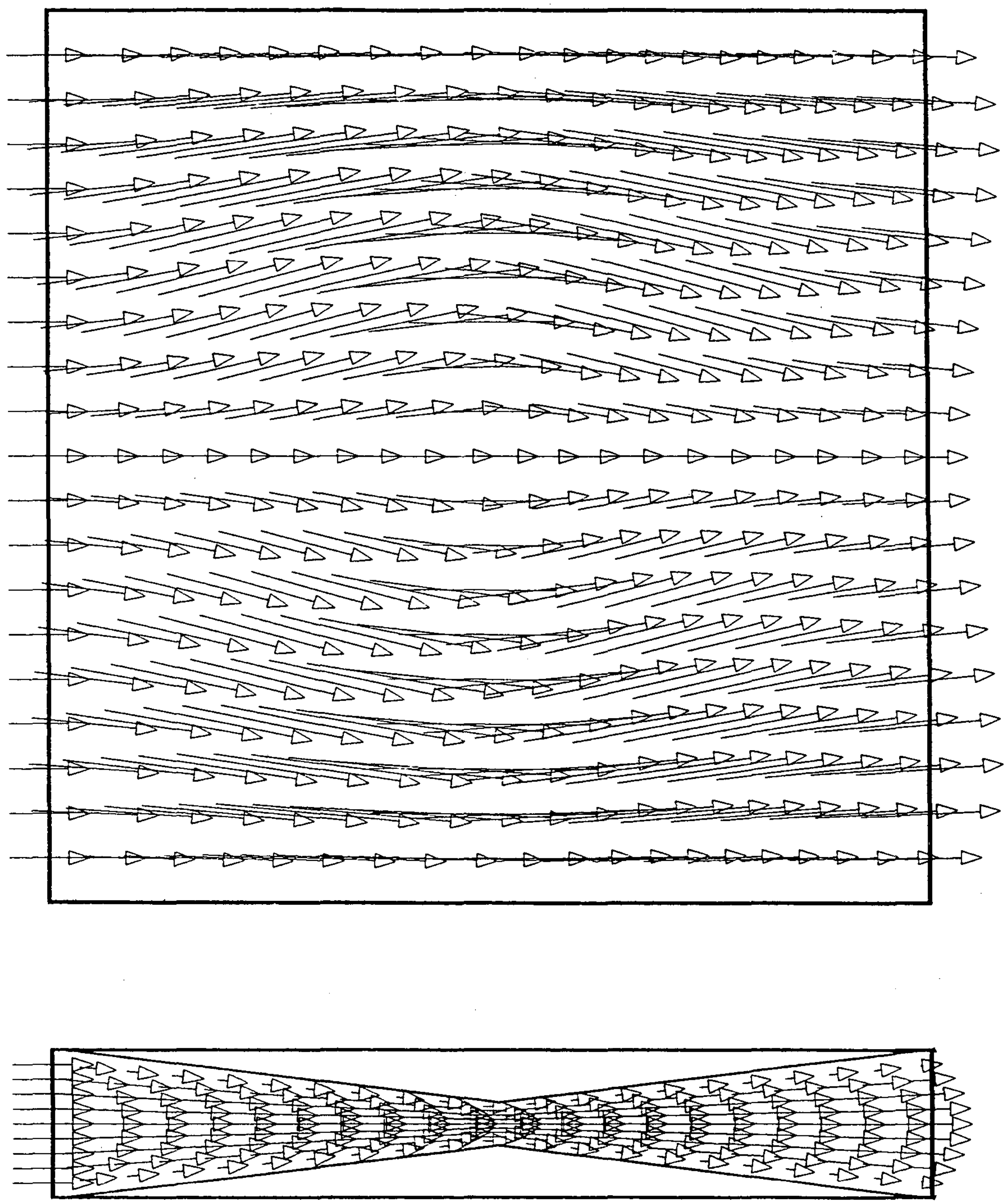


Figure 4.24. Velocity Vector Plot in a Three Dimensional Channel with a Constriction at the Center. Reynolds Number = 5.

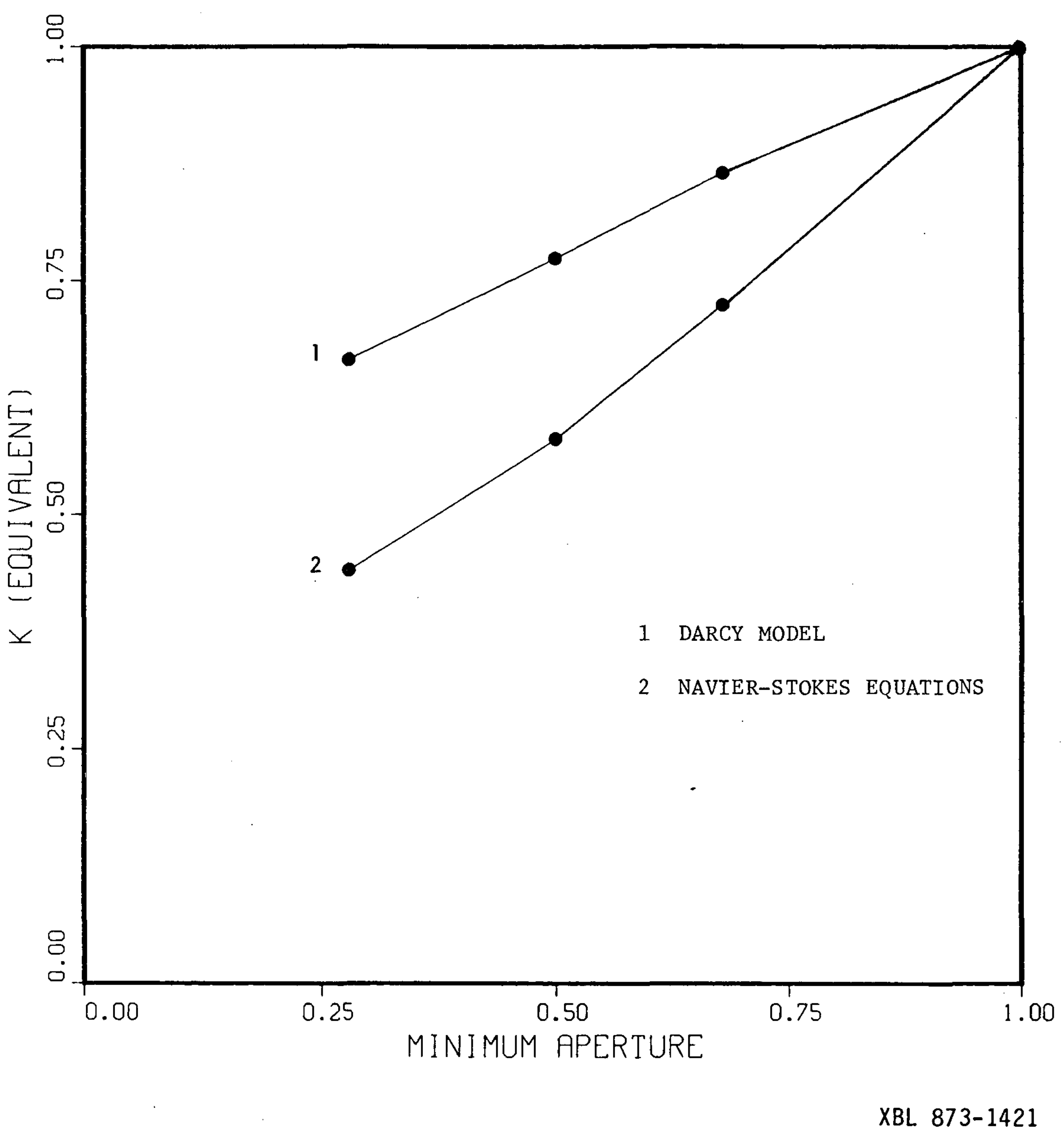


Figure 4.25. Plot of Equivalent Permeability of a Three Dimensional Channel with a Constriction. Comparison of Two Flow Models.

between the two solutions increases with decreasing minimum aperture. This is understandable because it results in an increasingly complex flow path. When the minimum aperture is 0.28, one obtains,

$$K_{eq} \text{ (Darcy)} = 0.6271$$
$$K_{eq} \text{ (Navier–Stokes)} = 0.458 \tag{4.2}$$

The difference between these two values is not large, but does emphasize the role of complexity of flow path on permeability. Figure 4.26 shows a plot of equivalent aperture of the channel, calculated as a square root of equivalent permeability. For the example studied here, its value is always larger than the minimum aperture, suggesting that the equivalent aperture could be determined as some average of the aperture distribution over the channel area. The Darcy value appears closer to the arithmatic average of maximum and minimum apertures, whereas the Navier-Stokes value shows a clear bias towards the minimum aperture.

Figure 4.27 shows grid generation in a channel whose aperture is a variable, and has a circular contact area of about 5 percent at the center. Figure 4.28 shows flow pattern in the channel at a Reynolds number of five. Figure 4.29 shows mean velocity as a function of Re for a parallel channel with and without a contact area. The response of both systems is linear over the range $0 < \text{Re} < 10$. Larger values of Re require more discretization and have not been studied here due to the extent of computation involved. Figure 4.30 shows a plot of equivalent permeability as a function of minimum aperture, with the obstacle in place. For larger minimum apertures, closer to unity, the curves lies below those shown in Figure 4.25. However, at smaller values ($\approx 0.28$) the curves approach those shown in Figure 4.25.

The finite difference method described in this report has been compared to a finite element calculation given by Muralidhar and Bodvarsson (1987). The geometry consists of a two-dimensional channel with one circular contact area, as shown in Figure 4.5. The velocity vector plot obtained in this work is shown in Figure 4.21. The equivalent

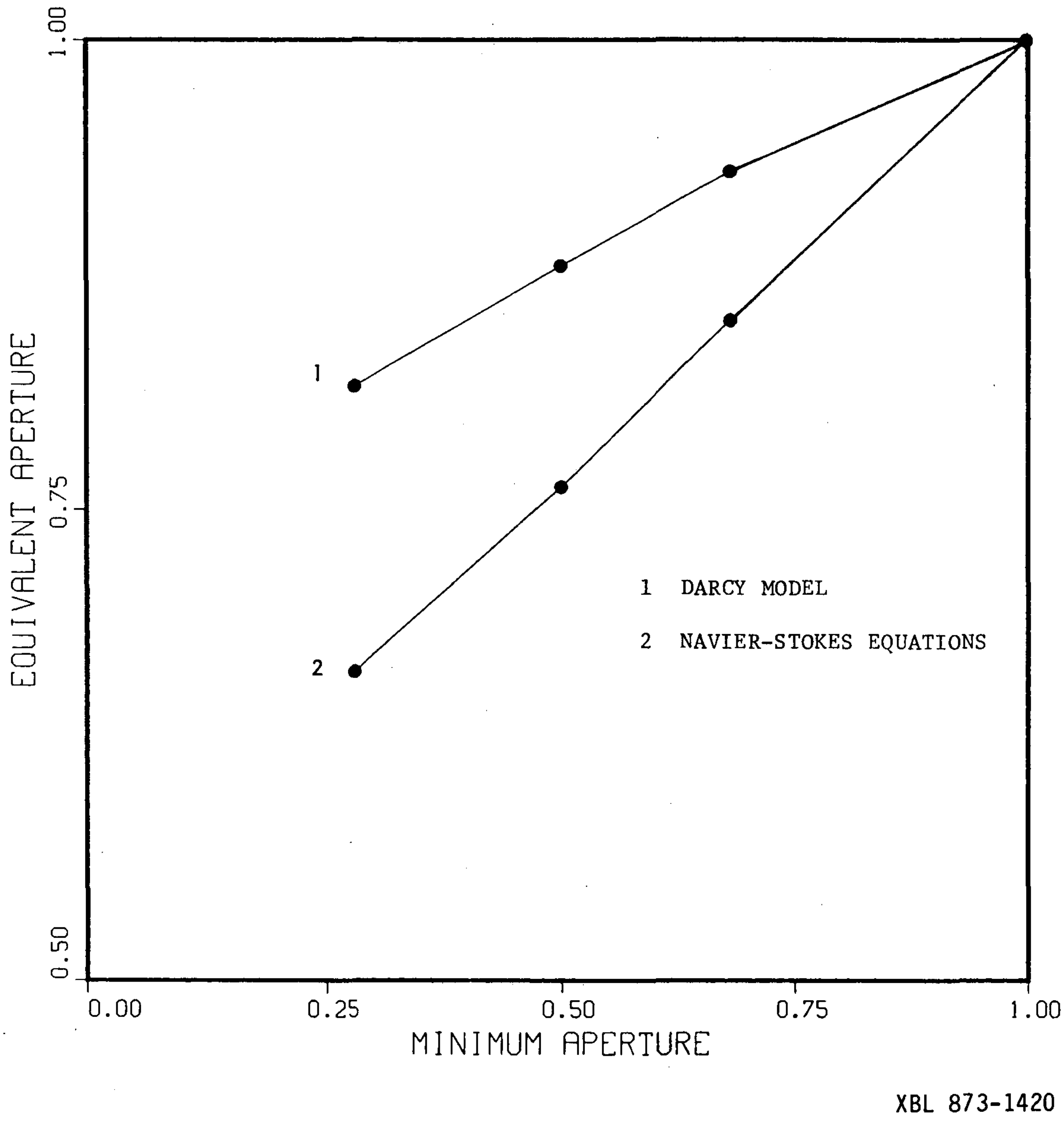


Figure 4.26. Plot of Equivalent Aperture of a Three Dimensional Channel with a Constriction. Comparison of Two Flow Models.

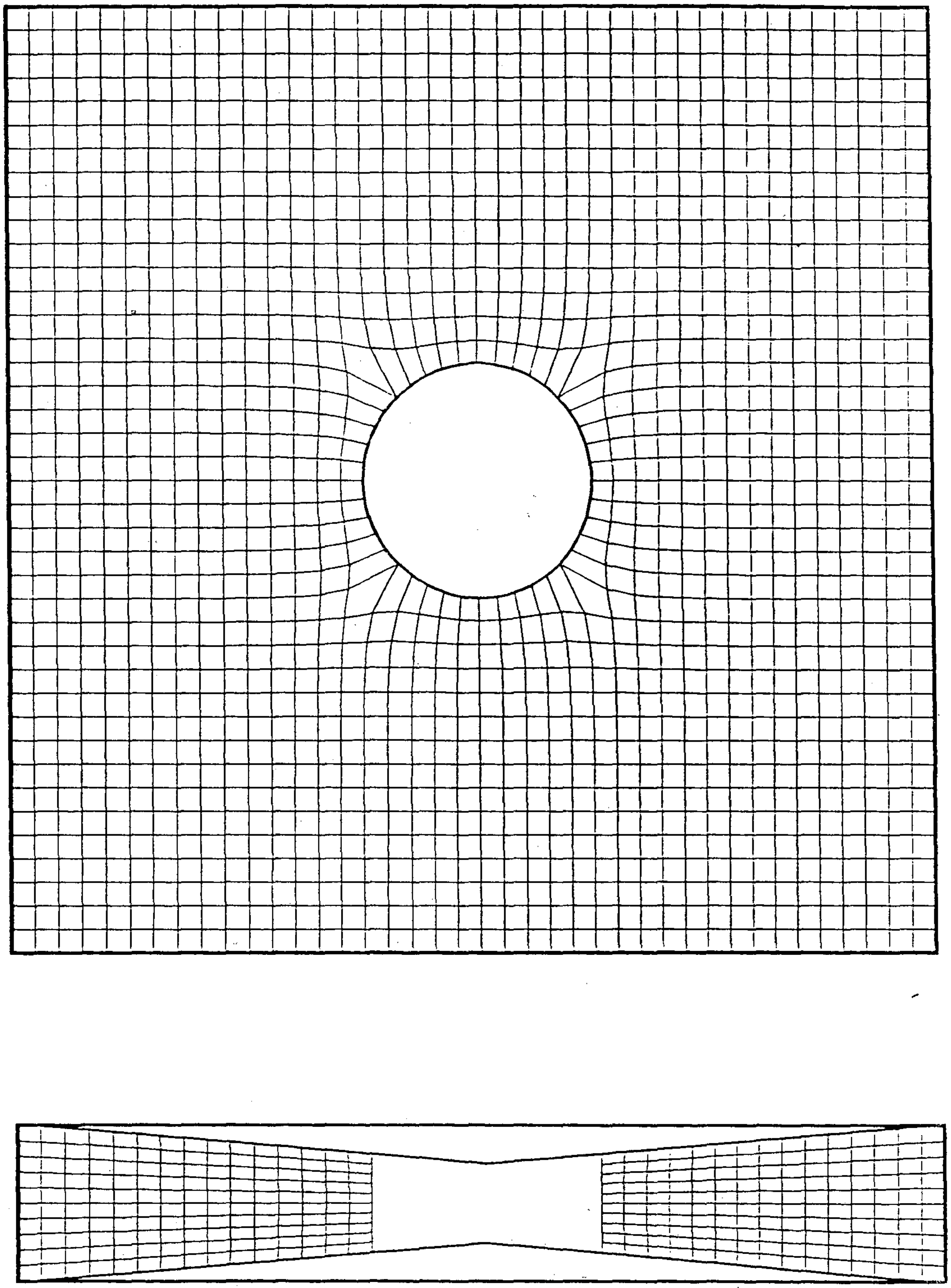

XBL 873-1434

Figure 4.27. Grid in a Three Dimensional Channel with a Constriction and a Circular Contact Area.

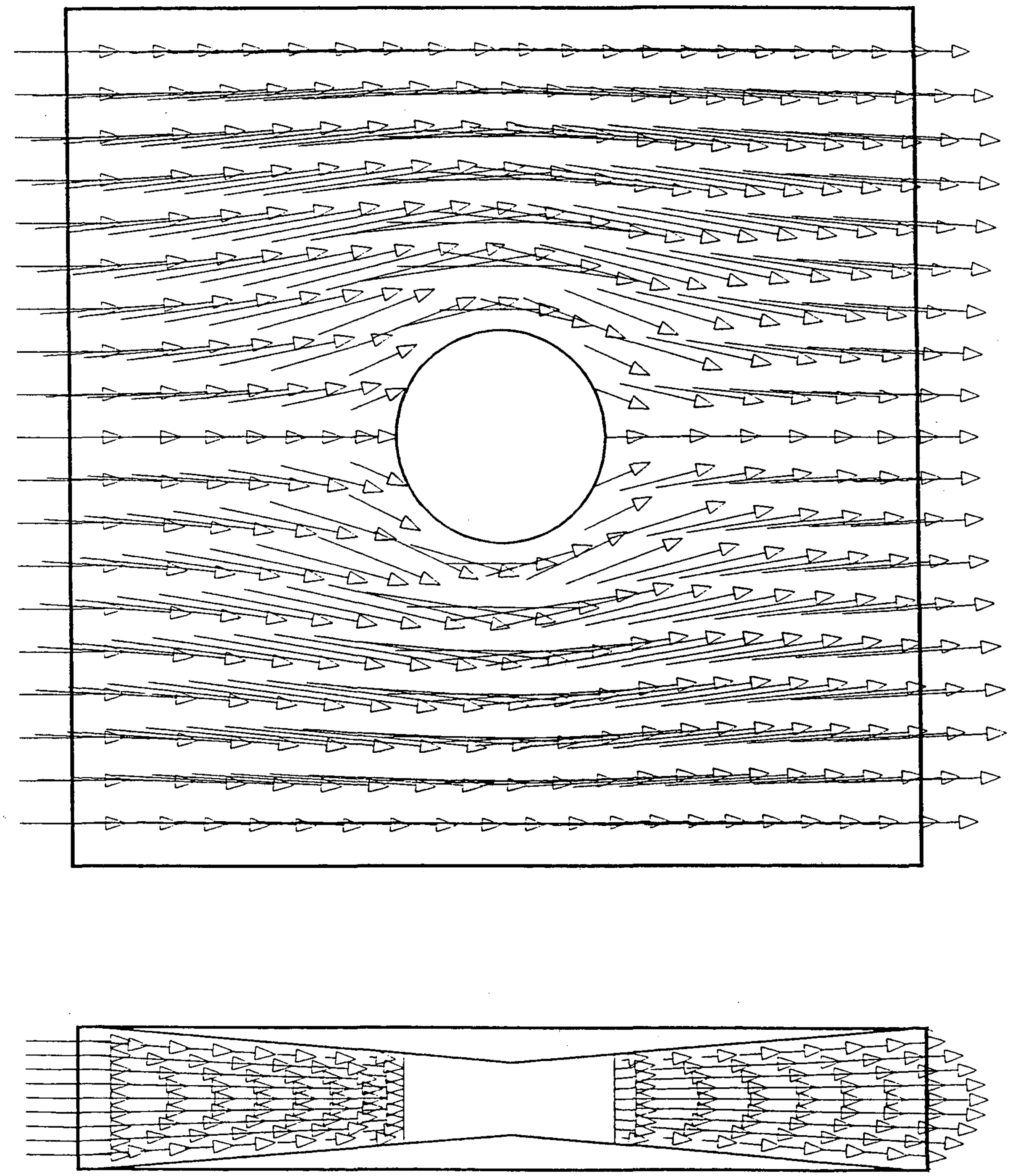

XBL 873-1433

Figure 4.28. Velocity Vector Plot in a Three Dimensional Channel with a Constriction and a Circular Contact Area. Reynolds Number = 5.

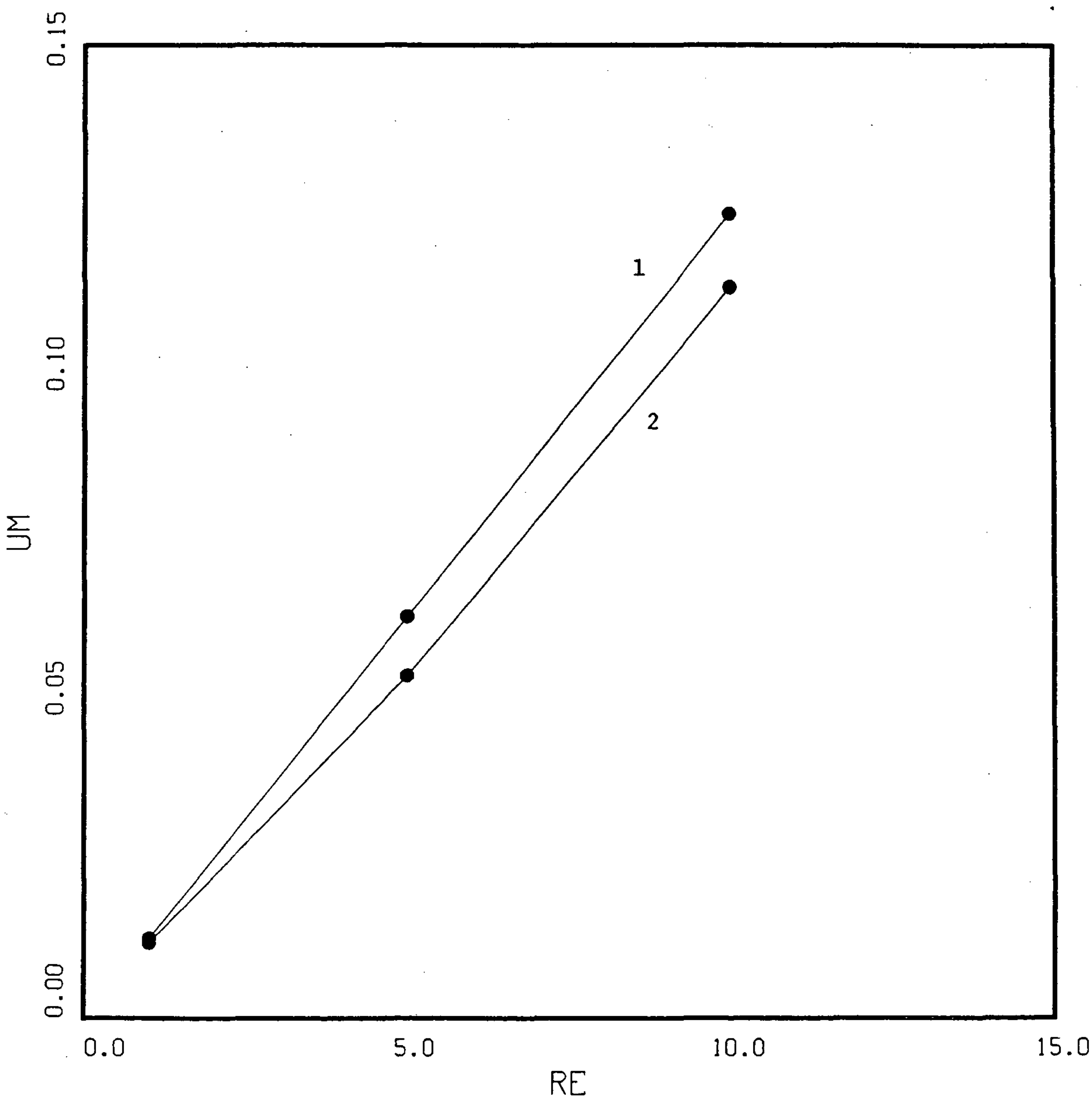


XBL 873-1432

Figure 4.29. Plot of Mean Velocity as a Function of Reynolds Number.
1. Parallel Three Dimensional Channel with no Contact Area,
2. Three Dimensional Channel with a Circular Contact Area, ($\approx$ 5 percent).

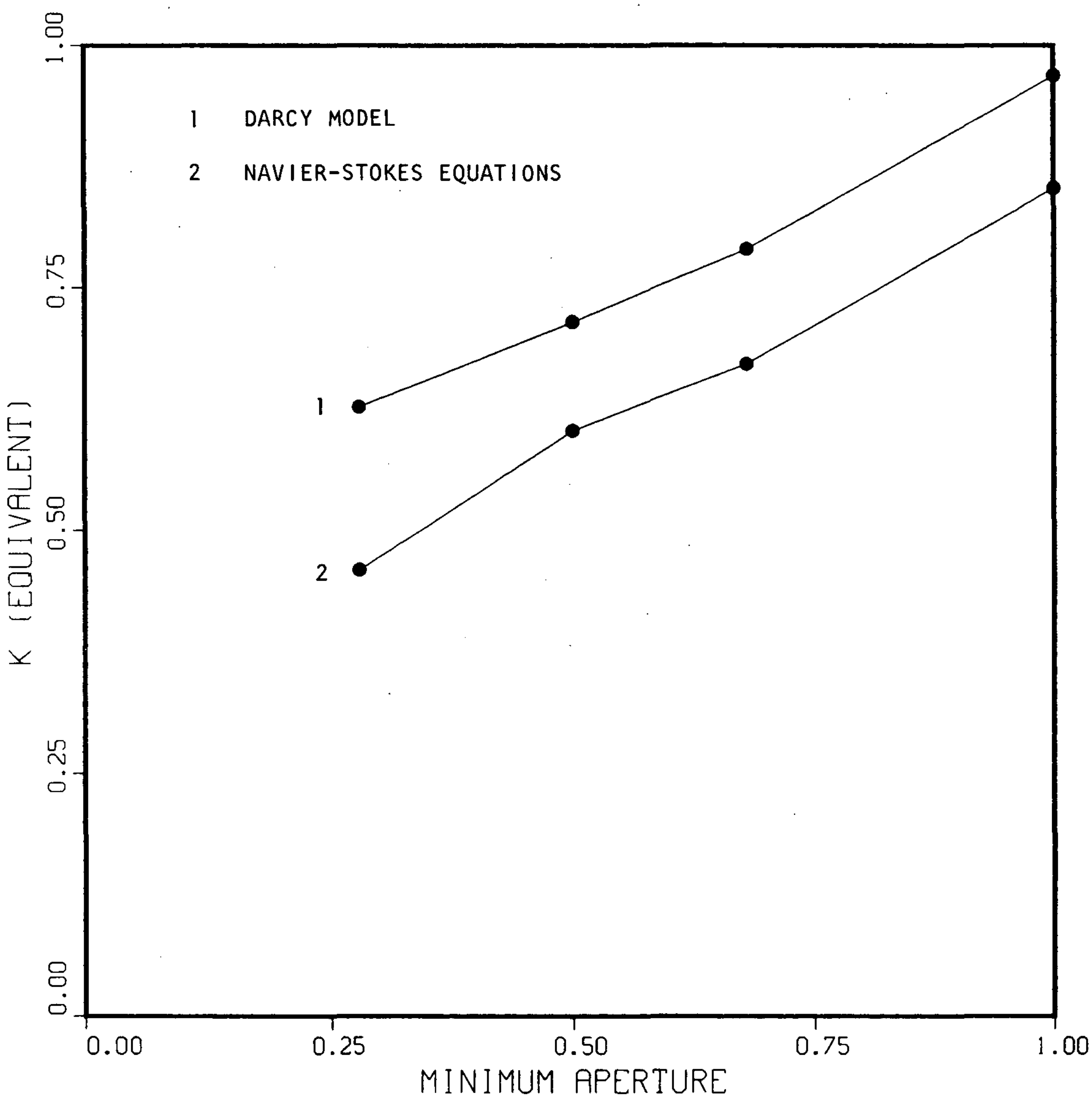


XBL 873-1419

Figure 4.30. Plot of Equivalent Permeability of a Three Dimensional Channel with a Circular Contact Area, and Variable Aperture. Comparison of Two flow Models.

permeability of the flow region, calculated by each procedure is as follows.

$$K_{eq}\,(\text{finite element}) = 0.2087 \tag{4.3}$$
$$K_{eq}\,(\text{finite difference}) = 0.1950$$

Figure 4.31 shows velocity profiles at two locations in the flow domain and agreement between the results of finite element and finite difference calculations is good.

## 4.4 Conclusions

This report describes a method to solve Navier-Stokes equations in complex two and three dimensional geometries. It has been used to solve for flow in model single fractures. This model treats fractures as channels with variable aperture and distributed contact areas. The complicated channel geometries are not well described by conventional orthogonal coordinate systems. This problem has been handled by coordinate transformation which generates a new coordinate system in which the fracture appears regular. The flow equations are written in terms of these coordinates and subsequently solved by finite differences. The flow is assumed to be steady and incompressible. The permeability of the flow domain is determined from the mean velocity which results from a prescribed pressure drop. This has been compared to the equivalent permeability calculated from Darcy's law, applied to a variable permeability region. The variability arises from assigning permeability as zero to contact areas and proportional to square of the local aperture elsewhere.

For the limited set of examples considered in this study, the following conclusions have been reached.

1. Over a range of $1 < Re < 20$, where Re is Reynolds number, inertial effects are small and flow still remains proportional to pressure drop across the fracture.

2. The Darcy permeability is always larger than the Navier-Stokes value. This is because Darcy's law does not correctly calculate pressure drops due to turning of the fluid. In some cases, this can be accounted for by the use of tortuosity

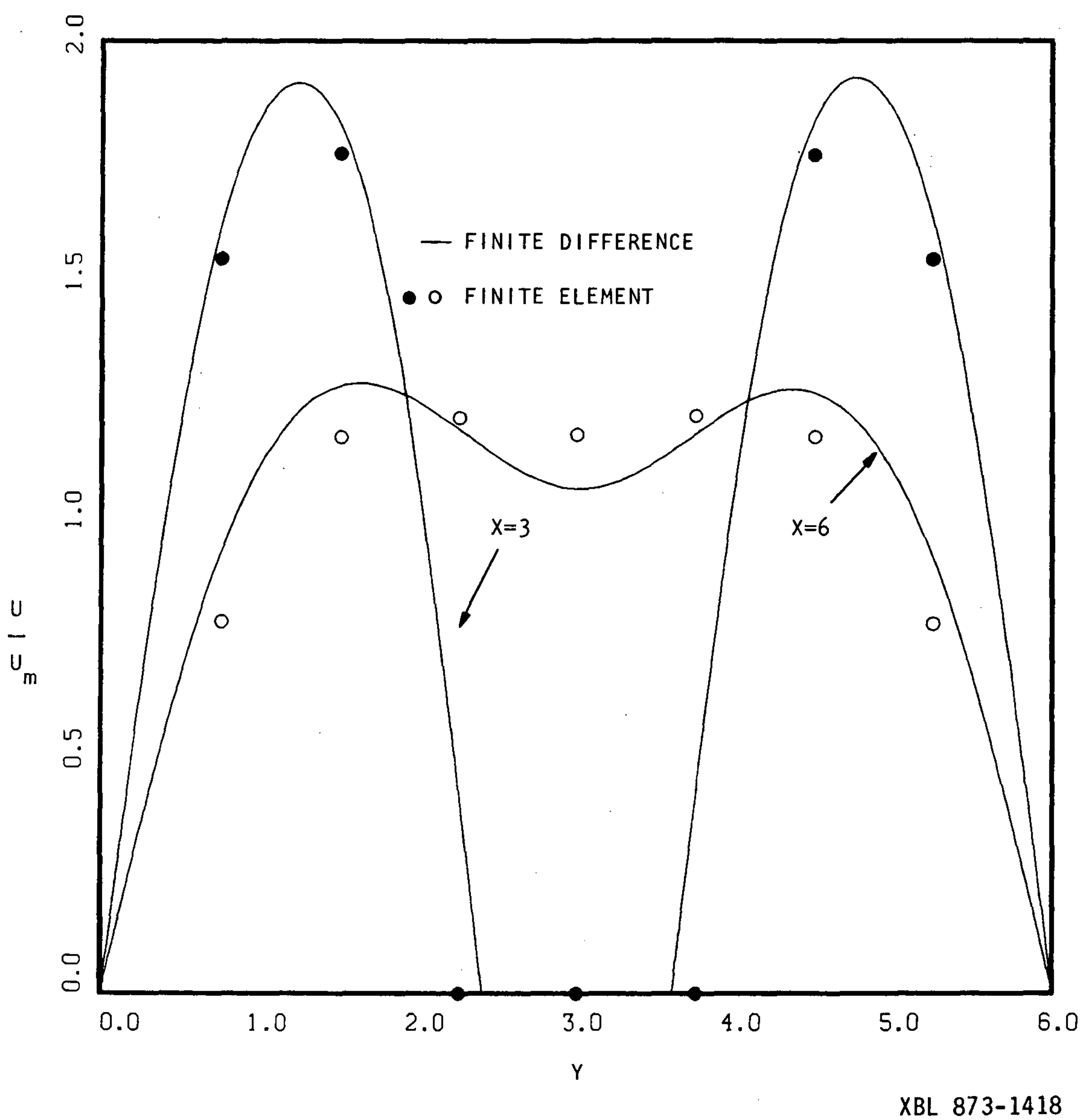


Figure 4.31. Comparison of Finite Element and Finite Difference Solution for Flow Past a Circular Obstacle, Re = 1

factors. The difference between the results of the two models increases as the tortuosity of the flow path increases.

3. A full three dimensional solution of Navier-Stokes equations requires extensive computation, and on an average, exceed the time for Darcy calculation by a factor of thirty. Since the difference in calculated flow rates by the two models is within an order-of-magnitude, the general use of Navier-Stokes equations as a tool for hydrogeology is not recommended. Exceptions are however possible in certain applications such as solute transport, where local velocities have to be calculated with accuracy.

Studies planned for the future involve the use of the technique developed in this report to solve the following problems.

(a) Flow in fractures with realistic and simulated aperture distribution.

(b) Flow in a fracture which is fed by another intersecting fracture.

(c) Extension to unsteady and solute transport problems.

(d) Dependence of equivalent permeability on fineness, distribution and percentage of contact area.

(e) Relationship between applied stress and equivalent permeability.

**REFERENCES**

Altus, E. and Bar-Yoseph, P., 1983, "A 3-D Finite Difference Solution for Orthotropic Laminated Composites Using Curvilinear Coordinates," *Computers and Structures,* Vol. 17, pp. 573-577.

Anderson, D. A., Tannehill, J. C., Pletcher, R. H., 1984, *Computational Fluid Mechanics and Heat Transfer,* McGraw Hill, New York.

Brackbill, M. V. and Saltzmann, J. S., 1982, "Adaptive Zoning for Singular Problems in Two Dimensions," *Journal of Computational Physics,* Vol. 46, pp. 342-368.

Churchill, R. V., 1960, *Complex Variables and Applications,* McGraw Hill, New York.

Eisman, P. R., 1985, "Grid Generation for Fluid Mechanics Computations," *Ann. Rev. Fluid Mechanics,* Vol. 17, pp. 487-522.

Goldman, A. and Kao, Y. C., 1981, "Numerical Solution to a Two-Dimensional Conduction Problem Using Rectangular and Cylindrical Body- Fitted Coordinate Systems," *Journal of Heat Transfer,* Vol. 103, pp. 753-758.

Greenberg, M. D., 1978, *Foundations of Applied Mathematics,* Prentice Hall.

Hughes, T. J. R., 1979, *Finite Element Methods for Convection Dominated Flows,* ASME, New York.

Muralidhar, K. and Bodvarsson, G.S., 1987, "Simulation of Flow on the Face of a Large Aperture Fault," LBL report in preparation.

Napolitano, M. and Orlandi, P., 1985, "Laminar Flow in a Complex Geometry: A Comparison", *Int. J. Numerical Methods in Fluids,* Vol. 5, pp. 667-683.

Patankar, S. V., 1980, *Numerical Heat Transfer and Fluid Flow,* Hemisphere, Washington, D. C.

Peyret, R. and Taylor, T. D., 1983, *Computational Methods of Fluid Flow,* Springer Verlog, New York.

Projan, V., Reiger, H. and Beer, H., 1981, "Numerical Analysis of Laminar Natural Convection between Concentric and Eccentric Cylinders," *Numer. Heat Transfer,* Vol. 4, pp. 131-146.

Pyrak-Nolte, L. J., Myer, L., Cook, N. G. W. and Witherspoon, P. A., 1987, "Hydraulic and Mechanical Properties of Natural Fractures in Low Permeability Rock," to be presented ast 6th International Congress on Rock Mechanics, held in Montreal, Canada, 30 August, 1987.

Schlichting, H., 1979, *Boundary-Layer Theory,* McGraw Hill, New York.

Thompson, J. F., Warsi, Z. U. A. and Mastin, C. W., 1982, "Boundary-Fitted Coordinate Systems for Numerical Solution of Partial Differential Equations - A Review," *J. Computational Physics* Vol. 47, pp. 1-108.

Thompson, J. F., Ed., 1982, *Numerical Grid Generation,* Elsevier Science Publishing Co., New York.

Winslow, A. M., 1966, *J. Computational Physics,* Vol. 1, p. 149.

Zienkiewicz, O. C., 1979, *The Finite Element Method,* McGraw Hill, New York.

## APPENDIX A

### Complete Forms of Coefficients Appearing in Equations 2.4

Coefficients appearing in Eqs. (2.4) are fully defined here. Those arising from Eq. (2.4a) are given first, and the permutation rules to generate the symbols in Eqs. (2.4b, 2.4c) are described next. The algebra involved is not written out since this can be directly performed through a computer program. The notation, (x,y,z) for Cartesian space and (u,v,w) for the transformed space is used here.

$$\alpha ux = \sum \alpha ux_i + \lambda \sum \alpha uxo_i \quad , \quad i = 1,2,3 \tag{A-1}$$

$$\alpha vx = \sum \alpha vx_i + \lambda \sum \alpha vxo_i$$

$$\alpha wx = \sum \alpha wx_i + \lambda \sum \alpha wxo_i$$

$$\alpha uy = \sum \alpha uy_i + \lambda \sum \alpha uyo_i$$

$$\alpha vy = \sum \alpha vy_i + \lambda \sum \alpha vyo_i$$

$$\alpha wy = \sum \alpha wy_i + \lambda \sum \alpha wyo_i$$

$$\alpha uz = \sum \alpha uz_i + \lambda \sum \alpha uzo_i$$

$$\alpha vz = \sum \alpha vz_i + \lambda \sum \alpha vzo_i$$

$$\alpha wz = \sum \alpha wz_i + \lambda \sum \alpha wzo_i$$

$$Ru = \sum Rx_i + \sum Sx_i + \sum Tx_i + \lambda \sum Rxo_i$$

The symbols on the right side of Equation (A-1) are given below. The following abbreviations have been used.

$$a1x(1) = y_v z_w - y_w z_v \tag{A-2}$$

$$a1x(2) = z_v x_w - z_w x_v$$

$$a1x(3) = x_v y_w - x_w y_v$$

(Note that a1x(2) can be obtained from a1x(1) by rotating $x \rightarrow y \rightarrow z \rightarrow x$. Similarly, a1x(3) can be derived from a1x(2). This notation is consistently used below.)

$$a2x(1) = x_v z_w - x_w z_v$$

$$a2x(2) = y_v x_w - y_w x_v$$

$$a2x(3) = z_v y_w - z_w y_v$$

$$a3x(1) = x_v y_w - x_w y_v$$

$$a3x(2) = y_v z_w - y_w z_v$$

$$a3x(3) = z_v x_w - z_w x_v$$

$$b1x(1) = y_u z_w - y_w z_u$$

$$b1x(2) = z_u x_w - z_w x_u$$

$$b1x(3) = x_u y_w - x_w y_u$$

$$b2x(1) = y_u z_v - y_v z_u$$

$$b2x(2) = z_u x_v - z_v x_u$$

$$b2x(3) = x_u y_v - x_v y_u$$

$$b3x(1) = x_w z_u - x_u z_w$$

$$b3x(2) = y_w x_u - y_u x_w$$

$$b3x(3) = z_w y_u - z_u y_w$$

$$b4x(1) = x_w y_u - x_u y_w$$

$$b4x(2) = y_w z_u - y_u z_w$$

$$b4x(3) = z_w x_u - z_u x_w$$

$$c1x(1) = x_u y_v - x_v y_u$$

$$c1x(2) = y_u z_v - y_v z_u$$

$$c1x(3) = z_u x_v - z_v x_u$$

$$d1x(1) = x_v z_u - x_u z_v$$

$$d1x(2) = y_v x_u - y_u x_v$$

$$d1x(3) = z_v y_u - z_u y_v$$

The second set of symbols are the following.

$$x1 = a2x(1) \cdot z_w + a3x(1) \cdot y_w \tag{A-3}$$

$$x2 = a2x(1) \cdot z_v + a3x(1) \cdot y_v$$

$$x3 = b3x(1) \cdot z_w + b4x(1) \cdot y_w$$

$$x4 = b3x(1) \cdot z_u + b4x(1) \cdot y_u$$

$$x5 = -d1x(1) \cdot z_v + c1x(1) \cdot y_v$$

$$x6 = -d1x(1) \cdot z_u + c1x(1) \cdot y_u$$

$$P1 = y_u z_{uw} - y_{uw} z_u$$

$$P2 = y_u z_{uv} - z_u y_{uv}$$

$$P3 = y_v z_{vw} - z_v y_{vw}$$

$$P4 = z_v y_{uv} - y_v z_{uv}$$

$$P5 = x_v z_{vw} - z_v x_{vw}$$

$$P6 = x_v y_{vw} - y_v x_{vw}$$

$$P7 = z_w y_{vw} - y_w z_{vw}$$

$$P8 = z_w\ y_{uw} - y_w z_{uw}$$

$$P9 = z_w x_{vw} - x_w z_{vw}$$

$$P10 = y_w x_{vw} - x_w y_{vw}$$

$$R1 = z_u x_{uw} - x_u z_{uw}$$

$$R2 = y_u x_{uw} - x_u y_{uw}$$

$$R3 = x_w z_{uw} - z_w x_{uw}$$

$$R4 = x_w y_{uw} - y_w x_{uw}$$

$$S1 = x_u z_{uv} - z_u x_{uv}$$

$$S2 = x_u y_{uv} - y_u x_{uv}$$

$$S3 = z_v x_{uv} - x_v z_{uv}$$

$$S4 = y_v x_{uv} - x_v y_{uv}$$

The following notation is used for quantities appearing in the smoothness integral.

$$Du = J^2(\nabla u)^2 = (a1x(1))^2 + (a1x(2))^2 + (a1x(3))^2 \tag{A-4}$$

$$Dv = J^2(\nabla u)^2 = (b1x(1))^2 + (b1x(2))^2 + (b1x(3))^2$$

$$Dw = J^2(\nabla w)^2 = (b2x(1))^2 + (b2x(2))^2 + (b2x(3))^2$$

$$Duv = J(\nabla u \cdot \nabla v) = -a1x(1) \cdot b1x(1) - a1x(2) \cdot b1x(2) - a1x(3) \cdot b1x(3)$$

$$Dvw = J^2(\nabla v \cdot \nabla w) = -b1x(1) \cdot b2x(1) - b1x(2) \cdot b2x(2) - b1x(3) \cdot b2x(3)$$

$$Dvw = J^2(\nabla u \cdot \nabla w) = a1x(1) \cdot b2x(1) + a1x(2) \cdot b2x(2) + a1x(3) \cdot b2x(3)$$

The following symbols appear exclusively in the orthogonality integral.

$$PO1 = a1x(2) \cdot z_w - a1x(3) \cdot y_w \tag{A-5}$$

$$PO2 = b1x(2) \cdot z_w - b1x(3) \cdot y_w$$

$$PO3 = b1x(3) \cdot y_v - b1x(2) \cdot z_v + a1x(3) \cdot y_u - a1x(2) \cdot z_u$$

$$RO1 = b2x(2) \cdot z_w - b2x(3) \cdot y_w - b1x(3) \cdot y_v + b1x(2) \cdot z_v$$

$$RO2 = b1x(3) \cdot y_u - b1x(2) \cdot z_u$$

$$RO3 = b2x(3) \cdot y_u - b2x(2) \cdot z_u$$

$$SO1 = a1x(3) \cdot y_v - a1x(2) \cdot z_v$$

$$SO2 = a1x(2) \cdot z_u - a1x(3) \cdot y_u + b2x(3) \cdot y_w - b2x(2) \cdot z_w$$

$$SO3 = b2x(2) \cdot z_v - b2x(3) \cdot y_v$$

Terms appearing in Eq. (A-1) are now defined. They are written in the same order as that of differentiation arising from the EL operator. This order is $\frac{\partial}{\partial u}\frac{\partial}{\partial x_u}(\nabla u)^2 J$, $\frac{\partial}{\partial v}\frac{\partial}{\partial x_v}(\nabla u)^2 J$, . . . $\frac{\partial}{\partial w}\frac{\partial}{\partial x_w}(\nabla w)^2 J$. This is followed by the terms arising from the orthogonality integral $I_o$, with $(\nabla u)^2$ replaced by $(\nabla u \cdot \nabla v)^2 J^4$ etc.

$$\alpha u x_1 = \frac{2}{J^3}(a1x(1))^2 Du \tag{A-6}$$

$$\alpha u y_1 = -\frac{2}{J^3}(a1x(1) \cdot a2x(1) Du$$

$$\alpha u z_1 = \frac{2}{J^3}\, a1x(1) \cdot a3x(1) \cdot Du$$

$$Rx_1 = \frac{2}{J^3}\, a1x(1)\, Du \left[x_u (a1x(1))_u - b1x(1) \cdot x_{uv} + x_{uw} b2x(1) - P1 \cdot x_v + x_w P2 \right]$$

$$- \frac{Du}{J^2}(a1x(1))_u - \frac{2a1x(1)}{J^2}\left[a1x(1) \cdot (a1x(1))_u + a2x(1) \cdot (a2x(1))_u + a3x(1) \cdot (a3x(1))_u \right]$$

$$\alpha v x_1 = 2\left(\frac{Du}{J^3}\, b1x(1) + \frac{2}{J^2}\, x1\right) b1x(1) + \frac{2}{J}(z_w^2 + y_w^2)$$

$$\alpha v y_1 = 2b3x(1)\left(\frac{Du}{J^3}\, b1x(1) + \frac{1}{J^2} x1\right) - \frac{2}{J}\, x_w y_w + \frac{2}{J^2}\, b1x(1)\left(z_w a1x(1) - x_w a3x(1)\right)$$

$$\alpha v z_1 = -2b4x(1)\left(\frac{Du}{J^3}\, b1x(1) + \frac{1}{J^2}\, x1\right) - \frac{2}{J}\, x_w z_w - \frac{2}{J^2}\, b1x(1)\left(a1x(1) \cdot y_w + x_w \cdot a2x(1)\right)$$

$$Rx_2 = \left\{ \left( -2b1x(1) \cdot \frac{Du}{J^3} - \frac{2}{J^2}\, x1 \right) \left( x_{uv}a1x(1) + P3 \cdot x_u - x_v(b1x(1))_v + x_{vw}b2x(1) + P4 \cdot x_w \right) \right]$$

$$+ \frac{2}{J} \left[ z_{vw} \cdot a2x(1) + y_{vw} \cdot a3x(1) + z_w \cdot P5 + y_w \cdot P6 \right]$$

$$+ \frac{Du}{J^2}\, (b1x(1))_v + \frac{2}{J^2}\, b1x(1) \left[ P3 \cdot a1x(1) + P5 \cdot a2x(1) + P6 \cdot a3x(1) \right]$$

$$\alpha wx_1 = 2b2x(1) \left[ \frac{b2x(1)}{J^3}\, Du + \frac{1}{J^2}\, x2 \right] + \frac{2}{J^2}\, b2x(1) \left( z_v a2x(1) + y_v a3x(1) \right] + \frac{2}{J}\, (y_v^2 + z_v^2)$$

$$\alpha wy_1 = 2d1x(1) \left[ \frac{Du}{J^3}\, b2x(1)) + \frac{1}{J^2}\, x2 \right] - \frac{2}{J^2}\, b2x(1) \left( x_v a3x(1) - z_v a1x(1) \right) - \frac{2}{J}\, x_v y_v$$

$$\alpha wz_1 = 2c1x(1) \left[ \frac{b2x(1)}{J^3}\, Du + \frac{1}{J^2}\, x2 \right] - \frac{2b2x(1)}{J^2} \left( a1x(1) \cdot y_v + a2x(1) \cdot x_v \right) - \frac{2}{J}\, x_v z_v$$

$$Rx_3 = 2 \left[ \left( \frac{Du}{J^3}\, b2x(1) + \frac{1}{J^2}\, x2 \right) \left( a1x(1) \cdot x_{uw} + P7 \cdot x_u - x_{vw} \cdot b1x(1) - x_v \cdot P8 + x_w(b2x(1))_w \right) \right]$$

$$- \frac{Du}{J^2}\, (b2x(1))_w - \frac{2b2x(1)}{J^2} \left[ a1x(1) \cdot P7 + a2x(1) \cdot P9 + a3x(1) \cdot P10 \right]$$

$$- \frac{2}{J} \left[ z_{vw} \cdot a2x(1) + y_{vw} \cdot a3x(1) + z_v \cdot P9 + y_v \cdot P10 \right]$$

(The remaining symbols can be obtained by permuting the indices $u \rightarrow v \rightarrow w \rightarrow u$ as given in the text. However, for completeness, all the symbols will be defined here.)

$$\alpha ux_2 = 2a1x(1) \left[ \frac{a1x(1)}{J^3} \cdot Dv + \frac{1}{J^2} x3 \right] + \frac{2a1x(1)}{J^2} \left( z_w b3x(1) + y_w b4x(1) \right) + \frac{2}{J}(y_w^2 + z_w^2)$$

$$\alpha uy_2 = -2a2x(1) \left[ \frac{Dv}{J^3}\, a1x(1) + \frac{1}{J^2} x3 \right] - \frac{2a1x(1)}{J^2} \left( x_w b4x(1) + z_w b1x(1) \right) - \frac{2}{J}\, x_w y_w$$

$$\alpha uz_2 = 2a3x(1) \left[ \frac{Dv}{J^3}\, a1x(1) + \frac{1}{J^2}\, x_3 \right] - \frac{2a1x(1)}{J^2} \left( x_w b3x(1) - y_w b1x(1) \right) - \frac{2}{J}\, x_w z_w$$

$$Sx_1 = 2\left[\left(\frac{Dv}{J^3}\, a1x(1) + \frac{1}{J^2}\, x3\right)\left(-x_{uv}\, b1x(1) - P1 \cdot x_v + x_{uw}\, b2x(1) + P2 \cdot x_w + x_u(a1x(1))_u\right)\right.$$

$$- \frac{Dv}{J^2}\,(a1x(1))_u - \frac{2}{J^2} a1x(1)\ \left[P1 \cdot b1x(1) + b3x(1) \cdot R1\right.$$

$$\left. + \ b4x(1) \cdot R2\right] - \frac{2}{J}\left[z_{uw} b3x(1) + y_{uw} b4x(1) + z_w\, R1 + y_w\, R2\right]$$

$$\alpha vx_2 = \frac{2}{J^3}\,(b1x(1))^2 Dv$$

$$\alpha vy_2 = \frac{2}{J^3} b1x(1) \cdot b3x(1) Dv$$

$$\alpha vz_2 = -\frac{2}{J^3} b1x(1) \cdot b4x(1) Dv$$

$$Sx_2 = \frac{-2}{J^3}\, b1x(1) Dv\left[-x_v(b1x(1))_v + b2x(1) \cdot x_{vw} + a1x(1) \cdot x_{uv} + x_w\, P4 + x_u\, P3\right]$$

$$+ \frac{Dv}{J^2}\,(b1x(1))_v + \frac{2b1x(1)}{J^2}\left[b1x(1) \cdot (b1x(1))_v + b3x(1) \cdot (b3x(1))_v + b4x(1) \cdot (b4x(1))_v\right]$$

$$\alpha wx_2 = -2b2x(1)\,\left(-\frac{Dv}{J^3}\, b2x(1) + \frac{2}{J^2}\, x4\right) + \frac{2}{J}\,(z_u^2 + y_u^2)$$

$$\alpha wy_2 = -2d1x(1)\left(-\frac{b2x(1)}{J^3}\, Dv + \frac{1}{J^2}\, x4\right) - \frac{2}{J}\, x_u y_u + \frac{2}{J^2}\, b2x(1)\,(z_u b1x(1) + x_u\, b4x(1))$$

$$\alpha wz_2 = -2c1x(1)\,\left(-\frac{b2x(1)}{J^3}\, Dv + \frac{1}{J^2}\, x4\right) - \frac{2}{J}\, x_u z_u + \frac{2}{J^2}\, b2x(1)\,(-b1x(1) \cdot y_u + b3x(1) \cdot x_u)$$

$$Sx_3 = \left[\left(\frac{2b2x(1)}{J^3}\, Dv - \frac{2}{J^2}\, x_4\right)\left(-\, b1x(1) \cdot x_{vw} - P8 \cdot x_v + x_w(b2x(1))_w + x_{uw} a1x(1) + x_u\, P7\right)\right]$$

$$+ \frac{2}{J}\,(b3x(1) \cdot z_{uw} + b4x \cdot y_{uw} + z_u\, R3 + y_u\, R4)$$

$$- \frac{Dv}{J^2}\,(b2x(1))_w - \frac{2}{J^2} b2x(1)(P8 \cdot b1x(1) + b3x(1) \cdot R3 + b4x(1) \cdot R4)$$

$$\alpha ux_3 = -2a1x(1)\left(\frac{-Dw}{J^3}\, a1x(1) + \frac{2}{J^2}\, x5\right) + \frac{2}{J}\,(z_v^2 + y_v^2)$$

$$\alpha uy_3 = 2a2x(1)\left(\frac{-a1x(1)}{J^3}\, Dw + \frac{1}{J^2}\, x5\right) - \frac{2}{J}\, x_v y_v - \frac{2}{J^2}\, a1x(1)\,\left(z_v b2x(1) - x_v\, c1x(1)\right)$$

$$\alpha uz_3 = -2a3x(1)\left(\frac{-a1x(1)}{J^3}\,Dw + \frac{1}{J^2}\,x5\right) - \frac{2}{J}\,x_v z_v + \frac{2}{J^2}\,a1x(1)\left(b2x(1)\cdot y_v - d1x(1)\cdot x_v\right)$$

$$Tx_1 = \left[\left(\frac{2a1x(1)}{J^2}\,Dw - \frac{2}{J^2}\,x5\right)\left(x_{uw}\,b2x(1) + x_w P2 + x_u(a1x(1))_u - b1x(1)\cdot x_{uv} - P1\cdot x_v\right)\right]$$

$$+ \frac{2}{J}\left(-z_{uv}d1x(1) + c2x(1)\cdot y_{uv} + z_v S1 + y_v\,S2\right) - \frac{1}{J^2}\,Dw(a1x(1))_u$$

$$- \frac{2}{J^2}\,a1x(1)\left(b2x(1)\cdot P2 - d1x(1)\cdot S1 + c1x(1)\cdot S2\right)$$

$$\alpha vx_3 = -2b1x(1)\left(\frac{-Dw}{J^3}\,b1x(1) + \frac{1}{J^2}\,x6\right) - \frac{2}{J^2}\,b1x(1)\,(-\,z_u d1x(1) + y_u c1x(1)) + \frac{2}{J}(y_u^2 + z_u^2)$$

$$\alpha vy_3 = -2b3x(1)\left(\frac{-Dw}{J^3}\,b1x(1) + \frac{x6}{J^2}\right) + \frac{2}{J^2}b1x(1)\cdot(x_u c1x(1) - z_u b2x(1)) - \frac{2}{J}\,x_u y_u$$

$$\alpha vz_3 = 2b4x(1)\left(\frac{-b1x(1)}{J^3}\,Dw + \frac{1}{J^2}\,x6\right) + \frac{2}{J^2}b1x(1)\left(-d1x(1)\,x_u + b2x(1)y_u\right) - \frac{2}{J}\,x_u z_u$$

$$Tx_2 = 2\left[\left(\frac{-b1x(1)}{J^3}\,Dw + \frac{1}{J^2}\,x6\right)(b2x(1)\cdot x_{vw} + P4\cdot x_w + x_{uv}a1x(1) + P3\cdot x_u - x_v(b1x(1))_v\right)$$

$$+ \frac{Dw}{J^2}(b1x(1))_v + \frac{2}{J^2}\,b1x(1)\left[b2x(1)\,P4 - d1x(1)\cdot S3 + c1x(1)\cdot S4\right]$$

$$- \frac{2}{J}\left[-d1x(1)\cdot z_{uv} + y_{uv}c1x(1) + z_u\cdot S3 + y_u\cdot S4\right]$$

$$\alpha wx_3 = \frac{2}{J^3}\,(b2x(1))^2\,Dw$$

$$\alpha wy_3 = \frac{2}{J^3}\,b2x(1)\,d1x(1)\,Dw$$

$$\alpha wz_3 = \frac{2}{J^3}\,b2x(1)\,c1x(1)\,Dw$$

$$Tx_3 = \frac{2}{J^3}\,b2x(1)\,Dw\left[x_w(b2x(1))_w + x_{uw}a1x(1) - x_{vw}b1x(1) + x_u\,P7 - x_v\,P8\right] - \frac{Dw}{J^2}\,(b2x(1))_w$$

$$- \frac{2}{J^2}\,b2x(1)\left[b2x(1)(b2x(1))_w + d1x(1)(d1x(1))_w + c1x(1)(c1x(1))_w\right]$$

The coefficients corresponding to the orthogonality integral (and distinguished from those of the smoothing integral by an 'o', e.g., $\alpha$uxo) are given completely here

$$\alpha uxo_1 = -2PO1(z_w a2x(1) + y_w a1x(3)) \tag{A-7}$$

$$\alpha vxo_1 = 2PO2(z_w b1x(2) - y_x b1x(3))$$

$$\alpha wxo_1 = 2PO3\,(z_u a2x(1) - z_v b1x(2) + y_u a1x(3) + y_v b1x(3)) - 4Duv(y_u y_v + z_u z_v)$$

$$\alpha uyo_1 = 2PO1(x_w a1x(3) - z_w a1x(1))$$

$$\alpha vyo_1 = 2PO2(x_w b1x(3) - z_w b1x(1))$$

$$\alpha wyo_1 = 2PO3(z_v b1x(1) - x_u a1x(3) - x_v b1x(3) + z_u a1x(1)) + 2Duv(x_u y_v + x_v y_u)$$

$$\alpha uzo_1 = 2PO1(y_w a1x(1) + x_w a2x(1))$$

$$\alpha vzo_1 = 2PO2(y_w b1x(1) - x_w b1x(2))$$

$$\alpha wzo_1 = 2PO3(-y_u a1x(1) - y_v b1x(1) - x_u a2x(1) + x_v b1x(2)) + 2Duv(x_u z_v + x_v z_u)$$

$$Rxo_1 = 2Duv\left[z_{uw} a1x(2) + z_w(a1x(2)_u - y_{uw} a1x(3) - y_w(a1x(3))_u\right]$$

$$+ 2PO1\Big[-P1 \cdot a1x(1) - b1x(1) \cdot (a1x(1))_u + a2x(1) \cdot R1 + b1x(2) \cdot (a2x(1))_u$$

$$+ R2 \cdot a1x(3) - b1x(3) \cdot (a1x(3))_u\Big]$$

$$+ 2Duv\left[z_{vw} b1x(2) + z_w(b1x(2))_v - y_{vw} b1x(3) - y_w(b1x(3))_v\right]$$

$$+ 2PO2\Big[- a1x(1)(b1x(1))_v - P3 \cdot b1x(1)$$

$$+ a2x(1)(b1x(2))_v + P5 \cdot b1x(2) - a1x(3)(b1x(3))_v - P6 \cdot b1x(3)\Big]$$

$$+ 2Duv\Big[-z_{vw} b1x(2) - z_{uw} a1x(2) + b1x(3) y_{vw} + a1x(3) y_{uw} - z_v\, R3$$

$$+ P9 \cdot z_u - R4 \cdot y_v + y_u\, P10\Big]$$

$$+ 2PO3\left[-P8 \cdot a1x(1) + P7 \cdot b1x(1) + R3 \cdot a2x(1) + P9 \cdot b1x(2) + R4 \cdot a1x(3) - b1x(3) \cdot P10\right]$$

$$\alpha uxo_2 = 2RO1\Big(z_v b1x(2) + z_w b2x(2) - y_v b1x(3) - y_w b2x(3)\Big) - 4Dvw(y_v y_w + z_v z_w)$$

$$\alpha vxo_2 = 2RO2(y_u b1x(3) - z_u b1x(2))$$

$$\alpha wxo_2 = 2RO3(y_u b2x(3) - z_u b2x(2))$$

$$\alpha uyo_2 = 2RO1(-z_v b1x(1) - z_w b2x(1) + x_v b1x(3) + x_w b2x(3)) + 2Dvw(x_v y_w + x_w y_v)$$

$$\alpha vyo_2 = 2RO2(z_u b1x(1) - x_u b1x(3))$$

$$\alpha wyo_2 = 2RO3(z_u b2x(1) - x_u b2x(3))$$

$$\alpha uzo_2 = 2RO1(y_w b2x(1) + y_v b1x(1) - x_v b1x(2) - x_w b2x(2)) + 2Dvw(x_v z_w + x_w z_v)$$

$$\alpha vzo_2 = 2RO2(x_u b1x(2) - y_u b1x(1))$$

$$\alpha wzo_2 = 2RO3(x_u b2x(2) - y_u b2x(1))$$

$$\begin{aligned}
Rxo_2 = {} & 2Dvw\Big[y_{uv} b1x(3) + y_u (b1x(3))_v - z_{uv} b1x(2) - z_u (b1x(2))_v\Big] \\
& + 2RO2\Big[b1x(2) \cdot S3 - b2x(1)(b1x(1))_v - P4 \cdot b1x(1) - S4 \cdot b1x(3) - b2x(3) \cdot (b1x(3))_v\Big] \\
& + 2Dvw\Big[y_{uw} b2x(3) - z_{uw} b2x(2) - z_u (b2x(2))_w + y_u (b2x(3))_w\Big] \\
& + 2RO3\Big[R4 \cdot b2x(3) - P8 \cdot b2x(1) - b1x(1) \cdot (b2x(1))_w \\
& \quad - b1x(2)\,(b2x(2))_w - R3 \cdot b2x(2) - b1x(3)\,(b2x(3))_w\Big] \\
& + 2Dvw\Big[z_{uw} b2x(2) + z_{uv} b1x(2) - y_{uw} b2x(3) - y_{uv} b1x(3) \\
& \quad - S1 \cdot z_w + R1 \cdot z_v - S2 \cdot y_w + R2 \cdot y_v\Big] \\
& + 2RO1\Big[-P2 \cdot b1x(1) - P1 \cdot b2x(1) + S1 \cdot b1x(2) - R1 \cdot b2x(2) - S2 \cdot b1x(3) + R2 \cdot b2x(3)\Big]
\end{aligned}$$

$$\alpha uxo_3 = 2SO1(y_v a1x(3) - z_v a1x(2))$$

$$\alpha vxo_3 = 2SO2(z_u a1x(2) - z_w b2x(2) + y_w b2x(3) - y_u a1x(3)) - 4Duw(y_u y_w + z_u z_w)$$

$$\alpha wxo_3 = 2SO3(z_v b2x(2) - y_v b2x(3))$$

$$\alpha uyo_3 = 2SO1(z_v a1x(1) - x_v a1x(3))$$

$$\alpha vyo_3 = 2SO2(-x_w b2x(3) + z_w b2x(1) - z_u a1x(1) + x_u a1x(3)) + 2Duw(x_w y_u + x_u y_w)$$

$$\alpha wyo_3 = 2SO3(x_v b2x(3) - z_v b2x(1))$$

$$\alpha uzo_3 = 2SO1(x_v a1x(2) - y_v a1x(1))$$

$$\alpha vzo_3 = 2SO2(-y_w b2x(1) + y_u a1x(1) + x_w b2x(2) - x_u a1x(2)) + 2Duw(x_w z_u + x_u z_w)$$

$$\alpha wzo_3 = 2SO3(y_v b2x(1) - x_v b2x(2))$$

$$\begin{aligned}
Rxo_3 = {} & 2Duw\left[z_{vw} b2x(2) + z_v(b2x(2))_w - y_{vw} b2x(3) - y_v(b2x(3))_w\right] \\
& + 2SO3\Big[P7 \cdot b2x(1) + P10 \cdot b2x(3) + (b2x(3))_w a1x(3) + (b2x(2))_w a1x(2) \\
& - P9 \cdot b2x(2) + (b2x(1))_w a1x(1)\Big] \\
& + 2Duw\left[y_v(a1x(3))_u + y_{uv} a1x(3) - z_{uv} a1x(2) - z_v(a1x(2))_u\right] \\
& + 2SO1\Big[P2 \cdot a1x(1) + b2x(1)(a1x(1))_u + b2x(2)(a1x(2))_u \\
& - S1 \cdot a1x(2) + b2x(3)(a1x(3))_u + S2 \cdot a1x(3)\Big] \\
& + 2Duw\Big[z_{uv} a1x(2) - z_{vw} b2x(2) - a1x(3) y_{uv} + y_{vw} b2x(3) \\
& - P5 \cdot z_u + z_w\, S3 - P6 \cdot y_u + y_w\, S4\Big] \\
& + 2SO2\left[a1x(1) \cdot P4 + P3\, b2x(1) - P5\, b2x(2) - S3\, a1x(2) + P6\, b2x(3) + S4\, a1x(3)\right]
\end{aligned}$$

The $\alpha$ coefficients are completely determined at this stage. The $\beta$ coefficients can be obtained from $\alpha$ and $\gamma$ coefficients from $\beta$, by rotating the variables as $x \to y \to z \to x$, termwise in Eqs. (3). This is done directly in the computer program, in the present work. Specific examples are given below. [ *Note:* It can be easily confirmed that the quantities J, Du, Dv, Dw, Duv, Dvw and Duw remain invariant to the cyclic rotation of indices.] The notation $\to$ is used to indicate the rotation $x \to y \to z \to x$.

**Example**

$$alx(1)_{\rightarrow} = (y_v z_w - y_w z_v)_{\rightarrow} = z_v x_w - z_w x_v = alx(2)$$

**Formulas for Determining $\beta$s and $\gamma$s.**

$$\beta ux = (\alpha uz)_{\rightarrow} \tag{A-8}$$

$$\beta vx = (\alpha vz)_{\rightarrow}$$

$$\beta wx = (\alpha wz)_{\rightarrow}$$

$$\beta uy = (\alpha ux)_{\rightarrow}$$

$$\beta vy = (\alpha vx)_{\rightarrow}$$

$$\beta wy = (\alpha wx)_{\rightarrow}$$

$$\beta uz = (\alpha uy)_{\rightarrow}$$

$$\beta vz = (\alpha vy)_{\rightarrow}$$

$$\beta wz = (\alpha wy)_{\rightarrow}$$

$$\gamma ux = (\beta uz)_{\rightarrow}$$

etc.

## APPENDIX B

### Complete Expressions for Gradient Boundary Conditions

The formulas arising from the application of Neumann boundary conditions are written out here. The derivation of these equations is outlined in Chapter 2. The notation used in Appendix A has also been employed here. After transformation of coordinates, the boundaries of the fracture can be identified as u = constant, v = constant and w = constant.

**u = constant**

$$x = \text{prescribed.} \tag{B-1}$$

$$\frac{\partial v}{\partial n} = 0, \text{ hence,}$$

$$y_u = \frac{\left[a1x(1)\, y_w\, z_u - a1x(2)b1x(2) - x_u\, y_w\, a1x(3)\right]}{\left(z_w\, a1x(1) - x_w\, a1x(3)\right)}$$

$$\frac{\partial w}{\partial n} = 0, \text{ hence,}$$

$$z_u = \frac{\left[a1x(1)\, y_u\, z_v + a1x(3)b2x(3) - x_u\, z_v a1x(2)\right]}{\left(y_v\, a1x(1) - x_v\, a1x(2)\right)}$$

**v = constant**

$$y = \text{prescribed.} \tag{B-2}$$

$$\frac{\partial u}{\partial n} = 0, \text{ hence,}$$

$$x_v = \frac{\left[b1x(3)\, y_v\, x_w - a1x(1)b1x(1) - x_w\, z_v\, b1x(2)\right]}{\left(y_w\, b1x(3) - z_w\, b1x(2)\right)}$$

$$\frac{\partial w}{\partial n} = 0, \text{ hence,}$$

$$z_v = \frac{\left[ y_v\, z_u\, b1x(1) - b2x(3)b1x(3) - x_v\, z_u\, b1x(2) \right]}{\left( y_u\, b1x(1) - x_u\, b1x(2) \right)}$$

**w = constant**

$$z = \text{prescribed.} \tag{B-3}$$

$$\frac{\partial u}{\partial n} = 0, \text{ hence,}$$

$$x_w = \frac{\left[ a1x(1)b2x(1) + x_v\, y_w\, b2x(3) - x_v\, z_w\, b2x(2) \right]}{\left( y_v\, b2x(3) - z_v\, b2x(2) \right)}$$

$$\frac{\partial v}{\partial n} = 0, \text{ hence,}$$

$$y_w = \frac{\left[ x_w\, y_u\, b2x(3) - z_w\, y_u\, b2x(1) - b2x(2)b1x(2) \right]}{\left( x_u\, b2x(3) - z_u\, b2x(1) \right)}$$

## APPENDIX C

### Grid Generation Equations in Two-Dimensional Geometries

Equations required to generate two dimensional grids are derived from the following variational problem,

$$\min I = I_s + \lambda I_o \tag{C-1}$$

where

$$I_s = \int \left[(\underset{\sim}{\nabla} u)^2 + (\underset{\sim}{\nabla} v)^2\right] d\underset{\sim}{x}$$

and

$$I_o = \int J^3 (\underset{\sim}{\nabla} u \cdot \underset{\sim}{\nabla} v)^2 \, d\underset{\sim}{x}$$

and

$\lambda$ is a specified parameter.

$\underset{\sim}{\nabla}$ is a two-dimensional gradient operator given as, $\underset{\sim}{\nabla} = (\frac{\partial}{\partial x}, \frac{\partial}{\partial y})$. J is the Jakobian of the transformation from (x,y) to (u,v) coordinates, i.e., $J = \frac{\partial(x,y)}{\partial(u,v)} = x_u y_v - x_v y_u$. The following rules are required in obtaining the Euler-Lagrange (EL) equations in the transformed space defined by the coordinates u and v.

$$u_x = \frac{y_v}{J} \ , \tag{C-2}$$

$$u_y = \frac{-x_v}{J} \ ,$$

$$v_x = \frac{-y_u}{J} \ ,$$

$$v_y = \frac{x_u}{J} \ ,$$

and can be derived from chain rule relationships. The EL operators are,

$$\mathrm{EL_u} = \frac{\partial}{\partial \mathrm{x}} - \frac{\partial}{\partial \mathrm{u}}\frac{\partial}{\partial \mathrm{x_u}} - \frac{\partial}{\partial \mathrm{v}}\frac{\partial}{\partial \mathrm{x_v}} \quad , \tag{C-3}$$

$$\mathrm{EL_v} = \frac{\partial}{\partial \mathrm{y}} - \frac{\partial}{\partial \mathrm{u}}\frac{\partial}{\partial \mathrm{y_u}} - \frac{\partial}{\partial \mathrm{v}}\frac{\partial}{\partial \mathrm{y_v}} \, .$$

The definition of the Jakobian also requires, $d\underset{\sim}{u} = \frac{1}{J}\, d\underset{\sim}{x}$. Application of Eqs. (C-3) on Eq. (C-1), along with Eq. (C-2) results in the following set of equations.

$$\alpha\mathrm{ux}\ \mathrm{x_{uu}} + \alpha\mathrm{vx}\ \mathrm{x_{vv}} + \alpha\mathrm{uy}\ \mathrm{y_{uu}} + \alpha\mathrm{vy}\ \mathrm{y_{vv}} + \mathrm{Ru} = 0 \tag{C-4}$$

$$\beta\mathrm{ux}\ \mathrm{x_{uu}} + \beta\mathrm{vx}\ \mathrm{x_{vv}} + \beta\mathrm{uy}\ \mathrm{y_{uu}} + \beta\mathrm{vy}\ \mathrm{y_{vv}} + \mathrm{Rv} = 0$$

Further,

$$\alpha\mathrm{ux} = \left(\frac{2}{J} - \frac{4}{J^2}\,\mathrm{x_u y_v} + \frac{2}{J^3}\,\mathrm{y_v^2\ FS}\right) + 2\lambda \mathrm{x_v^2} \ ,$$

$$\alpha\mathrm{vx} = \left(\frac{2}{J} + \frac{4}{J^2}\,\mathrm{x_v y_u} + \frac{2}{J^3}\,\mathrm{y_u^2\ FS}\right) + 2\lambda \mathrm{x_u^2}$$

$$\alpha\mathrm{uy} = \left(\frac{2}{J^2}\,\mathrm{x_u x_v} - \frac{2}{J^2}\,\mathrm{y_u y_v} - \frac{2}{J^3}\,\mathrm{x_v y_v\ FS}\right) + 2\lambda\ \mathrm{x_v y_v}$$

$$\alpha\mathrm{vy} = \left(\frac{2}{J^2}\,\mathrm{y_u y_v} - \frac{2}{J^2}\,\mathrm{x_u x_v} - \frac{2}{J^3}\,\mathrm{x_u y_u\ FS}\right) + 2\lambda \mathrm{x_u y_u}$$

$$\beta\mathrm{ux} = \left(\frac{2}{J^2}\,\mathrm{x_u x_v} - \frac{2}{J^2}\,\mathrm{y_u y_v} - \frac{2}{J^3}\,\mathrm{x_v y_v\ FS}\right) + 2\ \lambda \mathrm{x_v y_v}$$

$$\beta\mathrm{vx} = \left(\frac{2}{J^2}\,\mathrm{y_u y_v} - \frac{2}{J^2}\,\mathrm{x_u x_v} - \frac{2}{J^3}\,\mathrm{x_u y_u\ FS}\right) + 2\lambda \mathrm{x_u y_u}$$

$$\beta\mathrm{uy} = \left(\frac{2}{J} + \frac{4}{J^2}\,\mathrm{x_v y_u} + \frac{2}{J^3}\,\mathrm{x_v^2\ FS}\right) + 2\lambda \mathrm{y_v^2}$$

$$\beta\mathrm{vy} = \left(\frac{2}{J} - \frac{4}{J^2}\,\mathrm{x_u y_v} + \frac{2}{J^3}\,\mathrm{x_u^2\ FS}\right) + 2\lambda \mathrm{y_u^2}$$

$$\mathrm{FS} = \mathrm{x_u^2 + y_u^2 + x_v^2 + y_v^2} \ .$$

The source terms are given as,

$$Ru = -\frac{2}{J^2}\left[x_u(x_u y_{uv} - x_{uv} y_u) + x_v(x_{uv} y_v - x_v y_{uv})\right]$$

$$-\frac{2}{J^2}\left[y_v(x_v x_{uv} + y_v y_{uv}) - y_u(x_u x_{uv} + y_u y_{uv})\right]$$

$$-\frac{FS}{J^2}\left[\left(y_{uv} - \frac{2}{J}\, y_v\, (x_u y_{uv} - y_u x_{uv})\right) - (y_{uv} - \frac{2}{J}\, y_u(y_v x_{uv} - x_v y_{uv})\right]$$

$$+ 2\lambda\left[2FO\; x_{uv} + x_v(x_u x_{uv} + y_u y_{uv}) + x_u(x_v x_{uv} + y_v y_{uv})\right],$$

$$Rv = -\frac{2}{J^2}\left[y_u(x_u y_{uv} - y_u x_{uv}) + y_v(y_v x_{uv} - x_v y_{uv})\right]$$

$$+\frac{2}{J^2}\left[x_v(x_v x_{uv} + y_v y_{uv}) - x_u(x_u x_{uv} + y_u y_{uv})\right]$$

$$+\frac{FS}{J^2}\left[\left(x_{uv} - \frac{2x_v}{J}\,(x_u y_{uv} - y_u x_{uv})\right) - \left(x_{uv} - \frac{2}{J}\, x_u\, (y_v x_{uv} - x_v y_{uv})\right)\right]$$

$$+ 2\lambda\left[2y_{uv}\, FO + y_v\,(x_u x_{uv} + y_u y_{uv}) + y_u\,(x_v x_{uv} + y_v y_{uv})\right],$$

where $FO = x_u x_v + y_u y_v$.

The iteration scheme required to solve eqs. (C-4) is obtained (as in the text) by expanding the residuals of these equations in a Taylor's series up to the first order. The resulting equations are the following.

$$R_x^n + A_1\,\Delta x + B_1\,\Delta y = 0 \tag{C-5}$$

$$R_y^n + A_2\,\Delta x + B_2\,\Delta y = 0$$

$R_x$ and $R_y$ are the residuals of Eqs. (C-4) obtained by using approximate values of x and y.

$$A_1 = \frac{\partial R_x}{\partial x} = -2\,(\alpha ux + \alpha vx) \tag{C-6}$$

$$B_1 = \frac{\partial R_x}{\partial y} = -2\ (\alpha uy + \alpha vy)$$

$$A_2 = \frac{\partial R_y}{\partial x} = -2\ (\beta ux + \beta vx)$$

$$B_2 = \frac{\partial R_y}{\partial y} = -2(\beta uy + \beta vy)$$

$$\Delta x = x_{ij}^{n+1} - x_{ij}^{n}$$

$$\Delta y = y_{ij}^{n+1} - y_{ij}^{n}$$

The superscript n refers to the current level of iteration, and $\Delta x$ and $\Delta y$ are the necessary updates for the iteration scheme. They are obtained by simultaneously solving Eqs. (C-5) are given as,

$$\Delta x = (R_y^n \cdot B_1 - R_x^n B_2)/(B_2 A_1 - B_1 A_2) \qquad \text{(C-7)}$$

$$\Delta y = (R_x^n A_2 - R_y^n A_1)/(B_2 A_1 - B_1 A_2)$$

These corrections can be implemented on a finite-difference grid as discussed in the text.

**Boundary Conditions**

If all boundary conditions are of the Dirichlet type, they can be easily implemented by setting the corrections $\Delta x$ and $\Delta y$ as zero at the appropriate boundary nodes. On the other hand, if it is stipulated that the mesh lines intersect the physical boundaries at right angles (i.e., the Neumann condition), the equivalent mathematical expressions are the following.

**u = constant**

x is specified

$$\frac{\partial v}{\partial n} = 0 \qquad \text{(C-7)}$$

$$= \underset{\sim}{\nabla} v \cdot \underset{\sim}{n} = \underset{\sim}{\nabla} v \cdot \frac{\nabla u}{|\underset{\sim}{\nabla} u|}$$

Hence,

$$x_u x_v + y_u y_v = 0$$

$$y_u = -x_u x_v / y_v \quad , \qquad \text{determines y.}$$

**v = constant**

y is specified.

$$\frac{\partial u}{\partial n} = 0$$

$$= \underset{\sim}{\nabla} u \cdot \underset{\sim}{n} = \underset{\sim}{\nabla} u \cdot \frac{\underset{\sim}{\nabla} v}{|\underset{\sim}{\nabla} v|}$$

Hence,

$$x_u x_v + y_u y_v = 0$$

$$x_v = -y_u y_v / x_u \quad , \qquad \text{determines x.}$$

The iteration scheme and the boundary conditions can all be implemented within the framework of a second (or higher) order finite difference scheme.

## APPENDIX D

### Finite Difference Approximation of Equations Governing Flow in a Two Dimensional Complex Geometry

The Navier-Stokes equations in two dimensions can be extracted from Equations (3.5) by using the two dimensional form of the operator $\underset{\sim}{\nabla}$. Grid generation is used to handle complex geometry and is described in the text, and Appendices A and C. The flow equations given below are in terms of a generalized coordinate system ($\xi$, $\eta$) and it is assumed that the metric derivatives $\xi_x$, $\xi_y$ etc. are known from the grid generation procedure, at every nodal point in the flow domain. The momentum equations are given as follows.

$$\frac{\partial}{\partial \xi}\left\{ J \left[ \xi_x(\underset{\sim}{E}_i - \underset{\sim}{E}_v) + \xi_y (\underset{\sim}{F}_i - \underset{\sim}{F}_v) \right] \right\} + \tag{D-1}$$
$$\frac{\partial}{\partial \eta}\left\{ J \left[ \eta_x(\underset{\sim}{E}_i - \underset{\sim}{E}_v) + \eta_y (\underset{\sim}{F}_i - \underset{\sim}{F}_v) \right] \right\} = J\underset{\sim}{S}_p$$

The source term is,

$$\underset{\sim}{S}_p = -(p_x, p_y).$$

The Poisson equation of pressure is given as,

$$\frac{\partial}{\partial \xi}\left[ J\,(\xi_x\, p_x + \xi_y\, p_y) \right] + \frac{\partial}{\partial \eta}\left[ J(\eta_x p_x + \eta_y p_y) \right] = -JI_p \tag{D-2}$$

where

$$I_p = \underset{\sim}{\nabla} \cdot (\underset{\sim}{u} \cdot \underset{\sim}{\nabla}\, \underset{\sim}{u}) - \frac{1}{Re}\, \nabla^2 D, \quad \text{and}$$
$$D = \underset{\sim}{\nabla} \cdot \underset{\sim}{u}.$$

The subscripts i and v in Equation (D.1) refer to inertial and viscous terms respectively. The symbols used in this equation refer to the following.

$$\begin{aligned} \underset{\sim}{E}_i &= (u^2, uv) \\ \underset{\sim}{E}_v &= (\tau_{xx}, \tau_{yy}) \\ \underset{\sim}{F}_i &= (uv, v^2) \\ \underset{\sim}{F}_v &= (\tau_{xy}, \tau_{yy}) \end{aligned} \tag{D-3}$$

$$\tau_{xx} = \frac{2u_x}{Re}$$
$$\tau_{xy} = \frac{1}{Re}(u_y + v_x)$$
$$\tau_{yy} = \frac{2v_y}{Re}$$

u and v are the two components of velocity in x and y directions respectively. The generalized coordinates $\xi$ and $\eta$ form the computational space in which the fracture sides and contact areas appear regular. To this extent, only derivatives with respect to $\xi$ and $\eta$ have meaning and can be obtained on the computational space. However, the (x,y) derivatives are fully equivalent to the ($\xi$, $\eta$) derivatives through the chain rule,

$$\phi_x = \phi_\xi \, \xi_x + \phi_\eta \, \eta_x \tag{D-4}$$

and the metric derivatives are interchangeable as described in Appendix C. For example, $\xi_x = y_\eta/J$, where J is the Jakobian of the transformation from (x-y) plane to ($\xi - \eta$) plane. Using Equation (D-4), source terms such as $D = \underset{\sim}{\nabla} \cdot \underset{\sim}{u}$ can be evaluated as,

$$D = u_x + v_y \tag{D-5a}$$

or

$$D = \left\{ \frac{\partial}{\partial \xi} \left[ J(\xi_x u + \xi_y v) \right] + \frac{\partial}{\partial \eta} \left[ J(\eta_x u + \eta_y v) \right] \right\} / J \tag{D-5b}$$

For incompressible flow, D is exactly zero. However, for reasons mentioned in Chapter 3, it must be retained in all intermediate calculations of the flow field.

## Boundary Conditions

On all solid boundaries such as side walls and surface of the contact areas, the no-slip condition for the velocity field is imposed. Hence,

$$\underset{\sim}{u} = 0 \tag{D-6}$$

on solid surfaces. At inlet, the flow is specified as,

$$\begin{aligned} u &= u_m \\ v &= 0 \end{aligned} \tag{D-7}$$

where $u_m$, the mean velocity through the fracture is dependent on the pressure drop and contact areas, and must be determined as a part of the solution. Alternatively, the fracture geometry can be assumed to be periodic and the flow conditions taken to satisfy a periodicity condition (Equation 3.25). In case Equation (D-7) is used, an appropriate outflow condition is of the form,

$$\nabla \underset{\sim}{u} \cdot \underset{\sim}{n} = 0 \tag{D-8}$$

where $\underset{\sim}{n}$ is a unit normal on the exit plane. Equation (D-8) requires the flow to leave parallel to $\underset{\sim}{n}$ and is an approximation to flow conditions prevailing in the fracture. It is not expected to be valid for large flow rates, but is not a serious drawback since the interest of the present study is limited to small Reynolds number. Equation (D-8) can be expanded in the following manner. If the exit plane is denoted as $\xi =$ constant,

$$\underset{\sim}{n} = \frac{\nabla \xi}{|\nabla \xi|}$$

and for the u component of velocity, one obtains,

$$(u_x \xi_x + u_u \xi_y) = 0 \tag{D-9a}$$

Expanding Equation (D-9a),

$$u_\xi = u_\eta \frac{(y_\eta y_\xi + x_\eta x_\xi)}{(y_\eta^2 + x_\eta^2)} \tag{D-9b}$$

For a Cartesian system, the reduces to,

$$u_x = 0 \tag{D-9c}$$

The pressure is taken as specified at flow inlet and exit boundaries. For convenience, this can be expressed as,

$$\begin{aligned} p &= 1, \quad \text{inlet}, \\ p &= 0, \quad \text{exit}. \end{aligned} \tag{D-10}$$

On a solid wall, pressure is approximated from the reduced form of momentum equations, which include the no-slip condition. The equations are manipulated until the boundary conditions are expressible as,

$$p_\eta = f(u,v), \qquad \eta = \text{constant}, \tag{D-11}$$

or

$$p_\xi = g(u,v), \qquad \xi = \text{constant}.$$

As an example, consider a side wall $\eta = 0$. The y-momentum equation is,

$$p_y = \frac{1}{Re}(v_{xx} + v_{yy}) \tag{D-12}$$

Further,

$$v_{xx} = (v_\eta \eta_x + v_\xi \xi_x)_\eta \, \eta_x + (v_\eta \eta_x + v_\xi \xi_x)_\xi \, \xi_x,$$
$$v_{yy} = (v_\eta \eta_y + v_\xi \xi_y)_\eta \, \eta_y + (v_\eta \eta_y + v_\xi \xi_y)_\eta \, \xi_y$$

and

$$p_y = p_\eta \eta_y + p_\xi \xi_y.$$

Equation (D-12) can now be cast in the form of Equation (D-11) as,

$$p_\eta = \frac{1}{\eta_y}\left[\frac{1}{Re}(v_{xx} + v_{yy}) - p_\xi \xi_y\right] \tag{D-13}$$

**Treatment of Inertial Terms**

The inertial terms in Equation (D-1) are non-linear requiring the numerical scheme to be necessarily iterative. The convergence of the sequence of iterations is guaranteed only if the system of algebraic equations exhibits diagonal dominance. The construction of a numerical approximation of the inertial terms, which assures convergence is described below.

The $\xi$-component inertial terms in Equation (D-1) are,

$$\frac{\partial}{\partial \xi}\left[(J\xi_x u^2) + (J\xi_y uv)\right] + \frac{\partial}{\partial \eta}\left[(J\eta_x u^2) + (J\eta_y uv)\right]$$

In terms of the contravariant components of velocity (U,V), these terms can be written as,

$$\frac{\partial}{\partial \xi}(Uu) + \frac{\partial}{\partial \eta}(Vu),$$

where

$$U = y_\eta u - x_\eta v$$

and

$$V = x_\xi v - y_\xi u.$$

While u and v are the x and y components of the velocity vector, U and V can be interpreted as the components parallel to the $\xi$ and $\eta$ directions respectively. The numerical approximation is obtained in analogy to the Cartesian case, (with the use of a hybrid differencing scheme as described in Chapter 3) and is given below. The elementary computational cell is shown in Figure (D-1).

$$\frac{\partial}{\partial \xi}(Uu) \approx \frac{U_e u_e - U_w u_w}{\Delta \xi}$$

where

$$u_e = (\frac{u_E + u_p}{2}, u_p, u_E)$$

and

$$u_w = (\frac{u_W + u_p}{2}, u_W, u_p).$$

The value for $u_e$ chosen from the brackets depends on whether the grid Peclet number $Pe = U_e \Delta\xi Re$ follows one of the criteria,

$| Pe | < 2,$
$Pe > 2$ or
$Pe < -2,$ respectively.

In the case of $u_w$, the grid Peclet number is defined as

$$Pw = U_w \Delta\xi Re.$$

## Iteration Scheme

Using finite difference rules described in Chapter 3, Equations (D-1) and (D-2) can be written in terms of nodal values of velocity and pressure, as follows.

$$Ru = \alpha_{ue}u_E + \alpha_{uw}u_w + \alpha_{un}u_N + \alpha_{us}u_s + \alpha_{up}u_p + \alpha_{ve}v_E + \alpha_{vw}V_W + \alpha_{vn}v_N + \alpha_{vs}v_S + \alpha_{vp}v_p + Su \tag{D-14a}$$

$$Rv = \beta_{ve}v_E + \beta_{vw}v_w + \beta_{vn}v_N + \beta_{vs}v_S + \beta_{vp}v_p + \beta_{ue}u_E + \beta_{uw}u_W + \beta_{un}u_N + \beta_{us}u_S + \beta_{up}u_p + S_v \tag{D-14b}$$

$$Rp = \alpha_{pe}p_E + \alpha_{pw}p_W + \alpha_{pn}p_N + \alpha_{ps}p_s + \alpha_{pp}p_p + S_p \tag{D-14c}$$

Ru, RV and Rp are the residuals of the finite difference approximation of the momentum and pressure equations. As described in Chapter 2 and 3, corrections to a guessed flow

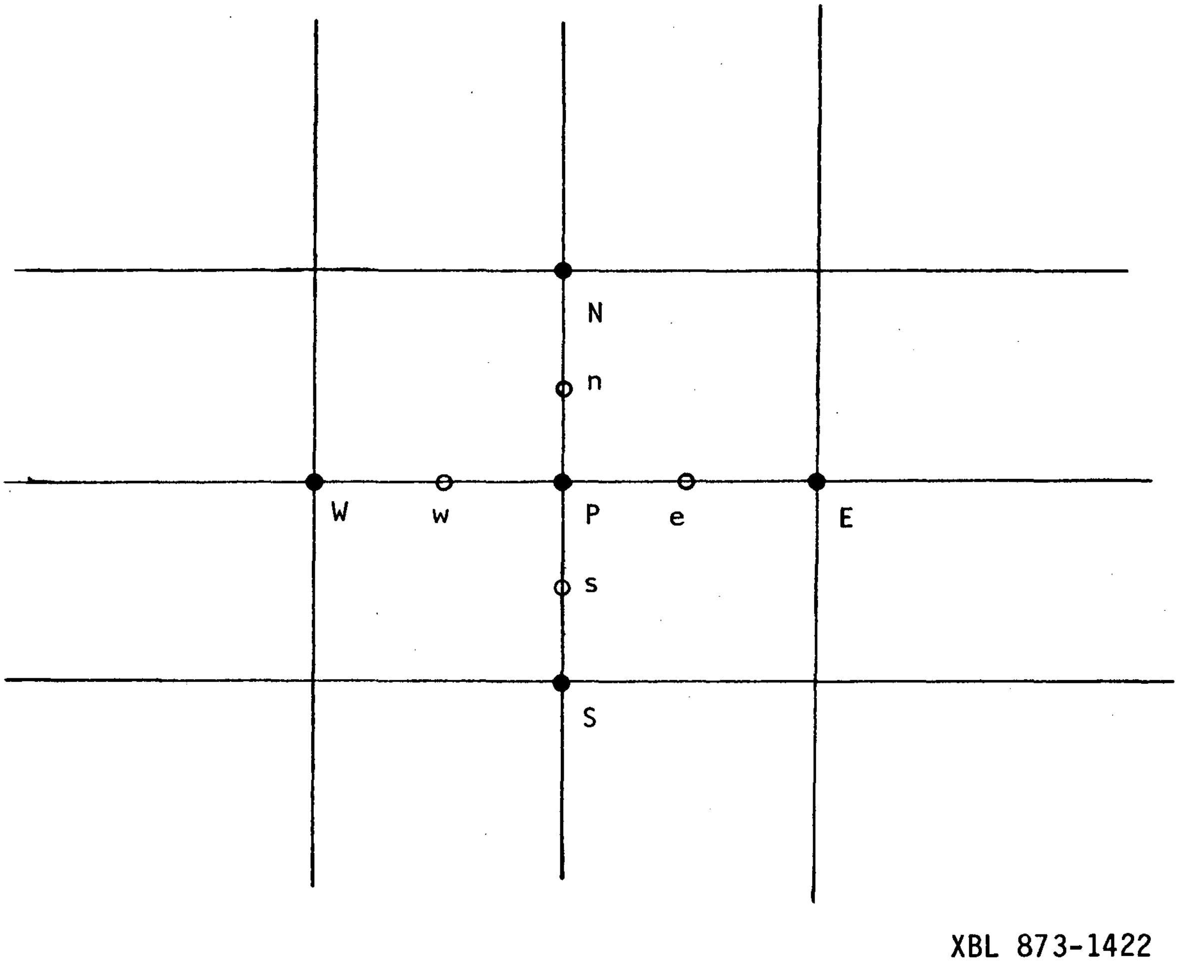


Figure D-1. Schematic of a Two Dimensional Computational Cell in the Transformed Flow Region.

field can be obtained from Equations (D-14) as follows.

$$\Delta u = \frac{(\alpha_{vp}Rv - \beta_{vp}Ru)}{Det}$$
$$\Delta v = \frac{(\beta_{up}Ru - \alpha_{up}Rv)}{Det} \qquad \text{(D-15)}$$
$$\Delta p = -\frac{Rp}{\alpha_{pp}}$$

and

$$Det = \alpha_{up}\beta_{vp} - \alpha_{vp}\beta_{up}$$

Equations (D-15) are repeatedly applied until these corrections become reasonably small

## Complete Form of Residuals

Coefficients appearing in Equations (D-14) are defined below. The following notation is used.

$$\phi_e = \frac{\phi_E + \phi_P}{2} \quad ,\phi_w = \frac{\phi_P + \phi_W}{2} \text{ etc.,}$$
$$(\quad)_w^e = (\quad)_e - (\quad)_w \text{, and}$$
$$(\quad)_{e,w} = (\quad)_e + (\quad)_w.$$

**Equation (D-14a)**

$$\alpha_{ue} = \left(\frac{2y_\eta^2 + x_\eta^2}{J\Delta\xi^2}\right)_e - \frac{Ue}{\Delta\xi}\left(\frac{1}{2}, 0, 1\right) Re \qquad \text{(D-16)}$$
$$\alpha_{uw} = \left(\frac{2y_\eta^2 + x_\eta^2}{J\Delta\xi^2}\right)_w + \frac{U_w}{\Delta\xi}\left(\frac{1}{2}, 1, 0\right) Re$$
$$\alpha_{un} = \left(\frac{2y_\xi^2 + x_\xi^2}{J\Delta\eta^2}\right)_n - \frac{V_n}{\Delta\eta}\left(\frac{1}{2}, 0, 1\right) Re$$
$$\alpha_{us} = \left(\frac{2y_\xi^2 + x_\xi^2}{J\Delta\eta^2}\right)_s + \frac{V_s}{\Delta\eta}\left(\frac{1}{2}, 1, 0\right) Re$$
$$\alpha_{up} = -\left(\frac{2y_\eta^2 + x_\eta^2}{J\Delta\xi^2}\right)_{e,w} - \left(\frac{2y_\xi^2 + x_\xi^2}{J\Delta\eta^2}\right)_{n,s}$$
$$- \frac{Re}{\Delta\xi}\left(\frac{U_e - U_w}{2}, U_e, -U_w\right) + \frac{Re}{\Delta\eta}\left(\frac{V_n - V_s}{2}, V_n, -V_s\right)$$
$$\alpha_{ve} = -\left(\frac{x_\eta y_\eta}{J\Delta\xi^2}\right)_e$$
$$\alpha_{vw} = -\left(\frac{x_\eta y_\eta}{J\Delta\xi^2}\right)_w$$

$$\alpha_{vn} = -\left(\frac{x_\xi y_\xi}{J\Delta\eta^2}\right)_n$$

$$\alpha_{vs} = -\left(\frac{x_\xi y_\xi}{J\Delta\eta^2}\right)_s$$

$$\alpha_{vp} = -\left(\alpha_{ve} + \alpha_{vw} + \alpha_{vn} + \alpha_{vs}\right)$$

$$Su = Su_1 + Su_2$$

where,

$$Su_1 = -Re(y_\eta p_\xi - y_\xi p_\eta)$$

and

$$Su_2 = -\frac{2}{\Delta\xi}\left(\frac{y_\eta y_\xi u_\eta}{J}\right)_w^e - \frac{2}{\Delta\eta}\left(\frac{y_\eta y_\xi u_\xi}{J}\right)_s^n - \frac{1}{\Delta\xi}\left(\frac{x_\eta x_\xi u_\eta - x_\eta y_\xi v_\eta}{J}\right)_w^e - \frac{1}{\Delta\eta}\left(\frac{x_\xi x_\eta u_\xi - x_\xi y_\eta v_\xi}{J}\right)_s^n$$

**Equation D-14b**

$$\beta_{ve} = \left(\frac{y_\eta^2 + 2x_\eta^2}{J\Delta\xi^2}\right)_e - \frac{U_e}{\Delta\xi}\left(\frac{1}{2}, 0, 1\right) Re \qquad \text{(D-17)}$$

$$\beta_{vw} = \left(\frac{y_\eta^2 + 2x_\eta^2}{J\Delta\xi^2}\right)_w + \frac{U_w}{\Delta\xi}\left(\frac{1}{2}, 1, 0\right) Re$$

$$\beta_{vn} = \left(\frac{y_\xi^2 + 2x_\xi^2}{J\Delta\eta^2}\right)_n - \frac{V_n}{\Delta\eta}\left(\frac{1}{2}, 0, 1\right) Re$$

$$\beta_{vs} = \left(\frac{y_\xi^2 + 2x_\xi^2}{J\Delta\eta^2}\right)_s + \frac{V_s}{\Delta\eta}\left(\frac{1}{2}, 1, 0\right) Re$$

$$\beta_{vp} = -\left(\frac{y_\eta^2 + 2x_\eta^2}{J\Delta\xi^2}\right)_{e,w} - \left(\frac{y_\xi^2 + 2x_\xi^2}{J\Delta\eta^2}\right)_{n,s} - - \frac{Re}{\Delta\xi}\left(\frac{U_e - U_w}{2}, U_e, - U_w\right) + \frac{Re}{\Delta\xi}\left(\frac{V_n - V_s}{2}, V_n, - V_s\right)$$

$$\beta_{ue} = -\left(\frac{x_\eta y_\eta}{J\Delta\xi^2}\right)_e$$

$$\beta_{uw} = -\left(\frac{x_\eta y_\eta}{J\Delta\xi^2}\right)_w$$

$$\beta_{un} = -\left(\frac{x_\xi y_\xi}{J\Delta\eta^2}\right)_n$$

$$\beta_{us} = -\left(\frac{x_\xi y_\xi}{J\Delta\eta^2}\right)_s$$

$$\beta_{up} = -\left(\beta_{ue} + \beta_{uw} + \beta_{un} + \beta_{us}\right)$$

$$S_v = Sv_1 + Sv_2 \ ,$$

where

$$Sv_1 = -\,Re\left(x_\xi p_\eta - x_\eta p_\xi\right)$$

and

$$Sv_2 = -\frac{2}{\Delta\xi}\left(\frac{x_\eta x_\xi v_\eta}{J}\right)_w^e - \frac{2}{\Delta\eta}\left(\frac{x_\eta x_\xi v_\xi}{J}\right)_s^n - \frac{1}{\Delta\xi}\left(\frac{y_\eta y_\xi v_\eta - y_\eta x_\xi u_\eta}{J}\right)_w^e - \frac{1}{\Delta\eta}\left(\frac{y_\xi y_\eta v_\xi - y_\xi x_\eta u_\xi}{J}\right)_s^n$$

**Equation D-14c**

$$\alpha_{pe} = \left(\frac{x_\eta^2 + y_\eta^2}{J\Delta\xi^2}\right)_e \qquad \text{(D-18)}$$

$$\alpha_{pw} = \left(\frac{x_\eta^2 + y_\eta^2}{J\Delta\xi^2}\right)_w$$

$$\alpha_{pn} = \left(\frac{x_\xi^2 + y_\xi^2}{J\Delta\eta^2}\right)_n$$

$$\alpha_{ps} = \left(\frac{x_\xi^2 + y_\xi^2}{J\Delta\eta^2}\right)_s$$

$$\alpha_{pp} = -\left(\alpha_{pe} + \alpha_{pw} + \alpha_{pn} + \alpha_{ps}\right)$$

$$S_p = Sp_1 + Sp_2$$

where

$$Sp_1 = -\left(\frac{(x_\eta x_\xi + y_\eta y_\xi)p_\eta}{J\Delta\xi}\right)_w^e - \left(\frac{(x_\eta x_\xi + y_\eta y_\xi)p_\xi}{J\Delta\xi}\right)_s^n$$

and

$$Sp_2 = J\left(\underset{\sim}{\nabla} \cdot (\underset{\sim}{u} \cdot \underset{\sim}{\nabla}\, \underset{\sim}{u}) - \frac{1}{Re}\,\nabla^2 D\right)$$

with

$$D = \underset{\sim}{\nabla} \cdot \underset{\sim}{u} \ .$$

The source term $Sp_2$ is computed pointwise on the grid, by expanding the form given above using chain rule (Equation D-4) and the inversion formulas for the metric derivatives (Equation C-2). A significant part of computing goes towards determining the source terms in Equations (D-16-D-18).

The iteration scheme given above continues until the corrections $\Delta u$, $\Delta v$ and $\Delta p$ are reasonably small ($\approx 10^{-5}$). Other measures are

1. convergence of the mean velocity through the fracture, and

2. divergence $D = |\underset{\sim}{\nabla} \cdot \underset{\sim}{u}|$, which must reduce with increasing number of iterations and also grid refinement. For an exact solution $D = 0$.

**Boundary Conditions**

Dirichlet boundary conditions (such as zero velocity on solid walls) is are imposed by setting the corrections ($\Delta u$ and$\Delta v$) as zero at the appropriate nodal points. Hence, the initial values at these nodes is preserved through the computation. However, the inlet flow condition (Equation D-7) has to be repeatedly applied since the mean velocity through the fracture (which is initially unknown) changes from one iteration to next. Gradient (Neumann) boundary conditions are treated in the following manner.

$$\phi_\eta = f \qquad \text{on } \eta = \text{constant},$$

can be approximated as,

$$\frac{(\phi_{j+1} - \phi_j)_i}{\Delta\eta} = f_{ij}, \text{ and hence,}$$

$$\phi_{ij} = \phi_{i,j+1} - f_{ij}\Delta\eta.$$

The gradient boundary conditions arise while solving for pressure and hold all solid walls, such as the fracture sides and the contact areas. When arbitrary shaped contact areas are mapped to squares, the corners of the squares introduce a break in the coordinate lines. An example of this is shown in Figure (D-2), for a circular contact area mapped to a square. Special treatment is required when such

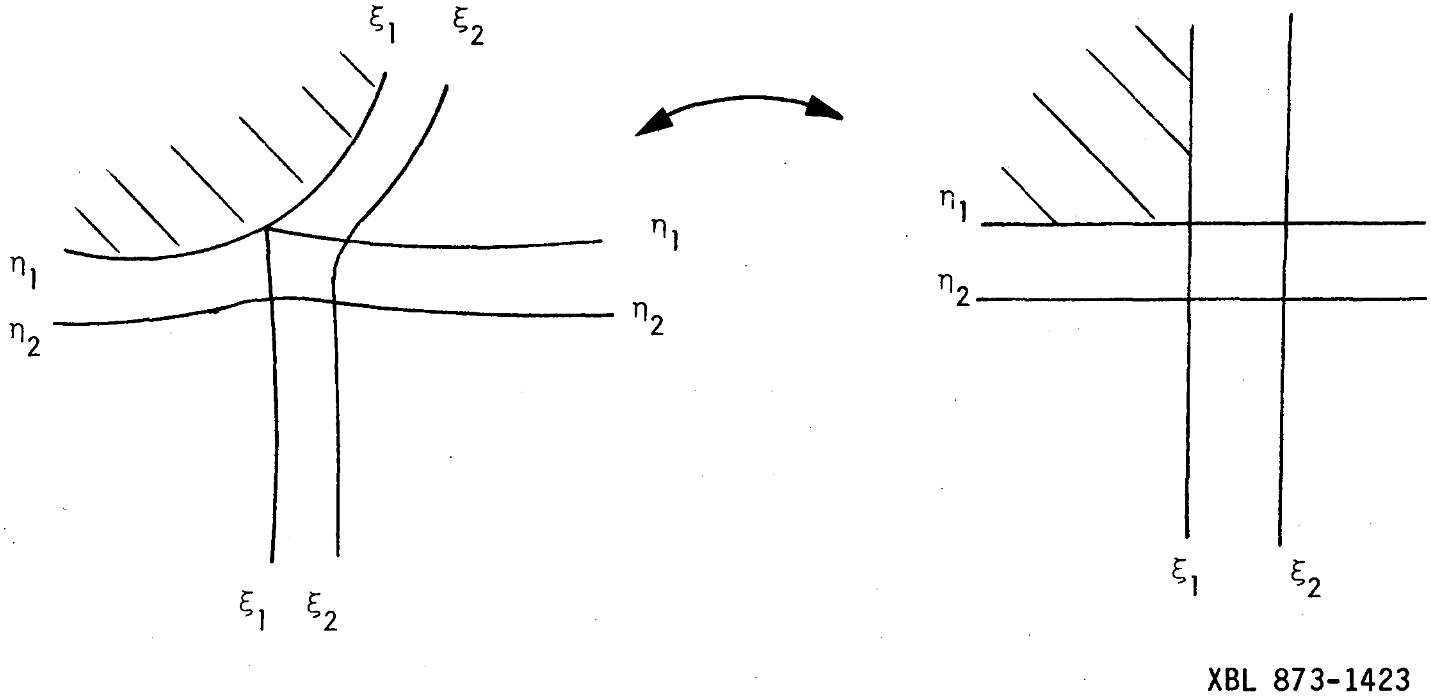


Figure D-2. Illustration of a Break in Coordinate Lines Arising from Grid Transformation. Note Lines $\xi = \xi_1$, and $\eta = \eta_1$.

instances are encountered. In the present work, the pressure boundary condition is derived from a local radial coordinate system. With reference to Figure (D-2), this can be written as follows

$$\frac{\partial p}{\partial r} = \frac{1}{Re}\frac{\partial^2 v_r}{\partial r^2} \tag{D-19}$$

where $v_r = u\cos\theta + v\sin\theta$. In two-dimensions, there are four special points for every contact area, on which Equation (D-19) is applied.

## APPENDIX E

### Finite Difference Approximation of Equations Governing Flow in a Three Dimensional Complex Geometry

The extension of the formulas given in Appendix D for solution of Navier-Stokes equations in a two dimensional geometry, to three dimensions is given below. The overall approach to solving the equations remains the same, and only the appropriate formulas are given in detail. It is assumed, as in Appendix D, that the grid-related derivatives are fully known from grid generation calculations. The Cartesian coordinates are (x,y,z) and the transformed coordinates are $(\xi,\eta,\gamma)$, in which all computation is performed. The fracture sides are given by $\xi$ (or $\eta$ or $\gamma$) = constant, and this facilitates easy applciation of boundary conditions. The Cartesian derivatives which appear below are evaluated in terms of $(\xi,\eta,\gamma)$ using the chain rule. For example,

$$u_x = u_\xi \xi_x + u_\eta \eta_x + u_\gamma \gamma_x \tag{E-1}$$

where $\xi_x = (y_\eta z_\xi - y_\xi z_\eta)/J$, etc., as given in Chapter 2 (Equation 2.5). This equivalence between the two coordinate systems is to be borne in mind while using the formulas given in the rest of this Appendix. Velocity components in the x, y and z directions are represented by symbols u, v and w respectively. Finite difference rules are valid only in the transformed space, where the grid is uniform.

### Navier-Stokes Equations

The three momentum equations are given in vector form as follows.

$$\begin{aligned}
&\frac{\partial}{\partial \xi}\left\{ J \left[ \xi_x(\underset{\sim}{E}_i - \underset{\sim}{E}_v) + \xi_y(\underset{\sim}{F}_i - \underset{\sim}{F}_v) + \xi_z(\underset{\sim}{G}_i - \underset{\sim}{G}_v) \right] \right\} \\
&+ \frac{\partial}{\partial \eta}\left\{ J \left[ \eta_x(\underset{\sim}{E}_i - \underset{\sim}{E}_v) + \eta_y(\underset{\sim}{F}_i - \underset{\sim}{F}_v) + \eta_z(\underset{\sim}{G}_i - \underset{\sim}{G}_v) \right] \right\} \\
&+ \frac{\partial}{\partial \gamma}\left\{ J \left[ \gamma_x(\underset{\sim}{E}_i - \underset{\sim}{E}_v) + \gamma_y(\underset{\sim}{F}_i - \underset{\sim}{F}_v) + \gamma_z(\underset{\sim}{G}_i - \underset{\sim}{G}_v) \right] \right\} \\
&= J \underset{\sim}{S} p \ ,
\end{aligned} \tag{E-2}$$

where

$$\underset{\sim}{E}_i = [u^2,uv,uw] \;,\; \underset{\sim}{E}_v = [\tau_{xx},\tau_{xy},\tau_{xz}]$$
$$\underset{\sim}{F}_i = [uv,v^2,vw] \;,\; \underset{\sim}{F}_v = [\tau_{xy},\tau_{yy},\tau_{yz}]$$
$$\underset{\sim}{G}_i = [uw,vw,w^2] \;,\; \underset{\sim}{G}_v = [\tau_{xz},\tau_{yz},\tau_{zz}]$$

and

$$\underset{\sim}{S}p = - [p_x,p_y,p_z].$$

Further,

$$\tau_{xx} = \frac{2u_x}{Re} \;,\; \tau_{xy} = \frac{1}{Re}(u_y + v_x),\; \tau_{xz} = \frac{1}{Re}(u_z + w_x)$$
$$\tau_{yy} = \frac{2v_y}{Re} \;,\; \tau_{yz} = \frac{1}{Re}(v_z + w_y),\; \tau_{zz} = \frac{2w_z}{Re} \;.$$

The Poisson equation of pressure is,

$$\frac{\partial}{\partial\xi}\left\{J[\xi_x p_x + \xi_y p_y + \xi_z p_z]\right\} + \frac{\partial}{\partial\eta}\left\{J[\eta_x p_x + \eta_y p_y + \eta_z p_z]\right\} + \frac{\partial}{\partial\gamma}\left\{J[\gamma_x p_x + \gamma_y p_y + \gamma_z p_z]\right\} = -JIp, \tag{E-3}$$

where,

$$Ip = \underset{\sim}{\nabla} \cdot (\underset{\sim}{u} \cdot \underset{\sim}{\nabla} \underset{\sim}{u}) - \frac{1}{Re} \nabla^2 D,$$
$$\underset{\sim}{\nabla} = (\frac{\partial}{\partial x}, \frac{\partial}{\partial y}, \frac{\partial}{\partial z}) \text{ and } D = \underset{\sim}{\nabla} \cdot \underset{\sim}{u} \;.$$

**Boundary Conditions**

As in Appendix D, the following boundary conditions apply.

$$\begin{array}{lll} \underset{\sim}{u} = 0 & \text{on all solid surfaces,} & \\ u = u_m & \text{(initially unknown)} & \\ v = 0 & & \text{at inlet,} \\ w = 0 & & \\ \underset{\sim}{\nabla} \underset{\sim}{u} \cdot \underset{\sim}{n} = 0 & \text{at exit .} & \end{array} \tag{3-4}$$

The last equation can be expanded as follows. Let $\xi$ = constant be the exit surface of a fracture. Then, $\underset{\sim}{n} = | \underset{\sim}{\nabla} \xi | / | \underset{\sim}{\nabla} \xi |$ and the exit boundary condition becomes,

$$\underset{\sim}{u}_x \xi_x + \underset{\sim}{u}_y \xi_y + \underset{\sim}{u}_z \xi_z = 0 \tag{E-4a}$$

This can be simplified to extract an expression for $\underset{\sim}{u}_\xi$ as in Appendix D. This expression is,

$$\underset{\sim}{u}_\xi = -\frac{\left[\underset{\sim}{u}_\eta(\xi_x\eta_x + \xi_y\eta_y + \xi_z\eta_z) + \underset{\sim}{u}_\gamma\,(\xi_x\gamma_x + \xi_y\gamma_y + \xi_z\gamma_z)\right]}{(\xi_x^2 + \xi_y^2 + \xi_z^2)} \tag{E-4b}$$

The pressure boundary conditions are,

$$\begin{aligned} p &= 1, && \text{inlet} \\ p &= 0, && \text{exit} \\ \underset{\sim}{\nabla} p \cdot \underset{\sim}{n} &= && \text{diffusion terms from Equation (E–1), on all no–slip boundaries.} \end{aligned} \tag{E-5}$$

Application of the gradient boundary condition of pressure accounts for a large part of computation and will be described below in some detail.

Consider a side boundary $\eta = 0$, or constant, on which the no-slip condition is imposed. On this boundary, $\underset{\sim}{u}_\xi = \underset{\sim}{u}_\gamma = 0$, and the Cartesian form of Equation (D-1) in the y-direction is,

$$p_y = \frac{1}{Re}\,(v_{xx} + v_{yy} + v_{zz}) \tag{E-6}$$

Each term can be expanded as follows, to account for coordinate transformation.

$$\begin{aligned} p_y &= p_\xi \xi_y + p_\eta \eta_y + p_\gamma \gamma_y, \\ v_{xx} &= \eta_{xx} v_\eta + \eta_x(v_{\eta\eta}\eta_x + 2v_{\eta\xi}2v_{\eta\xi}\xi_x + 2v_{\eta\gamma}\gamma_x) \end{aligned}$$

and similarly for $v_{yy}$ and $v_{zz}$. These, along with Equation (E-6) given an expression for $p_\eta$, which is the desired boundary condition for pressure. To improve accuracy, the velocity derivatives in the pressure boundary condition are calculated in a special manner. This involves using false nodes, as can be seen in Figure (E-1) and using the continuity equation to determine the velocities at these nodes. The continuity equation,

$$\underset{\sim}{\nabla} \cdot \underset{\sim}{u} = u_x + v_y + w_z = 0,$$

simplifies on a wall to,

$$u_\eta \eta_x + v_\eta \eta_y + w_\eta \eta_z = 0,$$

and so,

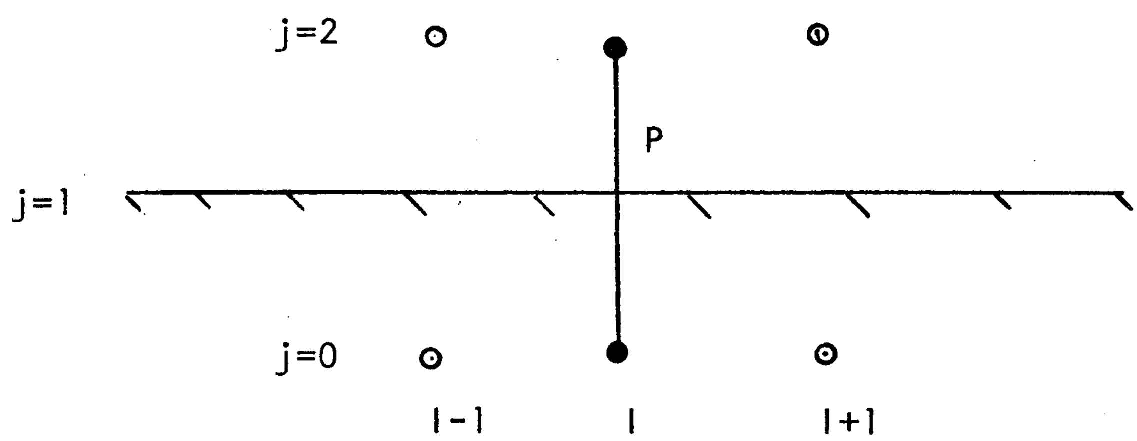


XBL 873-1424

Figure E.1. Distribution of Nodes at a No-Slip Boundary for Pressure Boundary Condition

$$v_\eta = -\frac{(u_\eta \eta_x + w_\eta \eta_z)}{\eta_y} \tag{E-7}$$

A second order finite-difference formula determines the velocity at node 0 as,

$$v_0 = v_2 - 2\Delta\eta v_\eta \tag{E-8}$$

Further,

$$v_{\eta\eta} = \frac{v_2 + v_0}{\Delta\eta^2}.$$

Mixed derivatives can be calculated using ghost nodes about the neighboring points of P (Figure E-1). This procedure has been used an all solid boundaries of the fracture, including the contact areas. The discretized version of Equation (E-4) - (E-8) is obtained in the same manner as in Appendix D, and is directly implemented in the computer program.

### Numerical Solution

The solution of Equations (E-2) and (E-3) is obtained by the approach outlined in Chapters 2 and 3 and Appendix D. Starting from an initial guess of the velocity and pressure field, Ru, Rv, Rw and Rp, the residual functions of Equations (E-2) and (E-3) are constructed. Since the solution is obtained on a grid, it is necessary to use finite difference rules, described in Chapter 3, to evaluate the derivatives of velocity and pressure. The corrections to the initial guess can be successively calculated by viewing the exact solution as a root of the residual function. This is described below.

$$Ru = \sum_i \alpha_{ui} u_i + \sum_i \alpha_{vi} v_i + \sum_i \alpha_{wi} w_i + Su \tag{E-9a}$$

$$Rv = \sum_i \beta_{ui} u_i + \sum_i \beta_{vi} v_i + \sum_i \beta_{wi} w_i + Sv \tag{E-9b}$$

$$Rw = \sum_i \gamma_{ui} u_i + \sum_i \gamma_{vi} v_i + \sum_i \gamma_{wi} w_i + Sw \tag{E-9c}$$

$$Rp = \sum_i \alpha_{pi} p_i + Sp \tag{E-9d}$$

In Equations (E-9), i takes on the symbols E, W, N, S, T, B and P, arising from a computational molecule shown in Figure (E-2). The corrections $\Delta \underset{\sim}{u}$ and $\Delta p$ can be

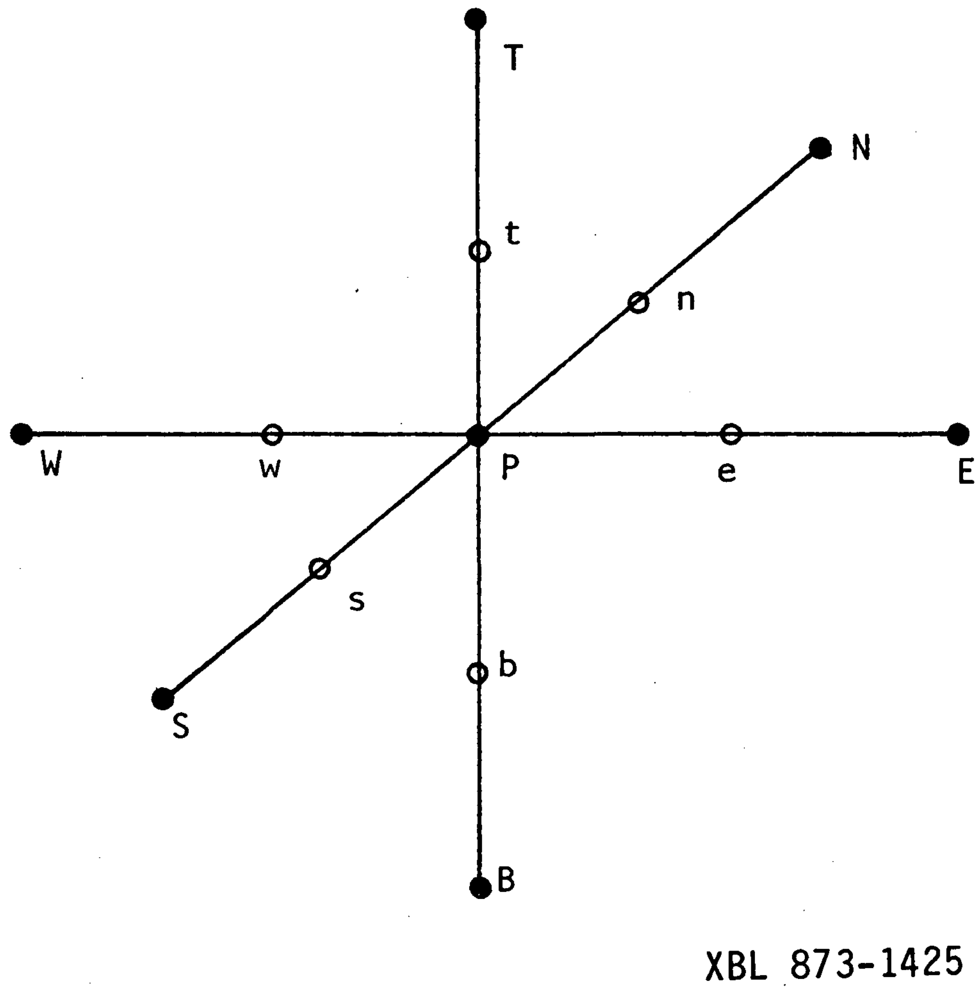


Figure E.2. A Three Dimensional Computational Molecule.

calculated as follows.

$$\Delta u = \text{Det } u/\text{Det}$$
$$\Delta v = \text{Det } v/\text{Det}$$
$$\Delta w = \text{Det } w/\text{Det}$$
$$\Delta p = -Rp/\alpha_{pp} \qquad \text{(E-10)}$$

where

$$\text{Det } u = \begin{vmatrix} -Ru & \alpha_{vp} & \alpha_{wp} \\ -Rv & \beta_{vp} & \beta_{wp} \\ -Rw & \gamma_{vp} & \gamma_{wp} \end{vmatrix},$$

$$\text{Det } v = \begin{vmatrix} \alpha_{up} & -Ru & \alpha_{wp} \\ \beta_{up} & -Rv & \beta_{wp} \\ \gamma_{up} & -Rw & \gamma_{wp} \end{vmatrix},$$

$$\text{Det } w = \begin{vmatrix} \alpha_{up} & \alpha_{vp} & -Ru \\ \beta_{up} & \beta_{vp} & -Rv \\ \gamma_{up} & \gamma_{vp} & -Rw \end{vmatrix}$$

and

$$\text{Det} = \begin{vmatrix} \alpha_{up} & \alpha_{vp} & \alpha_{wp} \\ \beta_{up} & \beta_{vp} & \beta_{wp} \\ \gamma_{up} & \gamma_{vp} & \gamma_{wp} \end{vmatrix}.$$

**Determination of Coefficients in Equations (E-9)**

Coefficients appearing in Equation (E-9) contain the finite difference approximations (including the grid spacing) arising from Equations (E-2) and (E-3). The flow equations contain both inertial and viscous terms and the sum contribution of each determines these coefficients. The treatment for each of these terms is given below.

**Inertial Terms**

The inertial terms, which define the acceleration of the fluid, are those with subscript i in Equations (E-2). These are given as

$$\left[J(\xi_x \underset{\sim}{E}_i + \xi_y \underset{\sim}{F}_i + \xi_z \underset{\sim}{G}_i)\right]_\xi +$$
$$\left[J(\eta_x \underset{\sim}{E}_i + \eta_y \underset{\sim}{F}_i + \eta_z \underset{\sim}{G}_i)\right]_\eta +$$

$$\left[J(\gamma_x \underset{\sim}{E}_i + \gamma_y \underset{\sim}{F}_i + \gamma_z \underset{\sim}{G}_i)\right]_\gamma \ .$$

These can be reduced to the form,

$$(U\underset{\sim}{u})_\xi + (V\underset{\sim}{u})_\eta + (W\underset{\sim}{u})_\gamma$$

where,

$$\begin{aligned} U &= J(\xi_x u + \xi_y v + \xi_z w) \ , \\ V &= J(\eta_x u + \eta_y v + \eta_z w) \ , \\ W &= J(\gamma_x u + \gamma_y v + \gamma_z w) \ . \end{aligned} \tag{E-11}$$

U, V and W are called the contravariant components of velocity, and represent those components which are orthogonal to the transformed coordinate system ($\xi$, $\eta$, $\gamma$). The form above is suitable for hybrid differencing, as described in Appendix D.

### Viscous Terms

The viscous terms can be split into two parts, one of which is linear in the flow and pressure variables, while the other has coupling terms which also render the equations non-linear. The linear terms produce coefficients which are common to all equations, while the non-linear terms contribute coefficients which are equation-specific. The linear part is,

$$\begin{aligned} &\left[J(\xi_x \phi_x + \xi_y \phi_y + \xi_z \phi_z)\right]_\xi + \\ &\left[J(\eta_x \phi_x + \eta_y \phi_y + \eta_z \phi_z)\right]_\eta + \\ &\left[J(\gamma_x \phi_x + \gamma_y \phi_y + \gamma_z \phi_z)\right]_\gamma + \ , \end{aligned}$$

where

$$\phi = (u,v,w,p) \ .$$

The non-linear part is,

$$\begin{aligned} &\left[J(\xi_x u_r + \xi_y v_r + \xi_z w_r)\right]_\xi + \\ &\left[J(\eta_x u_r + \eta_y v_r + \eta_z w_r)\right]_\eta + \\ &\left[J(\gamma_x u_r + \gamma_y v_r + \gamma_z w_r)\right]_\gamma \ , \end{aligned}$$

where

r = x for the u-equation,
r = y for the v-equation and
r = z for the w-equation.

These nonlinear terms do not appear in the pressure equation. In Cartesian coordinates, this viscous coupling is identically zero. It arises only with coordinate transformation because the velocity components (u,v,w) do not form an orthogonal triad on the computational space of $(\xi, \eta, \gamma)$.

Each of the coefficients in Equation (E-9) has three parts, arising from the inertial terms, the linear viscous terms and the coupling viscous terms. These are fully given below.

**Notation**

$$\mathrm{Ge} = \frac{1}{\Delta\xi^2}\left[J(\xi_x^2 + \xi_y^2 + \xi_z^2)\right]_e \quad , \quad [\ ]_e = \frac{[\ ]_E + [\ ]_P}{2}$$

$$\mathrm{Gw} = \frac{1}{\Delta\xi^2}\left[J(\xi_x^2 + \xi_y^2 + \xi_z^2)\right]_w$$

$$\mathrm{Gn} = \frac{1}{\Delta\eta^2}\left[J(\eta_x^2 + \eta_y^2 + \eta_z^2)\right]_n$$

$$\mathrm{Gs} = \frac{1}{\Delta\eta^2}\left[J(\eta_x^2 + \eta_y^2 + \eta_z^2)\right]_s$$

$$\mathrm{Gt} = \frac{1}{\Delta\gamma^2}\left[J(\gamma_x^2 + \gamma_y^2 + \gamma_z^2)\right]_t$$

$$\mathrm{Gb} = \frac{1}{\Delta\gamma^2}\left[J(\gamma_x^2 + \gamma_y^2 + \gamma_z^2)\right]_b$$

$$\mathrm{Gp} = -(\mathrm{Ge} + \mathrm{Gw} + \mathrm{Gn} + \mathrm{Gs} + \mathrm{Gt} + \mathrm{Gb})$$

$$\mathrm{Ae} = \frac{\mathrm{Ue}}{\Delta\xi}\,[\tfrac{1}{2}, 0, 1]\ \mathrm{Re}$$

$$\mathrm{Aw} = -\frac{\mathrm{Uw}}{\Delta\xi}\,[\tfrac{1}{2}, 1, 0]\ \mathrm{Re}$$

$$\mathrm{An} = \frac{\mathrm{Vn}}{\Delta\eta}\,[\tfrac{1}{2}, 0, 1]\ \mathrm{Re}$$

$$\mathrm{As} = \frac{-\mathrm{Vs}}{\Delta\eta}\,[\tfrac{1}{2}, 0, 1]\ \mathrm{Re}$$

$$\mathrm{At} = \frac{\mathrm{Wt}}{\Delta\gamma}\,[\tfrac{1}{2}, 0, 1]\ \mathrm{Re}$$

$$\mathrm{Ab} = -\frac{\mathrm{Wb}}{\Delta\gamma}\,[\tfrac{1}{2}, 0, 1]\ \mathrm{Re} \quad ,$$

where the quantity in square brackets is chosen according to,

$|\text{Pec}| < 2$,

Pec $>2$ or

Pec $<-2$

respectively. Pec is the grid Peclet number, defined as, Pec $=$ Ue $\Delta\xi$ Re for Ae, Pec $=$ Vn $\Delta\eta$ Re for An etc. Lastly,

$$\text{Ap} = \frac{\text{Re}}{\Delta\xi}\left[\frac{\text{Ue} - \text{Uw}}{2}\ ,\ \text{Ue},\ -\text{Uw}\right] + \frac{\text{Re}}{\Delta\eta}\left[\frac{\text{Vn} - \text{Vs}}{2}\ ,\text{Vn},\ -\text{Vs}\right]$$
$$+ \frac{\text{Re}}{\Delta\xi}\left[\frac{\text{Wt} - \text{Wb}}{2}\ ,\text{Wt},\ -\text{Wb}\right] .$$

**Equation (E-9a)**

$$\alpha_{ue} = \frac{1}{\Delta\xi^2}\,(J\xi_x^2)_e + \text{Ge} - \text{Ae}$$

$$\alpha_{uw} = \frac{1}{\Delta\xi^2}\,(J\xi_x^2)_w + \text{Gw} - \text{Aw}$$

$$\alpha_{un} = \frac{1}{\Delta\eta^2}\,(J\eta_x^2)_n + \text{Gn} - \text{An}$$

$$\alpha_{us} = \frac{1}{\Delta\eta^2}\,(J\eta_x^2)_s + \text{Gs} - \text{As}$$

$$\alpha_{ut} = \frac{1}{\Delta\gamma^2}\,(J\gamma_x^2)_t + \text{Gt} - \text{At}$$

$$\alpha_{ub} = \frac{1}{\Delta\gamma^2}\,(J\gamma_x^2)_b + \text{Gb} - \text{Ab}$$

$$\alpha_{up} = -\frac{1}{\Delta\xi^2}\left[(J\xi_x^2)_e + (J\xi_x^2)_w\right] - \frac{1}{\Delta\eta^2}\left[(J\eta_x^2)_n + (J\eta_x^2)_s\right]$$
$$- \frac{1}{\Delta\gamma^2}\left[(J\gamma_x^2)_t + (J\gamma_y^2)_b\right] + \text{Gp} - \text{Ap}$$

$$\alpha_{ve} = \frac{1}{\Delta\xi^2}\,(J\xi_x\xi_y)_e$$

$$\alpha_{vw} = \frac{1}{\Delta\xi^2}\,(J\xi_x\xi_y)_w$$

$$\alpha_{vn} = \frac{1}{\Delta\eta^2}\,(J\eta_x\eta_y)_n$$

$$\alpha_{vs} = \frac{1}{\Delta\eta^2}\,(J\eta_x\eta_y)_s$$

$$\alpha_{vt} = \frac{1}{\Delta\gamma^2}\,(J\gamma_x\gamma_y)_t$$

$$\alpha_{vb} = \frac{1}{\Delta\gamma^2}\,(J\gamma_x\gamma_y)_b$$

$$\alpha_{vb} = \frac{1}{\Delta\gamma^2}\,(J\gamma_x\gamma_y)_b$$

$$\alpha_{vp} = -(\alpha_{ve} + \alpha_{vw} + \alpha_{vn} + \alpha_{vs} + \alpha_{vt} + \alpha_{vb})$$

$$\alpha_{we} = \frac{1}{\Delta\xi^2}(J\xi_x\xi_z)_e$$

$$\alpha_{ww} = \frac{1}{\Delta\xi^2}(J\xi_x\xi_z)_w$$

$$\alpha_{wn} = \frac{1}{\Delta\eta^2}(J\eta_x\eta_z)_n$$

$$\alpha_{ws} = \frac{1}{\Delta\eta^2}(J\eta_x\eta_z)_s$$

$$\alpha_{wt} = \frac{1}{\Delta\gamma^2}(J\gamma_x\gamma_z)_t$$

$$\alpha_{wb} = \frac{1}{\Delta\gamma^2}(J\gamma_x\gamma_z)_b$$

$$\alpha_{wp} = -(\alpha_{we} + \alpha_{ww} + \alpha_{wn} + \alpha_{ws} + \alpha_{wt} + \alpha_{wb})$$

$$Su = Su_1 + Su_2 + Su_3 \quad ,$$

where

$$Su_1 = -ReJ\,(p_\xi\xi_x + p_\eta\eta_x + p_\gamma\gamma_x) \quad ,$$

$$\begin{aligned} Su_2 = & \frac{1}{\Delta\xi}\Big[J\xi_x(\eta_x u_\eta + \gamma_x u_\gamma) + J\xi_y(\eta_y u_\eta + \gamma_y u_\gamma) + J\xi_z(\eta_z u_\eta + \gamma_z u_\gamma)\Big]_w^e \\ & + \frac{1}{\Delta\eta}\Big[J\eta_x(\xi_x u_\xi + \gamma_x u_\gamma) + J\eta_y(\xi_y u_\xi + \gamma_y u_y) + J\eta_z(\xi_z u_\xi + \gamma_z u_\gamma)\Big]_s^n \\ & + \frac{1}{\Delta\gamma}\Big[J\gamma_x(\xi_x u_\xi + \eta_x u_\eta) + J\gamma_y(\xi_y u_\xi + \eta_y u_\eta) + J\gamma_z(\xi_z u_\xi + \eta_z u_\eta)\Big]_b^t \quad , \end{aligned}$$

where

$$\Big[\quad\Big]_w^e = \Big[\quad\Big]_e - \Big[\quad\Big]_w \quad ,$$

and

$$\begin{aligned} Su_3 = & \frac{1}{\Delta\xi}\Big[J\eta_x(\xi_x u_\eta + \xi_y v_\eta + \xi_z w_\eta) + J\gamma_x(\xi_x u_\gamma + \xi_y v_\gamma + \xi_z w_\gamma)\Big]_w^e \\ & + \frac{1}{\Delta\eta}\Big[J\xi_x(\eta_x u_\xi + \eta_y v_\xi + \eta_z w_\xi) + J\gamma_x(\eta_x u_\gamma + \eta_y v_\gamma + \eta_z w_\gamma)\Big]_s^n \\ & + \frac{1}{\Delta\gamma}\Big[J\xi_x(\gamma_x u_\xi + \gamma_y v_\xi + \gamma_z w_\xi) + J\eta_x(\gamma_x u_\eta + \gamma_y v_\eta + \gamma_z w_\eta)\Big]_b^t \quad . \end{aligned}$$

**Equation (E-9b)**

$$\beta_{ue} = \alpha_{ve}$$

$\beta_{uw} = \alpha_{vw}$ etc., until

$$\beta_{up} = \alpha_{vp}$$

$$\beta_{ve} = \frac{1}{\Delta\xi^2}(J\xi_y^2)_e + Ge - Ae$$

$$\beta_{vw} = \frac{1}{\Delta\xi^2} (J\xi_y^2)_w + Gw - Aw$$

$$\beta_{vn} = \frac{1}{\Delta\eta^2} (J\eta_y^2)_n + Gn - An$$

$$\beta_{vs} = \frac{1}{\Delta\eta^2} (J\eta_y^2)_s + Gs - As$$

$$\beta_{vt} = \frac{1}{\Delta\gamma^2} (J\gamma_y^2)_t + Gt - At$$

$$\beta_{vb} = \frac{1}{\Delta\gamma^2} (J\gamma_y^2)_b + Gb - At$$

$$\beta_{vp} = -\frac{1}{\Delta\xi^2} \left[(J\xi_y^2)_e + (J\xi_y^2)_w\right] - \frac{1}{\Delta\eta^2} \left[(J\eta_y^2)_n + (J\eta_y^2)_s\right] - \frac{1}{\Delta\gamma^2} \left[(J\gamma_y^2)_t + (J\gamma_y^2)_b\right] + Gp - Ap$$

$$\beta_{we} = \frac{1}{\Delta\xi^2} (J\ \xi_y\ \xi_z)_e$$

$$\beta_{ww} = \frac{1}{\Delta\xi^2} (J\ \xi_y\ \xi_z)_w$$

$$\beta_{wn} = \frac{1}{\Delta\eta^2} (J\ \eta_y\ \eta_z)_n$$

$$\beta_{ws} = \frac{1}{\Delta\eta^2} (J\ \eta_y\ \eta_z)_s$$

$$\beta_{wt} = \frac{1}{\Delta\gamma^2} (J\ \gamma_y\ \gamma_z)_t$$

$$\beta_{wb} = \frac{1}{\Delta\gamma^2} (J\ \gamma_y\ \gamma_z)_b$$

$$\beta_{wp} = -(\beta_{we} + \beta_{ww} + \beta_{wn} + \beta_{ws} + \beta_{wt} + \beta_{wb})$$

$$Sv = Sv_1 + Sv_2 + Sv_3$$

where

$$Sv_1 = -ReJ\ (p_\xi\xi_y + p_\eta\eta_y + p_\gamma\gamma_y),$$

$Sv_2 = (Su_2)$ with u replaced by v,

$$Sv_3 = \frac{1}{\Delta\xi} \Big[J\eta_y(\xi_x u_\eta + \xi_y v_\eta + \xi_z w_\eta) + J\gamma_y\ (\xi_x u_\gamma + \xi_y v_\gamma + \xi_z w_\gamma)\Big]_w^e + \frac{1}{\Delta\eta} \Big[J\xi_y(\eta_x u_\xi + \eta_y v_\xi + \eta_z w_\xi) + J\gamma_y\ (\eta_x u_\gamma + \eta_y v_\gamma + \eta_z w_\gamma\Big]_s^n + \frac{1}{\Delta\gamma} \Big[J\xi_y\ (\gamma_x u_\xi + \gamma_y v_\xi + \gamma_z w_\xi) + J\eta_y(\gamma_x u_\eta + \gamma_y v_\eta + \gamma_z w_\eta)\Big]_b^t$$

**Equation (E-9c)**

$$\gamma_{ue} = \alpha_{we}$$

$\gamma_{uw} = \alpha_{ww}$ etc., until

$$\gamma_{up} = \alpha_{wp}$$
$$\gamma_{ve} = \beta_{we}$$
$$\gamma_{vw} = \beta_{ww} \quad \text{etc., until}$$
$$\gamma_{vp} = \beta_{wp}$$
$$\gamma_{we} = \frac{1}{\Delta\xi^2}\,(J\xi_z^2)_e + Ge - Ae$$
$$\gamma_{ww} = \frac{1}{\Delta\xi^2}\,(J\xi_z^2)_w + Gw - Aw$$
$$\gamma_{wn} = \frac{1}{\Delta\eta^2}\,(J\eta_z^2)_n + Gn - An$$
$$\gamma_{ws} = \frac{1}{\Delta\eta^2}\,(J\eta_z^2)_s + Gs - As$$
$$\gamma_{wt} = \frac{1}{\Delta\gamma^2}\,(J\gamma_z^2)_t + Gt - At$$
$$\gamma_{wb} = \frac{1}{\Delta\gamma^2}\,(J\gamma_z^2)_b + Gb - Ab$$
$$\gamma_{wp} = -\frac{1}{\Delta\xi^2}\left[(J\xi_z^2)_e + (J\xi_z^2)_w\right] - \frac{1}{\Delta\eta^2}\left[(J\eta_z^2)_n + (J\eta_z^2)_s\right] - \frac{1}{\Delta\gamma^2}\left[(J\gamma_z^2)_t + (J\gamma_z^2)_b\right] + Gp - Ap$$
$$Sw = Sw_1 + Sw_2 + Sw_e$$

where,

$$Sw_1 = -Re\, J(p_\xi\xi_z + p_\eta\eta_z + p_\gamma\gamma_z)\ ,$$
$$Sw_2 = (Su_2) \text{ with u replaced by w,}$$
$$Sw_3 = \frac{1}{\Delta\xi}\left[J\eta_z(\xi_x u_\eta + \xi_y v_\eta + \xi_z w_\eta) + J\gamma_z(\xi_x u_\gamma + \xi_y v_\gamma + \xi_z w_\gamma)\right]_w^e + \frac{1}{\Delta\eta}\left[J\xi_z(\eta_x u_\xi + \eta_y v_\xi + \eta_z w_\xi) + J\gamma_z(\eta_x u_\gamma + \eta_y v_\gamma + \eta_z w_\gamma)\right]_s^n + \frac{1}{\Delta\gamma}\left[J\xi_z(\gamma_x u_\xi + \gamma_y v_\xi + \gamma_z w_\xi) + J\eta_z(\gamma_x u_\eta + \gamma_y v_\eta + \gamma_z w_\eta)\right]_b^t$$

**Equation (E-9d)**

$$\alpha_{pe} = Ge$$
$$\alpha_{pw} = Gw \quad \text{etc., until}$$
$$\alpha_{pp} = Gp$$
$$Sp = Sp_1 + Sp_2, \quad \text{where}$$
$$Sp_1 = J\left[\nabla \cdot (\underset{\sim}{u} \cdot \nabla \underset{\sim}{u}) - \frac{1}{Re}\nabla^2 D\right] \text{ and } D = \nabla \cdot \underset{\sim}{u}\ ,$$
$$Sp_2 = (Su_2) \text{ with u replaced by p.}$$

Equations (E.10) can be fully evaluated everywhere in the flow domain, except on the boundaries, where Equations (E.4) and (E.5) apply. The flow and pressure field can now be repeatedly computed till the corrections $\Delta \underset{\sim}{u}$ and $\Delta p$ become smaller than some prescribed value (say $10^{-5}$).

## APPENDIX F

### Relationship between Darcy's Law and Navier-Stokes Equations

The Darcy equations governing flow in a fracture are given in Chapter 3, and are repeated below for convenience.

$$\frac{\partial}{\partial x} (K_l \; h \; \frac{\partial p}{\partial x}) + \frac{\partial}{\partial y} (K_l \; h \; \frac{\partial p}{\partial y}) = 0 \tag{F.1}$$

$$p \; (0,y) = 1 \tag{F.2}$$

$$p \; (L,y) = 0$$

$$p_y \; (x,0) = p_y \; (x,L) = 0$$

Here, L is taken as the size of the fracture (assumed to be a square), p is pressure, x and y are coordinate directions in the plane of the fracture and z is a direction normal to both x and y. $K_l$ is local permeability and based on the cubic law, it is proportional to the square of the local fracture aperture. Equations (F.1) and (F.2) are derivable from Navier-Stokes equations by a series of simplifications which are outlined in this Appendix. These simplifying assumptions help understand the difference between the results of Darcy's law and Navier-Stokes equations and allows one to decide which model is required in a given physical application. This is particularly important since the computational time required to solve Navier-Stokes equations can exceed that for Darcy's law by a factor of hundred or more.

The Navier-Stokes equations along with the incompressibility constraint are given in Chapter 3 and also repeated below.

$$\underset{\sim}{\nabla} \cdot \underset{\sim}{u} = 0 \tag{F.3}$$

$$\underset{\sim}{u} \cdot \underset{\sim}{\nabla} \; \underset{\sim}{u} = -\underset{\sim}{\nabla} p + \frac{1}{Re} \; \underset{\sim}{\nabla}^2 \underset{\sim}{u} \tag{F.4}$$

**Assumption 1**

Inertial terms are negligible. This changes Equations (F.4) to,

$$- \underset{\sim}{\nabla} p + \frac{1}{Re} \nabla^2 \underset{\sim}{u} = 0 \tag{F.5}$$

**Assumption 2**

The component of velocity parallel to the z axis, i.e., normal to the fracture plane is negligible in comparison to the other two, namely u and v. The system of equations can now be written as follows.

$$u_x + v_y = 0 \tag{F.6a}$$

$$- \frac{\partial p}{\partial x} + \frac{1}{Re} \nabla^2 u = 0 \tag{F.6b}$$

$$- \frac{\partial p}{\partial y} + \frac{1}{Re} \nabla^2 v = 0 \tag{F.6c}$$

$$w = 0 \tag{F.6d}$$

**Assumption 3**

In the momentum equations (F.6b-F.6b), the gradients in the z-direction dominate those in x and y directions. Hence

$$\nabla^2 \equiv \frac{\partial^2}{\partial x^2} + \frac{\partial^2}{\partial y^2} + \frac{\partial^2}{\partial z^2} \approx \frac{\partial^2}{\partial z^2} \; .$$

The reduced set of Navier-Stokes equations are now obtained as given below.

$$\begin{aligned} &u_x + v_y = 0 \\ &-p_x + \frac{1}{Re} u_{zz} = 0 \\ &-p_y + \frac{1}{Re} v_{zz} = 0 \end{aligned} \tag{F.7}$$

Darcy's law can be recovered from Equations (F.7) by averaging them over the fracture aperture h(x,y). Noting that $p_x$ and $p_y$ are constant across the fracture aperture (since $p_z = 0$, from Equation (F.6d)). One has the following:

$$\int_0^h (u_x + v_y) \, dz = 0, \tag{F.8a}$$

$$\int_0^h \left(-p_x + \frac{1}{Re} u_{zz}\right) dz = 0, \tag{F.8b}$$

$$\int_0^h \left(-p_y + \frac{1}{Re} v_{zz}\right) dz = 0. \tag{F.8c}$$

Hence,

$$\frac{\partial \overline{u}}{\partial x} + \frac{\partial \overline{v}}{\partial y} = 0, \tag{F.9}$$

where

$$\overline{u} = \int_0^h u \, dz,$$

$$\overline{v} = \int_0^h v \, dz.$$

From Equations (F.8b) and (F.8c),

$$u = \frac{1}{2} p_x \, Re \, z \, (z - h) \quad ,$$

$$v = \frac{1}{2} p_y \, Re \, z \, (z - h) \quad ,$$

$$\overline{u} = - p_x \, Re \, \frac{h^3}{12} \quad ,$$

$$\overline{v} = - p_y \, Re \, \frac{h^3}{12} \quad .$$

Defining $K_l = \dfrac{h^2}{12}$ , Equation (F.9) can be written as,

$$\frac{\partial}{\partial x}\left(K_l \; h \, \frac{\partial p}{\partial x}\right) + \frac{\partial}{\partial y}\left(K_l \; h \, \frac{\partial p}{\partial y}\right) = 0 \tag{F.10}$$

This is identical to Equation (F.1).

Assumption 3 clearly shows that Darcy's law ignores pressure drops related to the turning of the fluid, i.e., the tortuosity of the flow path.

*LAWRENCE BERKELEY LABORATORY*
*TECHNICAL INFORMATION DEPARTMENT*
*UNIVERSITY OF CALIFORNIA*
*BERKELEY, CALIFORNIA 94720*